High Brightness Light Sources for Defence Applications

Mhairi Ann Martin

Submitted for the degree of Doctor of Engineering

Heriot-Watt University

School of Engineering and Physical Sciences

April 2014

ACADEMIC REGISTRY

Research Thesis Submission

Name*:*	Mhairi Ann Martin		
School/PGI:	Engineering and Physical Sciences		
Version: *(i.e. First, Resubmission, Final)*	Final	Degree Sought (Award **and** Subject area)	EngD (Photonics)

Declaration

In accordance with the appropriate regulations I hereby submit my thesis and I declare that:

1) the thesis embodies the results of my own work and has been composed by myself
2) where appropriate, I have made acknowledgement of the work of others and have made reference to work carried out in collaboration with other persons
3) the thesis is the correct version of the thesis for submission and is the same version as any electronic versions submitted*.
4) my thesis for the award referred to, deposited in the Heriot-Watt University Library, should be made available for loan or photocopying and be available via the Institutional Repository, subject to such conditions as the Librarian may require
5) I understand that as a student of the University I am required to abide by the Regulations of the University and to conform to its discipline.

* *Please note that it is the responsibility of the candidate to ensure that the correct version of the thesis is submitted.*

Signature of Candidate*:*		Date:	

Submission

Submitted By *(name in capitals):*	MHAIRI ANN MARTIN
Signature of Individual Submitting:	
Date Submitted:	

For Completion in the Student Service Centre (SSC)

Received in the SSC by *(name in capitals):*			
1.1 Method of Submission *(Handed in to SSC; posted through internal/external mail):*			
1.2 E-thesis Submitted (**mandatory for final theses)**			
Signature:		Date:	

ACKNOWLEDGEMENTS

I would like to thank my supervisors, colleagues and most of all, my friends for their support during the EngD.

ABSTRACT

This thesis contains the results of the work that was carried out between February 2009 and September 2012 in the area of high brightness light sources for defence applications. The work follows two main themes, namely nonlinearity in optical fibres and optical parametric oscillators (OPOs). Initially, the prospect of creating an ultrafast light source from solid core microstructured fibre via the phenomenon of modulation instability is discussed alongside supercontinuum generation and its value as a broad bandwidth source in countermeasures. What follows concerns OPOs in the infrared, both external (extracavity) and internal (intracavity) to a laser cavity, with the former is of benefit for high power applications, whereas the latter allows the OPO to operate more effectively at lower powers. The extracavity OPO section discusses a 2-stage conversion from 1064nm to 2128nm with the second stage design for conversion to ~5000nm, and the intracavity work is directed at both enabling a single frequency source for spectroscopy and examining the relationship between output coupling and the resonant OPO and laser fields.

Table of Contents

1 Introduction

The remit of an Engineering Doctorate is to extend the knowledge and commercial capabilities of the industrial sponsor which, in this case, is BAE Systems. The aim of the work carried out for BAE Systems was to engineer new mid-IR wavelength sources to enable new applications in the areas of Directional Infra-Red Counter Measures (DIRCM) and gas sensing. This thesis describes the results of a number of investigations into the development of mid-IR sources based around lasers. However, during the economic downturn a number of funding avenues became difficult to access ultimately having an effect on the direction and extent of the work that was carried out. The defence applications for the mid-IR technology will be described before introducing the technical work that was carried out. This is followed by a discussion of the difficulties that were faced as a result of the economic climate at the time and a timeline of events.

1.1 Application areas

Much of the research carried out during an Engineering Doctorate project is driven by either a gap in the market or the desire to enter a new market – despite the difficulties in funding this research the motivation remains the same.

Countermeasures continually evolve as new threats emerge and counter-counter measures become more sophisticated. It is for this reason that a section of work was directed in identifying new sources which could be deployed in this area. The interest in the area of the infrared beyond 8 micrometers is driven by the desire to create more complex and effective countermeasures. Whereas in the realm of spectroscopy, in the defence arena there are new threats emerging such as improvised explosive devices (IEDs) where the need is to be able to detect them prior to detonation but also for this technology to be man-portable and energy efficient. This next section aims to look in a bit more detail at the requirements for these devices before going back into the technical overview prior to the main body of the thesis.

1.1.1 DIRCM

The aim of Directional Infra-Red Counter Measures is to prevent the missile from acquiring the target. To do this, the countermeasure must engage with the missile in a way which changes its course. The IR source must mimic the IR signature of the target

as effectively as possible given environmental constraints such as atmospheric transmission. Figure 1.1 shows a mid-IR image of a combat aircraft which clearly shows the contrast between the cold sky and the heat radiation emitted specifically from the engines.

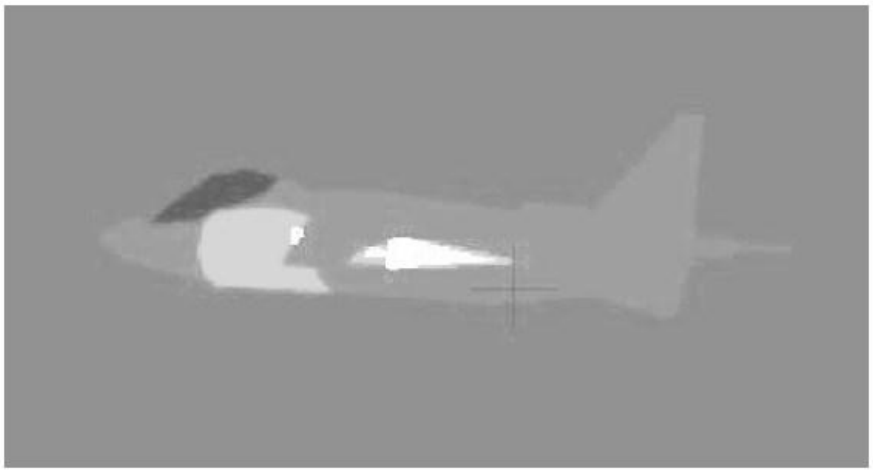

Figure 1.1: Mid-IR image (3 – 5 µm) of a combat aircraft [1.1]

If the region between 3 and 5 µm is identified as the key area which the missile is seeking, in order to specify the wavelength targets for the countermeasure source, this should be compared with the atmospheric transmission window (shown in Figure 1.2).

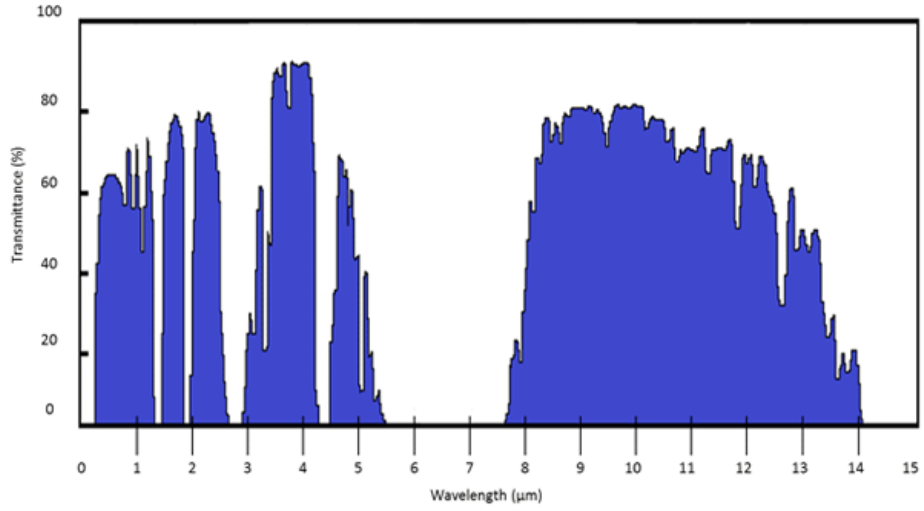

Figure 1.2: Atmospheric transmission [1.2]

In order to have maximum resistance against potential threats, it is advantageous for the IR source to operate across several wavelengths – which is why the OPO is so attractive. PPLN is a nonlinear material which can be used to build an OPO which has available wavelengths at either side of the water absorption peak at ~4.3 µm. The real

advantage, as threats continue to evolve and counter-counter measures become more efficient, is to be able to access the 8 – 12 μm region where the atmospheric transmission is still high and the range of sources available for countering threats is higher, and therefore less predictable. It is for this reason that ZGP/OP-GaAs are of interest in this thesis.

The power requirement is derived from the exact nature of the threat which has to be overcome and the types of atmosphere the beam has to propagate. Realistically, these figures lie within government bodies, but nominally an upper limit of 10W average power has been assumed here with nanosecond pulses as this is fitting with the resources that were available for the work. Practically, longer pulse durations (CW/nanoseconds rather than pico- or femtoseconds) would be of advantage to best mimic a real heat signature.

1.1.2 Gas Spectroscopy using continuous wave intracavity OPOs

The second application area for the latter chapters of this thesis is that of spectroscopy. It is known that one of the newest threats in war zones today is the use of improvised explosive device which are largely unrecognisable until the point of detonation – the ability to identify these threats is clearly very desirable. These bombs are made from explosive materials which have a chemical signature which could potentially be picked up – at distance – using some form of spectroscopic tool. Back-scatter gas absorption spectroscopy based on the IC-OPO has been patented [1.3] and demonstrations of methane detection down to 30ppm.m have been made with only 50mW of idler [1.4], with 205mW of idler in the VECSEL ICOPO been demonstrated [1.5] there is significant scope for this to be a useful tool for gas imaging. More recent demonstrations of using the ICOPO for hyperspectral imaging of VOCs have been made M^2 Lasers – results shown in Figure 1.3 for sensing at 2.75 μm showing distinct spectral features for each of the compounds.

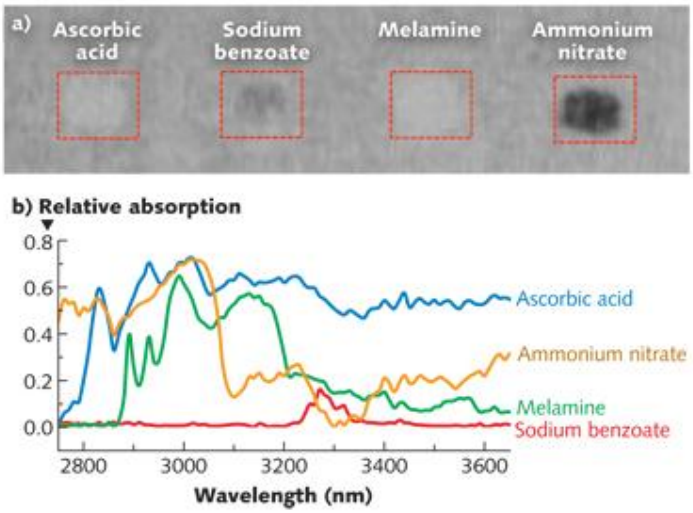

Figure 1.3: Ascorbic acid, sodium benzoate, melamine, and ammonium nitrate shown as (a) RAW images at 2.75 µm and processed across a wider wavelength region [1.6]

The technical advantages of moving to a continuous wave infrared source are an increase in spectral resolution as a consequence of the reduction in linewidth due to the time bandwidth product. For example, the source used to see the signatures in Figure 1.3 has a pulse duration of ~10nm and corresponding linewidth of 10cm^{-1} or 300 GHz, whereas a continuous wave product could achieve linewidths down to the kHz regime close to the theoretical limit.

PETN, RDX and SEMTEX-H are all explosives which have been used in IEDs, all with discernable spectra between 1000 and 1450cm^{-1} (6.8 – 10 µm) – shown below. The ability to 'see' in this regime would be of definite benefit for the detection of such compounds and this is something which is possible with the further development of IC-OPOs based on materials such as ZGP and OP-GaAs.

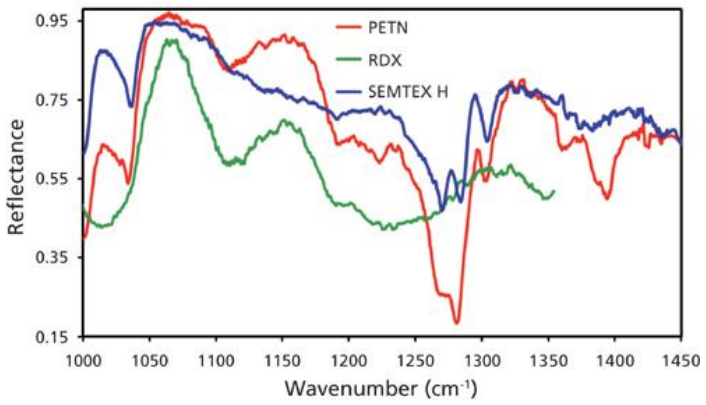

Figure 1.4: Reflectance spectra of common explosives used in IEDs (from 10 to 6.8µm) [1.8]

1.2 Technical challenges

Having looked at the applications areas for the research carried out in this thesis the technical areas will now be introduced below in the order in which they appear in the thesis. Firstly, there is a literature review examining the potential for engineering optical pulse break-up in microstructured fibre to generate an ultrafast laser-like source in the near IR (~1064nm), before changing direction to the main body of experimental work which investigates the potential of using three nonlinear materials in Optical Parametric Oscillators for wavelengths deeper into the IR (2 – 5μm) in terms of both power scaling and single frequency oscillation in two different configurations. The experimental work finishes with an examination of the effects of varying the output coupling from an OPO and the extent to which this can be altered and still achieve reasonable optical output over the wavelengths of interest.

1.2.1 Short pulse generation in microstructured fibre

At the time of the work being carried out, there were no mature direct emission laser lines in the 3 -5 μm wavelength range with the only way of accessing this region being via an OPO for which high intensity laser light is required. Before high power continuous wave diode bars were available, the only way to achieve the intensities required for OPOs was to use mode-locked or Q-switched lasers which require additional intracavity complexity to allow them to function in these modes of operation.

An awareness of the dynamics of supercontinuum generation in fibres following recent (at the time) demonstrations of ultrabroadband continuum that exploited the high intensities possible in the narrow core diameters afforded by the manufacturing techniques of microstructured fibres led to the question of whether the pulse break-up which contributes to supercontinuum generation could somehow be isolated and controlled independently to create an all-fibre ultrafast source.

It is concluded from this work that an OPO would be a more effective countermeasure source as the wavelength can be more tightly controlled and therefore achieve more power in these areas, rather than be at the mercy of broadening mechanisms whose range is largely defined by the power in the fibre.

1.2.2 Narrow linewidth OPO for mid IR generation using ZGP

In order to pump OP-GaAs, or ZGP as it turned out, it is necessary to have a narrow linewidth source with wavelength >2 μm due to material absorption at those

wavelengths. Traditionally, ZGP is pumped with a Holmium laser pumped by a Thulium fibre laser, however this gives a fixed pump wavelength without any flexibility to characterise the material over a wider tuning range. Using an intracavity diffraction grating in a PPLN OPO would provide a narrow linewidth tuneable source around the pump wavelength allowing the ZGP OPO to be fully characterised.

A narrow linewidth OPO source was achieved however the power available from this initial OPO stage was insufficient to raise the ZGP OPO above threshold. The end of the chapter covering this work will detail the subsequent work that could have been carried out to try to improve the performance of the PPLN OPO had the funding not been withdrawn.

1.2.3 Single frequency operation of a VECSEL pumped Intracavity OPO

The Nonlinear Optics group at St Andrews are interested in developing a spectroscopy tool for the detection of gases, including Volatile Organic Compounds (VOCs) for application (ultimately) in war zones where potentially the IC-OPO can be used as an imaging tool to 'see' VOC signatures coming from Improvised Explosive Devices (for example).

As the initial secondment was extended due to a lack of resource to pursue a VECSEL IC-OPO power scaling option – this would have required new pump diodes and associated focussing optic assemblies for re-shaping the beam, potentially PPLN with a larger cross section and possibly a new VECSEL chip – it was decided that the refinement of the IC-OPO to a single frequency source would be a more efficient use of the limited resources available.

It was assumed that since a stand-alone VECSEL tends to operate on a reasonably stable single longitudinal mode (with occasional mode hops), that the insertion of PPLN would not affect this stability and a single frequency OPO would be readily achieved as the dynamics of the OPO mirror those of the laser cavity. However, it was found that this was not the case and upon insertion of the nonlinear material the frequency behaviour of the cavity was very erratic and at best would hold a single frequency for a few seconds before collapsing into a chaotic state.

The perusal of a single frequency mode of operation was taken from 2 angles – forcing a single mode by using frequency selective elements that would suppress the unwanted modes, and the hypothesis that there were parasitic cavities formed due to non-optimal

coatings which were feeding back into the main cavity and causing the instabilities. The former approach worked reasonably well, however due to the very tight constraints that were put on the cavity, the OPO did not operate sufficiently above threshold for measurements to be taken. The latter approach was considered in 2 different ways – by designing a potential cavity based around Brewster cut PPLN (negating the need for coatings), and by getting the PPLN re-coated to a tighter anti-reflection specification (Laseroptik) and wedged to break symmetry. The second approach was taken following in-depth assessment of the coatings from a range of AR coated nonlinear materials which suggested this was a less risky way of furthering the work.

This section of work ran up against the time limit of the 4-year funded period for the EngD and the final experiments yielded poor results as a consequence of an aging pump diode which was not providing enough power to get the OPO above threshold. The crystal transmission was characterised external to the laser but showed a poorer anti-reflection that was specified and also poorer than on the original coating.

1.2.4 Variable output coupling of an IC-OPO

One of the attractive qualities of an OPO is that it generates multiple wavelengths with a single pump source. In the context of DIRCM this is attractive as it makes the countermeasure more difficult to overcome/block.

In the extracavity configuration, the pump beam is not resonated within the cavity as there is sufficient gain on a single pass to generate the signal, leaving the remainder free to pass through the OPO and be used for other purposes. The idler beam is never resonated and exits the cavity as a consequence of the parametric generation. In the extracavity case, the intensities afforded by a continuous wave laser do not lend themselves to reaching the threshold power required for nonlinear processes. The most efficient way to do this is to place the nonlinear material inside the high finesse laser cavity where the intensity is highest, leaving the pump output as low as it can be from the parasitic losses of a high reflectivity coating. This leaves the intracavity OPO only generating idler radiation for use in any given application, which is less useful for DIRCM. Due to the interdependence of the OPO cavity and the pump laser cavity, the dynamics lead to a somewhat ‘chicken and egg’ when it comes to optimising the losses on each of the cavities involved. If more pump output coupling is required, there is less available for down conversion and similarly there is more signal required there is less

pump available due to the increased OPO threshold induced by increasing the signal cavity losses.

The results from some modelling are shown in this chapter alongside experimental results confirming, for the first time, the relationships between thresholds and output coupling in an intracavity OPO based on a theoretical analysis published by Dunn in the Handbook of Optics [1.7].

1.3 The climate of the programme

The direction of this programme of work was heavily affected by the financial difficulties of the defence sector. The purpose of this section is to outline the work that was carried out under various funding streams and the reason behind its termination.

1.3.1 Laser Coalition

This Engineering Doctorate project was sponsored by BAE Systems via the Laser Coalition Project which was a Dstl funded programme looking at novel laser sources for a range of applications from burst illumination (BIL) to high power mid-infrared (mid-IR) lasers. The programme was due to conclude in August 2011 after 3 years, however it was funded during a time when the recession was beginning to impact government budgets and, as lower Technology Readiness Level (TRL) is of lower priority in the short term, the programme was cancelled after just 1 year.

The initial aim of the EngD project under the Laser Coalition was to investigate whether ultrafast, high peak power pulses could be generated using fibre geometry in preference to the traditional solid state arrangement using titanium sapphire making the architecture more robust to alignment problems and potentially cheaper, with a smaller footprint. The budget allocation in the first instance did not include provisions for material resources in the EngD project, so no practical demonstrations were possible in the first 6 months. However, the programme as a whole was terminated at the first annual review meeting where there was an opportunity to review resource allocation. What follows from this is Chapter 3 which looks at the literature surrounding the area of modulation instability in microstructured fibres and whether it can be applied to generating designer pulses as a consequence of dispersion management.

1.3.2 Transformational Technology Programme

The loss of the laser coalition had a large short term impact on the members of the group at the BAE Systems Advanced Technology Centre (ATC) as this was due to

account for a significant amount of the work for that time, as well as the EngD project. Funding was, however, secured through an internal BAE funding programme, the Transformational Technology Programme (TTP) which was to look at the longer term aspirations of the BAE business units in contrast to the Engineering Capability Programme (ECP) which funded research into technologies which were for more immediate deployment. At that time, protecting platforms using laser based technologies was seen as a priority due to interest from BAE business units both in the UK and Australia and therefore some of the Laser Coalition projects were funded under the TTP. This allowed the continuation of the work on mid-IR OPOs, specifically in the development of OPOs based on the novel material Orientation Patterned Gallium Arsenide (OP-GaAs). This was where the EngD work was diverted following a lack of suitable funding opportunities for the work which had already been started.

OP-GaAs, as a material used for frequency conversion in the mid-IR, was first published in 2007 by Schunemann from BAE Systems in Nashua, USA. Following extensive communication between BAE USA/UK it was understood that some of this material could be borrowed under an inter-governmental agreement, The Technical Cooperation Programme (TTCP), however this could not bypass the International Traffic in Arms (ITAR) regulations which made exporting the material very difficult. The potential ITAR implications were not fully appreciated at the time as the material was assumed to be of only research use, however this turned out to be a significantly more complex and drawn out set of procedures than anyone could have predicted making this a much higher risk project than was initially anticipated. Ultimately the difficulty in sourcing the material outlived the project that it was intended to be used for. By means of contingency, the funding which had been allocated to the procurement (or otherwise) of OP-GaAs was redirected towards obtaining a different nonlinear material for mid-IR conversion – Zinc Germanium Phosphide (ZGP) which was secured before the re-organisation of the BAE Systems funding streams.

BAE Systems ATC underwent a review of all projects funded under the ECP/TTP in April 2010, putting a freeze on all project spending for this time. This lasted for several months and resulted in the restructuring of the budgets of the ECP/TTP into a centralised budget which was supported and projects directed by the business units, rather than by a committee within the Shared Services part of the business, leading to the prioritisation of short term objectives which did not include the work detailed here.

The timing of the re-structuring led to premature termination on the work on the ZGP OPO before reaching a more satisfying conclusion.

The work carried out at BAE in this area is described in Chapter 4 – the design and build of a narrow linewidth optical parametric oscillator to use as a pump source for a second optical parametric oscillator based on ZGP.

1.3.3 EPSRC

In an attempt to mitigate the effects of turbulent defence funding and constantly shifting priorities, an opportunity to work in academia was taken. Due to the existing collaboration between the University of St Andrews and BAE Systems which had been established under the Laser Coalition, a move to the Nonlinear Optics group at the University of St Andrews seemed viable. The opportunity to embark on a knowledge transfer secondment to learn more about IC-OPOs aligned well with the interest of BAE in demonstrating the intracavity OPO (IC-OPO). This was originally intended to be a 6 week placement in October 2010 from which components could be bought to replicate the system at the ATC. However, following the restructuring of internal BAE Systems budgets to align more closely with the needs of their business units, it was concluded that there was more opportunity to make progress on the intracavity OPO system in St Andrews, working on developing a single frequency intracavity OPO based on Vertical External Cavity Surface Emitting Lasers (VECSELs), than to risk further disruption by staying at the ATC. Over time the scope of the work carried out at the University of St Andrews was extended to include an additional project looking at experimental validation of the output coupling of the IC-OPO.

At the time when the secondment began, an EPSRC proposal prepared by the group in collaboration with the Institute of Photonics (Strathclyde University) had been submitted and was awaiting approval. This was due to cover, amongst other things, the development of the single frequency IC-OPO source based on Periodically Poled Lithium Niobate (PPLN) and the extension of this to use 2 μm VECSELs as a pump laser for OP-GaAs.

Ultimately this project was rejected in September 2011 resulting in a significant compromise in progress as it was not possible to investigate all the necessary trial configurations/experimental arrangements that in the course of a properly funded programme would have been explored in order to make rapid progress.

1.3.4 Conclusion

In conclusion, the availability of funding played a significant role in the evolution of the programme and had an effect on the final state outputs. The following is a timeline of what research was carried out at which location.

When	Work Undertaken	Location	Funded By
Sept 2008 – Feb 2009	Taught coursework	University of St Andrews	N/A
Feb 2009 – Oct 2010	Extracavity OPO – Chapters 2 and 3	BAE Systems Advanced Technology Centre, Bristol	Laser Coalition/TTP
Oct 2010 – July 2012	Intracavity OPO – Chapters 4, 5 and 6	University of St Andrews	Unfunded

1.4 Conclusion

This introduction has outlined the technical work undertaken over the duration of the funded programme, described the key application areas to which this work is relevant and also contextualised this within the challenging economic circumstances that influenced the direction of some of the work that was carried out. The work has contributed to a broader understanding of the engineering tolerances required for mid-IR lasers and generation, which is important for the field. The results will be embedded within BAE Systems and used as an engineering template for future projects and products.

1.5 References

[1.1] M. A. Richardson, "The anatomy of the MANPAD - art. no. 67380H," Technologies for Optical Countermeasures IV (6738), H7380-H7380 (2007)

[1.2] Opto-E website http://www.opto-e.com/infra-red-resources-theory.php accessed 4/4/14

[1.3] D. J. M. Stothard, M. H. Dunn and C. F. Rae, "Detector/Imager" US Patent 7,995,204 (published Aug 2011)

[1.4] D. J. M. Stothard, M. H. Dunn and C. F. Rae, "Hyperspectral Imaging of gases with a continuous-wave pump enhanced optical parametric oscillator," *Optics Express*, vol. 12, no. 5, pp. 947 – 955, 2004

[1.5] D. J. M. Stothard, J.-M. Hopkins, D. Burns, and M. H. Dunn, "Stable, continuous-wave, intracavity, optical parametric oscillator pumped by a semiconductor disk laser (VECSEL)," Opt. Express 17, 10648-10658 (2009).

[1.6] N. Hempler, J. Nicholls and G. Malcolm, "Spectral Imaging: Active hyperspectral sensing and imaging for remote spectroscopy applications", Laser Focus World, vol. 49, issue 1, 2013 (accessed online – 29/3/14: http://www.laserfocusworld.com/articles/print/volume-49/issue-11/features/spectral-imaging-active-hyperspectral-sensing-and-imaging-for-remote-spectroscopy-applications.html)

[1.7] M. Ebrahimzadeh and M. H. Dunn, "Ch. 22 – Optical Parametric Oscillators" in *Handbook of Optics*, 2001, pp. 2.42 – 22.50

2 Fibre

This chapter deals with a 6 month period of work at the beginning of the doctorate during which the theoretical question of whether microstructured fibre can be optimized for defence-like applications was addressed.

The motivation behind moving to fibre-based technologies is the capacity for reducing the footprint of a system. Traditionally Titanium Sapphire (Ti:S) lasers are used to generate ultrafast pulses however these are complex systems which are very sensitive to misalignment. The advantage of ultrafast laser sources is that the pulse energy is high which is essential for nonlinear conversion, important for the generation of wavelengths in the infrared (~2 – 5 μm) where direct emission sources have traditionally been less well established due to a lack of availability of efficient gain media. This was true at the time of this investigation, but as outlined in the literature section the availability of direct emission sources in the infrared, for example bandgap engineered semiconductors such as Quantum Cascade Lasers, is increasing which may, over time, displace nonlinear conversion techniques in countermeasure technologies.

It was highlighted in a previous EngD project carried out at BAE Systems that in microstructured fibres used for continuum generation the incident pulses are temporally fragmented, via the modulation instability effect, over the length of the fibre [2.1]. There are two lines of enquiry stemming from this observation: i) can this effect be isolated to make a more compact, high power, ultrafast system at lower cost and ii) can the spectral power density of the continuum be increased without resulting in further broadening. If it were possible, the former could potentially simplify a mode locked fibre laser, which would only operate at low pulse energies due to the broadening effects (this will be discussed more fully in the following section). Being able to increase the spectral power density independently of the extent of the broadening would create a spectral fingerprint which could penetrate the atmosphere and be more useful in countering threats. The target spectral power density was nominally set to 50mW/nm, over a range of 100nm, with no specification of the centre wavelength.

Before going on to discuss the proposed scheme and how it could feasibly work with regards both of the points raised above, the advantages and disadvantages of alternative technologies will be discussed.

There are a number of factors which need to be considered when designing an ultrafast laser; a gain medium with a large gain bandwidth, such that the time-bandwidth product gives the required pulse duration, a suitable mode-locking technique, for example, passive mode-locking using a saturable absorber and dispersion has to be very carefully managed in the cavity. When this is compared to the very simplest of laser cavities, such as the Nd: YAG laser, it would clearly be advantageous to move to a simpler scheme. One possible alternative could be to mode-lock a fibre laser, however in order to achieve the pulse energies required for conversion to the infrared, this scheme would be impractical due to broadening effects as well as the presence of photodarkening over time in Yb, a key dopant in fibre lasers. Examples of all-fibre ultrafast lasers include Chong (2006) [2.2] who produced 120mW of 170fs and then later Lefrançois (2010) [2.3] who produced 12W average power at 115fs. If it were possible to control the effect of modulation instability in a single length of fibre (or multiple lengths of fibre spliced together), there could potentially be a very simple, very compact solution to generating ultrafast pulses.

Increasing the spectral bandwidth of mid-IR laser lines could be achieved by operating an Optical Parametric Oscillator (OPO) at degeneracy, which would create a spectrum which could span at least 100nm (degenerate OPOs will be discussed in later chapters in more detail). However, the degenerate condition is always twice the pump wavelength which is too predictable from a defence standpoint. The idea behind introducing some broadening in the IR wavebands is to increase the complexity and reduce the predictability of the IR fingerprint making it more challenging to defeat. For airborne countermeasures, the key wavelengths which are targeted coincide with areas of atmospheric transmission (~3 – 5 μm) with sufficient power in the beam to penetrate over some distance.

Having looked at the alternatives and the motivation behind this work, in the following sections the proposed scheme will be outlined, with the concepts of modulation instability examined together with the mechanisms of continuum generation.

2.1 Modulation instability

In this section the aim is to discuss the origin of Modulation Instability (MI) and whether this effect could be used to “re-create” the Ti:S in terms of an ultrafast laser

source which could be used for pumping nonlinear processes, e.g. OPOs. The block diagram of the scheme is shown in Figure 2.1.

Figure 2.1: Block diagram showing the key components of the hypothetical ultrafast MI system

The pump laser would ideally be a continuous wave source, but for the purposes of the investigation, experimental work was postulated for an off-the-shelf, 1064nm, Q-Switched laser.

As mentioned, the original awareness of the MI effect within the BAE Systems originated from work carried out using microstructured fibres [2.1]; however the MI effect has far deeper roots than this. MI creates a train of optical solitons and the two are usually discussed in parallel. Soliton generation in fibre results from modulation instability, this is a consequence of pumping a fibre in its anomalous dispersion regime or broadening from normally pumping a fibre spilling into the anomalous regime and becoming unstable. Modulation instability is the term used to describe an effect in which deviations from a periodic waveform are re-inforced by nonlinearity, not restricted to optical fibre. The recent resurgence of interest in this area is due to the flexibility in the design of microstructured fibre – careful design of dispersion and nonlinearity can result in endless propagation of solitons as they broaden [2.4].

The rest of this chapter proceeds as follows; MI will be derived numerically from the nonlinear Schrodinger equation, before going on to discuss specific examples where pulsed outputs have been generated that are of interest to our application.

2.1.1 The Origin of Modulation Instability

Numerically, Modulation Instability can be derived from the Nonlinear Schrödinger Equation (NLSE) [2.4]

$$i\frac{\delta A}{\delta z}+\frac{i\alpha}{2}A-\frac{\beta_2}{2}\frac{\delta^2 A}{\delta T^2}+\gamma|A|^2A=0 \tag{2.1}$$

Where A is the amplitude of the phase envelope, β_2 is the nonlinear dispersion co-efficient, $\gamma=\frac{n_2\omega_0}{cA_{eff}}$ (nonlinear parameter) T is time and α is loss (= 0 for NLSE, but shown here for completeness). This can be solved to obtain a steady state solution:

$$\overline{A}=\sqrt{P_o}\exp\left(i\phi_{NL}\right) \tag{2.2}$$

Which is perturbed such that:

$$\overline{A}=\left(\sqrt{P_o}+a\right)\exp\left(i\phi_{NL}\right) \tag{2.3}$$

Where P_o is incident power, $\phi_{NL}=\gamma P_o z$ is the nonlinear phase shift induced by self-phase modulation and "a" is the perturbation.

Substituting equation 2.3 into equation 2.1 (and linearizing in "a") the solution should be considered in the following form:

$$a(z,T)=a_1\exp[i(Kz-\Omega T)]+a_2\exp[i(Kz-\Omega T)] \tag{2.4}$$

Where K and Ω are the wavenumber and frequency of the perturbation respectively; this set of equations has a nontrivial solution only when K and Ω satisfy the following dispersion relation:

$$K=\pm\frac{1}{2}|\beta_2\Omega|\sqrt{[\Omega^2+sgn(\beta_2)\Omega_c^2]} \tag{2.5}$$

Where Ω_c is the central frequency of the perturbation and is given by;

$$\Omega_c^2=\frac{4\gamma P_o}{|\beta_2|}=\frac{4}{|\beta_2|L_{NL}} \tag{2.6}$$

In the time domain, this corresponds to a period of: $T_m = \frac{2\pi}{\Omega_c}$

It is seen from equation 2.5 that the dispersion relation has square root dependence, thus there is a point of instability around the modulation frequency. If the fibre is pumped in the normal regime ($\beta_2 > 0$), the solution is real and the system is stable against perturbation, however if the system is pumped in the anomalous regime ($\beta_2 < 0$) it will be imaginary and the perturbation grows exponentially with distance propagated through the fibre [2.5].

There are length metrics which take into account the dispersion and nonlinearity of a fibre which can be used to deduce the length of fibre over which a certain effect is important for pulse evolution.

$$L_D = \frac{T_o^2}{|\beta_2|} \tag{2.7}$$

$$L_{NL} = \frac{1}{\gamma P_o} \tag{2.8}$$

Where T_o is the initial width of a pulse, P_o is the peak power of the incident pulse and the other symbols hold their usual meaning. If $L_D << L_{NL}$, then dispersion effects dominate and conversely if $L_D >> L_{NL}$, then nonlinear effects dominate. These metrics are useful both in applications where nonlinearity needs to be minimised, for example, fibre communications, and cases where the nonlinearity is to be exploited, as is the case for continuum generation.

Considerations with this approach in relation to defence applications include the required power per pulse. Optimising the fibre for use with higher pump pulses will require careful design of the fibre parameters to get the desired effect. If N is the soliton number, and N = 1 is the fundamental soliton (which undergoes no transformation over the length of fibre), then

$$N^2 = \frac{L_D}{L_{NL}} = \frac{\gamma P_o T_o^2}{|\beta_2|} \tag{2.9}$$

from which $P_o = \frac{|\beta_2|}{\gamma T_o^2}$.

If N > 1 and the fibre is perfect, the soliton will periodically contract and split into a number of distinct pulses before merging again to recover its original shape [2.4]. The higher order solitons are best avoided in the context of pulsed operation, however it will be seen later in the chapter that they are key to continuum generation. From equation 2.9, by substituting N = 1 for the fundamental soliton, it can be seen that there is an inverse relationship between pulse length and the power in the generated soliton.

2.1.2 Examples of Pulse Trains generated via Modulation Instability

Generating a controlled soliton train from a single laser input is not possible. From a single CW input, the process would be driven by noise and solitons would be created with no fixed relationship to each other. The most effective way of generating a train of pulses with fixed repetition rate is via the beating of two sources to achieve a pulse train which has the repetition rate equal to the frequency difference between the two sources. For example, Greer *et al* [2.6] (1989) demonstrated 130 fs pulses at 2 THz on a picosecond envelope by beating 1.319 μm and 1.307μm sources (schematic shown in Figure 2. below).

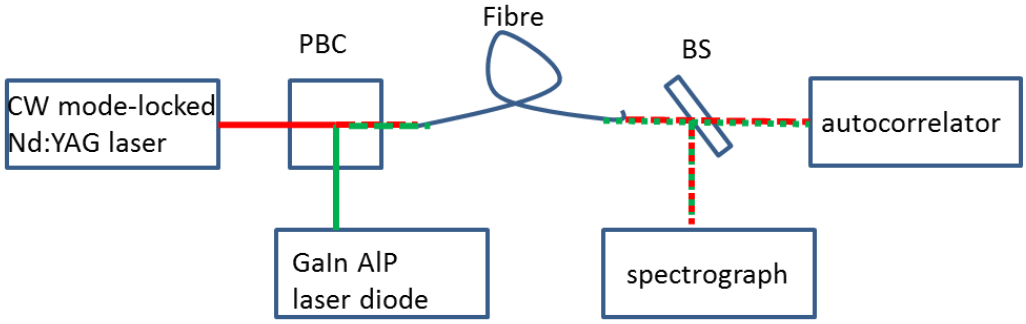

Figure 2.2: Replicated from Greer [2.6] (1989). The Nd:YAG and diode fields are coupled together via the polarising beam cube (PBC) and focussed into the fibre by a microscope objective. Following the fibre, the light is re-collimated using a matching microscope objective and split by the beamsplitter (BS) into the diagnostics.

By beating CW fields, researchers have used the ability to tailor the dispersion of novel fibres to chirp and subsequently compress pulses. Researchers from the Institut Carnot de Bourgogne in France have demonstrated the use of multiple fibres in series to engineer the repetition rate and pulse duration of the output [2.7],[2.8] and [2.9] (see Figure 2.3). Most recently Fortier *et al* (2008) [2.9] generated 380fs pulses with a repetition rate of 160GHz and average powers of up to 400mW. This was achieved

using 3 different lengths of fibre to engineer a beat signal into well separated Gaussian-like pulses (using Non-Zero Dispersion Shifted Fibre (NZ-DSF)), create linearly chirped pulses (using Highly Non-Linear Fibre (HNLF)) and temporally compress the pulses (SMF-28) – this is shown schematically in Figure 2.3 with the stages denoted as F1, F2 and F3 respectively.

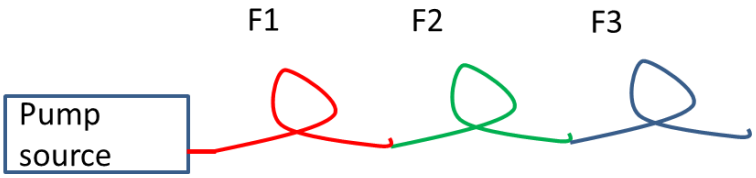

Figure 2.3 : Schematic of cascading fibre lengths to tailor pulse characteristics. The fibres could be spliced together or free-space coupled

Also in the realm of ultrafast sources based on dual frequency beating Mamyshev *et al* [2.10] in 1991 demonstrated 490fs pulses at 200GHz, whilst Chernikov *et al* [2.11] in 1993 demonstrated 250fs solitons at 113GHz, both using dispersion decreasing fibres in which the dispersion is reduced along the fibre length by tapering the core. By using such a fibre, the compressive effect is enhanced and at the very minimum the condition for fundamental soliton propagation is maintained. In the earlier analysis, loss terms were ignored however if these were included the solitons generated would disperse over the length of the fibre. This can be understood qualitatively by considering Equation 2.9; if loss is included in that expression causing the peak power to reduce exponentially over the fibre length, the fundamental soliton (N = 1) can be maintained if the dispersion were to reduce exponentially along the fibre.

The wavelengths over which the previous work has been demonstrated corresponds to wavelengths popular in telecommunications (~1300nm or 1550nm), although it is hoped that through fibre design they could be tailored where necessary to more appropriate wavelengths for any countermeasure application in the infrared (3 - 5μm).

2.1.3 Conclusion

After an initial statement that it is not possible to create a train of controlled pulses from a single laser source, the compromise of multiple lasers and cascaded fibres gives a range of interesting solutions which could be useful for some applications, however the initial interest was in using this technique to simplify an ultrafast laser and generally the methods described in this chapter so far would not be suitable. In conclusion, there have been demonstrations of ultrafast pulses from all-fibre systems however the powers

achieved in the literature are of the order of milliWatts, rather than the several Watts required for the application. The wavelengths described in the literature (~1300nm) would have to be displaced either further into the IR (3 – 5μm) or closer to 1μm where the output could be used as a source for frequency conversion using, for example, an OPO. In order to extract gain from an ultrafast OPO, the path length of the OPO has to match the repetition rate of the pump laser therefore the high repetition rates achieved with MI would lead to ultra-compact synchronously pumped OPOs. Although perhaps extreme, a 160GHz repetition rate for example would correspond to a cavity length of 1.9mm which practically could be a nonlinear crystal with HR coatings on each face. The higher repetition rates achievable with this technique rival the highest repetition rates from mode locked lasers such as the 1GHz (cavity length ~150cm) achieved by Schratweiser *et al* [2.12]. To the best of the author's knowledge there have been no demonstrations of nonlinear conversion of the output from such sources.

2.2 Tailoring continuum generation for high spectral power density in restricted wavelength regions

Having discussed the implications of MI as a method for generating ultrafast pulses in isolation, we will now apply MI and soliton theory (as well as other nonlinear effects) in the context of continuum generation. Significant effort in this field has gone into understanding the mechanisms behind supercontinuum generation, but the variables we are interested in here are that of increasing spectral power density and defining that wavelength region.

This section will start by discussing why microstructured fibres are significant in this context before briefly describing the effects that are important in continuum generation and then moving on to highlight specific examples from the literature which show promise for high spectral density and wavelength selection.

2.2.1 Summary of Supercontinuum Generation in Microstructured Fibre

Optical fibre has provided one of the most significant and widely used means of communication since its first use in the 1970s, with continuing research in terms of loss reduction and maximising bandwidth. Standard optical fibre is limited in use to wavelengths around 800 nm and 1550 nm due to residual water absorption in the material and the choice of materials used. Microstructured fibres use holes in the cladding layer to create guiding effects. Such fibres may have a hollow core in which case guiding is normally via a photonic bandgap effect. If a solid core, it is possible to

guide light via total internal reflection, with the average refractive index of the cladding reduced due to the holes. The hollow-core photonic bandgap fibre has potential applications in the delivery of high powers and was the subject of a thesis completed at BAE Systems (Filton) [2.1].

The small diameter core (~3.4 μm [2.29]) which can be achieved in some designs of microstructured fibres means that higher intensities can be generated and nonlinear effects can be more readily harnessed. This has mostly been exploited to create a supercontinuum which can be used in a number of applications including coherence tomography [2.13], flow cytometry [2.14] and measurement of carrier-envelope offset in frequency combs [2.15] to name but a few. The recent resurgence of the field of supercontinuum generation was sparked by Knight *et al* and the group at the Optoelectronics Research Centre in Southampton with the first demonstration of Photonic Crystal Fibres (or microstructured fibre as we are referring to it here) [2.16] and then by Ranka [2.17] in 2000, where the first supercontinuum was demonstrated which spanned more than an octave. A number of significant developments have been made by the group at the University of Bath who demonstrated endlessly single mode fibre from 337 – 1550nm [2.18] as well as numerous advances in mid-IR guidance [2.19], mid-IR fibre lasers [2.20] and gas detection [2.21] in hollow core fibre. Another main driver in the development of microstructured fibre is in creating ultra-low loss fibres in the telecom regions which could potentially result in significant commercial gains, for example, the Corning fibre SMF-28 has a 1.7dB/km loss at 1550nm [2.22] where an analysis showed that the ultimate low loss limit in PCF is 0.1dB/km [2.23] although the lowest loss achieved to date has been 0.48dB/km [2.24].

Having highlighted some of the range of applications where microstructured fibres have been exploited, the basic characteristics of solid core microstructured fibre and their relevance to continuum generation will be outlined before going on to discuss the possibility of increasing spectral power density over a narrow wavelength region.

2.2.2 Contributions to SCG

Solid core microstructured fibre, like standard optical fibre, has an anomalous and normal dispersion regime. One key feature of this fibre is that the fabrication process allows a greater level of control over the wavelength of the zero dispersion point, and the shape of the dispersion curve. This is achieved by varying the material from which

the fibre is drawn, the size of the central defect, and the pitch (Λ) and size (d) of the air holes in the cladding (as illustrated in Figure 2.4). The characteristics of the dispersion curve play a critical part in the evolution of the continuum, and will be discussed further in this section.

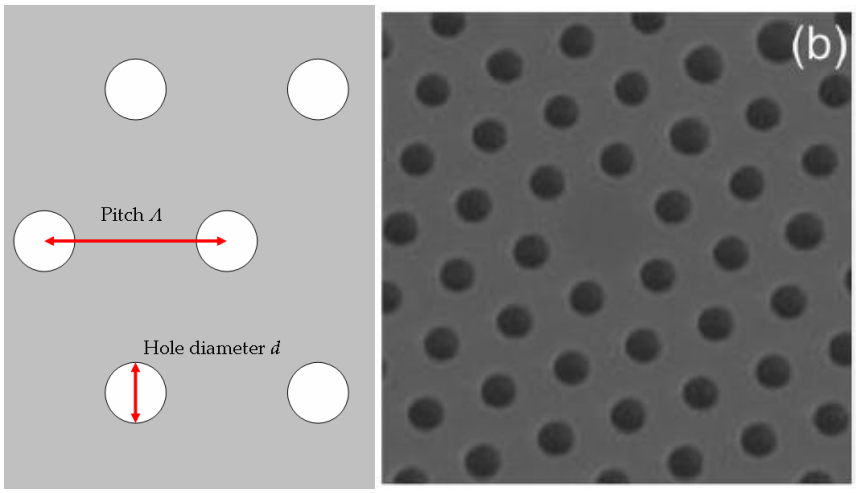

Figure 2.4 : Definitions of physical parameters in solid core microstructured fibre; (b) Scanning Electron microscope image of solid core microstructured fibre [2.27]

To further the investigation in the realms of supercontinuum generation, the case of a silica (solid core) microstructured fibre will be examined. This type of fibre is fabricated to have an array of nominally identical holes with a central defect (no hole) in which the light is guided, the following table shows general trends in how the zero dispersion point changes with the pitch/hole diameter ratio, and laterally how it is affected by the size of the central defect. There are, of course, limitations to these generalisations and these will also be stated.

Table 2.1: General trends in dispersion tailoring

Constant fibre parameter	Variable fibre parameter	Movement of ZDP
d/Λ	core diameter reduced	Moves to shorter wavelengths
Core diamater	d/Λ reduced	Moves to longer wavelengths

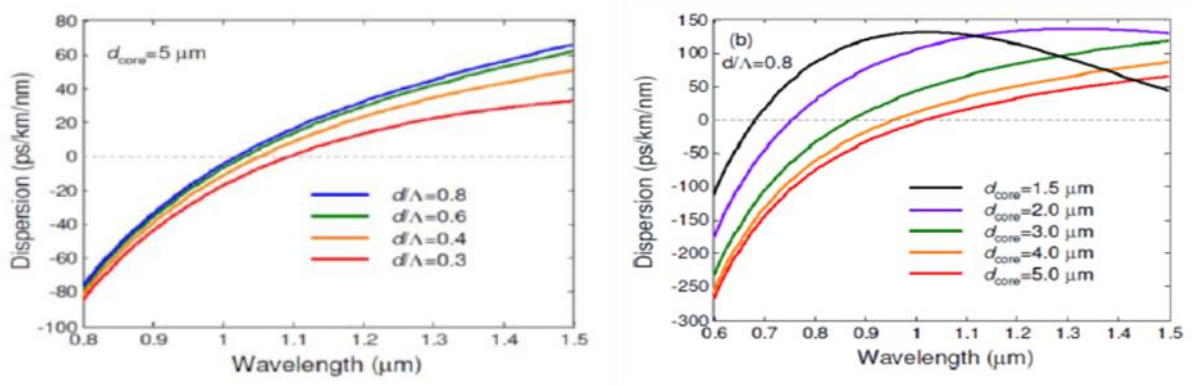

Figure 2.5 : Simulation results extracted from Kumar [2.25] (2013) showing the extent of tailoring achievable by varying d/Λ (left) and the fibre core diameter (right)

There is a limit to the extent to which these trends can be pursued, once d / Λ is small (e.g. 0.4), and if the core is already small (e.g. 3μm), then the zero dispersion point cannot be moved any further. From this point, if further reduction is required then d / Λ must be increased in order for the core diameter to be reduced [2.25]. This is indicative of the trade-off between material (manipulation of the core size) and waveguide dispersion (affected by the pitch/hole spacing) which have to be considered jointly. For supercontinuum generation a small core size is essential for maximising nonlinearity, so d / Λ will be large [2.26].

In addition to modifying the structure in its entirety as described above, d / Λ could be varied radially, with smaller holes closer to the core to affect the dispersion and larger holes further from the core to ensure that the mode field area is kept small, or the holes filled with some liquid to further tune the refractive index profile of the material [2.39]. In the normal regime, dispersive effects such as self-phase modulation are dominant and MI will only occur when/if the continuum is red-shifted beyond the zero dispersion point into the anomalous regime.

When pumped in the anomalous dispersion regime, the incident pulses will undergo a combination of temporal break-up via MI (as discussed in the previous section) and subsequently chromatic spreading. There are a number of nonlinear effects which contribute to continuum evolution including; Raman-induced energy exchange, four wave mixing, soliton self-shifting, cross wave modulation and self-phase modulation [2.27]. The contribution of each of these effects to the resulting output is dependent on the pump conditions. Following the temporal splitting of the input field, if the soliton bandwidth is sufficiently large (or the pulse sufficiently short), the short wavelength

edge can pump the long wavelength edge resulting in soliton self-frequency shift [2.4]. It is common in spectra generated by pumping in the anomalous regime to see pump side lobes which are indicative of solitons being generated at the Stokes and anti-Stokes wavelengths, this is illustrated in Figure 2.6) for a microstructured fibre pumped with a Q-switched, frequency doubled laser at 532nm with pulse duration of 0.8 ns (peak powers as indicated in the figure).

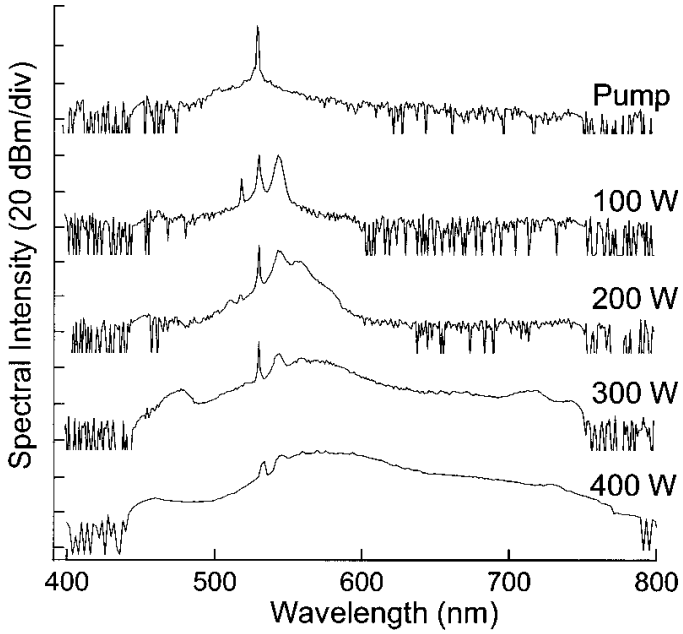

Figure 2.6 : Spectra of anomalous pumping of microstructured fibre over a range of pump powers [2.28]

In addition, Figure shows the effect of increasing pump power on the extent of the continuum. The correlation between the extent of the continuum and the input power is consistent across all pumping regimes, in each case the spectral power density may increase, but the primary effect is in broadening the spectrum.

If we examine the trade-off between nonlinearity and dispersion, extending into the visible region (with a 1 micron pump laser) can be most readily achieved by pumping close to the zero dispersion point to encourage coupling of dispersive waves into the normal region, whereas for extension further into the IR it is important to prolong the interaction between the generated solitons which happens where the dispersion to nonlinearity ratio is roughly constant with respect to wavelength [2.29].

As mentioned, one of the key features of microstructured fibre which enables continuum generation is the ability to generate high fields in the small core to harness nonlinear effects. In order to do this high incident powers are required which were

traditionally only achievable using mode-locked lasers. With the advances made in fibre lasers in recent years there have been a number of results using a continuous input which results in smoother spectra with increased flatness [2.29], [2.30], [2.31]. In the case of a CW input the field is fragmented temporally due to MI which then goes on to broaden the spectrum in a similar way to short pulse pumping where smoothness is attributed to the nature of un-seeded MI, as the solitons which are produced have variable duration, peak power and repetition rate.

2.2.3 Examples of Supercontinuum Generation in Microstructured Fibre

Having described some of the key contributing effects to continuum generation, this section will highlight a number of examples of how pump source and fibre engineering can be used to tailor the extent of the continuum. The majority of research in this field is directed at maximising the spectral width, whereas for countermeasure applications it is more advantageous to have a narrower spectral width with increased power density. However, by understanding how the continuum evolves in its various schemes, an appropriate configuration for narrower bandwidth with higher spectral power density may be obtained. In the following discussion, the fibres considered are limited to silica since they are the most mature in this young field and are not as environmentally sensitive as special mid-IR fibres such as fluoride or ZBLAN.

In addition to using a single length of fibre to create an effect, there are examples where a number of fibre lengths have been cascaded to generate a broader continuum than a single length. Kutz *et al* used two lengths of fibre with different dispersion characteristics to engineer a CW input to exploit the effects of MI in high dispersion fibres before using a low dispersion fibre to enhance the continua further via Raman effects [2.32]. Kudlinski *et al* [2.33] used a similar approach but used a dispersion decreasing fibre as the second length in order to extend the continuum into the visible region through dispersive wave trapping.

There have been a number of interesting examples of techniques implemented to both restrict the wavelength range and increase the spectral power density of generated continua. Cumberland *et al* [2.31] and Travers *et al* [2.29] in 2008 both demonstrated spectral power densities of 50mW/nm (flatness of ~10dB over 840nm) by using a CW beam which had been fibre amplified coupled into a fibre with two zero dispersion wavelengths. This spectral power density has since been improved upon by Song *et al*

[2.30] who achieved up to 70mW/nm exploiting all-normal dispersion in single mode fibre with greater than 12dB flatness over 640nm using a nanosecond MOPA configuration with two pre-amplifier stages.

Whilst using the same type of fibre, the increase in pump power used between [2.31] and [2.29] showed different broadening mechanisms at work. In [2.31] there was 50W pump available with a 20m length of fibre, and in [2.29] 170W of pump with a 17m length of fibre. By using 170W of pump power, dispersive waves in the normal dispersion regime are excited, resulting in much broader continua in the visible part of the spectrum, compared with the 50W pump. The high spectral power densities were maintained in both cases between 1.06 – 1.4 microns which is between the zero dispersion points (0.81 and 1.73 microns) This suggests that there is a limit to how much the spectral power density can be increased without extending the continuum. Mussot *et al* [2.34] details a theoretical study showing that the continuum is bound by the zero dispersion wavelengths of the fibre, increasing the spectral power density in that region. As the anomalous dispersion regime exists only between these points, there is no soliton self-frequency shifting beyond the second zero dispersion point so the broadening does not extend beyond the dispersive waves formed in the normal regime on either side.

2.2.4 Summary

To summarise, controlling both the spectral range and spectral power density of a continuum is not a trivial task. The spectral range can be controlled to an extent via tailoring of the zero dispersion point (if a fixed pump wavelength is assumed) such that the anomalous regime is restricted in width, or by pumping sufficiently far from this point that there is walk-off between the various contributing processes such that they are halted. Increasing spectral power density is simply achieved by using higher power pump lasers, however the increase in power will be spread across the continuum and will extend it further rather than solely drive up the spectral power density. This is not what is required for the countermeasure application.

The examples which have been discussed are in relation to SCG in the visible regime, whereas for countermeasures the interest lies in the infrared. Advances in SCG in the infrared have lagged behind those in the visible due to difficulty in manufacturing fibres with sufficient transmission and quality to exploit the mechanisms described here. A theoretical investigation was carried out in 2009 by Price *et al* [2.40] and a practical

demonstration of 7.1W between 1.9μm and 3.9μm by Yang *et al* [2.41]. This practical demonstration in 2013 is far from the spectral density achieved by Travers in the visible in 2008 with a far simpler design [2.28].

2.3 Conclusion

In this chapter the physics of modulation instability and supercontinuum generation have been discussed in relation to the design flexibility afforded by microstructured fibres. The initial aim of this investigation was to conclude as to whether the fibre technology discussed in this chapter could be used to create a countermeasure source capable of several Watts in the 3 – 5μm waveband over a spectral range of a ~100nm. To the best of the author's knowledge, at the time that this work was carried out (February 2009 – August 2009) there were no high power (5W < P < 10W) demonstrations of mid-IR supercontinuum generation leading to the belief that this is something that would require significant resource to develop within the project at that time.

Using fibre to generate ultrafast pulses has been demonstrated using multiple lengths of fibre with varying dispersion characteristics. This concept could be engineered for the wavelengths which are of interest in this area. However the time and effort required for creating reliable models and designing microstructured fibres is not something which would provide good value to the company for a stand-alone engineering doctorate project, unless there was access to the resources held by groups who have many years of experience in this field. Therefore, this chapter exists as a literature review of the methods used to create known pulse trains from fibre (section 2.1) and a review of the mechanisms and demonstrations of supercontinuum generation in the visible wavelength region using silica fibre. To progress the work in any meaningful way would require partnering with a university with expertise in this area.

The engineering of a narrow spectrum from the techniques afforded by continuum generation in microstructured fibre, however, is more ambitious. The main driver in using microstructured fibres is that when the various nonlinear effects interact under the correct conditions, a broad continuum is generated – attempting to reduce its extent would deviate from their design purpose. The powers that would be required and the wavelength ranges are not suitable for this avenue of exploitation. With this in mind, it

may be advantageous to look at non-microstructure alternatives for a more broadband laser-like source, for example, tapering a standard fibre to small core diameters will create a more limited continuum [2.35], and degenerate OPOs can span 10's of nanometres in the ~2 μm region using PPLN and recent demonstrations have shown extensive continua from 2.6 – 6.1 μm using ultrafast sources [2.36]. As stated above, anything involving the design, manufacture and reproducibility of special fibres is expensive both in terms of time and budget and there was insufficient business interest to commit the required resource.

Since the initial work on this project was undertaken, there have been significant advances in the area of mode locked fibre lasers which, in retrospect, would have taken this chapter in a completely different direction. One of the key issues with fibre lasers is the nonlinear broadening caused by high energy pulses in small core fibres which limits their feasibility in short pulse configurations despite favourable characteristics such as superior thermal conductivity and beam quality. Some mode-locked fibre lasers use large mode area fibres, enabled by advances in the area of microstructured fibre, followed by pulse compression techniques using bulk optics to compensate for nonlinear broadening, for example Tunnerman *et al* demonstrated pulse energies of 741nJ at 711fs (post-fibre compression from 13.75ps) [2.37]. Other examples include high pulse energies with pulse durations comparable to Q-switched lasers, such as Fedotov *et al* who demonstrated 4μJ pulses of 10ns duration in an all-fibre configuration [2.38] which are arrived at by compromising pulse duration for pulse energy.

Ultimately the decision to re-direct the overarching project stemmed from the withdrawal of funding to the Laser Coalition. The termination of the funding led to a re-evaluation of priorities within the company in the short term, and although the premise of the Engineering Doctorate scheme is to look at technologies which would be complementary to the activities on the roadmap of the company in which the EngD student is placed there was no funding in place to continue this work specifically. Additionally, the fibre technology described in this chapter is not the most efficient way of generating mid-IR appropriate for countermeasure applications, with mid-IR Optical Parametric Oscillators offering better options for power scalability.

2.4 References

[2.1] T. Delmonte, "Studies into the Potential Uses for Microstructured Fibres in Aerospace and Defence Applications," EngD Thesis, Heriot Watt University, 2008.

[2.2] A. Chong, J. Buckley, W. Renninger, and F. Wise, "Femtosecond fiber laser," vol. 14, no. 21, pp. 660–662, 2006.

[2.3] S. Lefrançois, K. Kieu, Y. Deng, J. D. Kafka, and F. W. Wise, "Scaling of dissipative soliton fiber lasers to megawatt peak powers by use of large-area photonic crystal fiber," *Optics letters*, vol. 35, no. 10, pp. 1569–1571, May 2010.

[2.4] Agrawal, *Nonlinear Fibre Optics*, 4th ed. Academic Press, 2007.

[2.5] P. K. Shukla and J. J. Rasmussen, "Modulational instability of short pulses in long optical fibers," *Optics letters*, vol. 11, no. 3, p. 171, Mar. 1986.

[2.6] E. Greer and D. Patrick, "Generation of 2 THz repetition rate pulse trains through induced modulational instability," *Electronics Letters*, vol. 25, no. 18, pp. 9–11, 1989.

[2.7] S. Pitois, C. Finot, J. Fatome, B. Sinardet, and G. Millot, "Generation of 20-GHz picosecond pulse trains in the normal and anomalous dispersion regimes of optical fibers," *Optics Communications*, vol. 260, no. 1, pp. 301–306, Apr. 2006.

[2.8] C. Finot, J. Fatome, S. Pitois, and G. Millot, "All-Fibered High-Quality Low Duty-Cycle 20-GHz and 40-GHz Picosecond Pulse Sources," *IEEE Photonics Technology Letters*, vol. 19, no. 21, pp. 1711–1713, Nov. 2007.

[2.9] C. Fortier, B. Kibler, J. Fatome, C. Finot, S. Pitois, and G. Millot, "All-fibered high-quality low duty-cycle 160-GHz femtosecond pulse source," *Laser Physics Letters*, vol. 5, no. 11, pp. 817–820, Nov. 2008.

[2.10] P. V. et. al. Mamyshev, "Generation of Fundamental Soliton Trains for Communication Lines," *IEEE Journal of Quantum Elecronics*, vol. 27, no. 10, pp.2347- 2355, 1991.

[2.11] S. Chernikov, "114 Gbit/s soliton train generation through Raman self • scattering of a dual frequency beat signal in dispersion decreasing optical fiber," *Applied Physics Letters* vol. 63, no. 3, p. 293, 1993.

[2.12] T. Schratwieser, "Highly efficient 1 GHz repetition-frequency femtosecond Yb3+: KY (WO4) 2 laser," *Optics letters*, vol. 37, no. 6, pp. 1133–1135, 2012.

[2.13] G. Humbert, W. Wadsworth, S. Leon-Saval, J. Knight, T. Birks, P. St J Russell, M. Lederer, D. Kopf, K. Wiesauer, E. Breuer, and D. Stifter, "Supercontinuum generation system for optical coherence tomography based on tapered photonic crystal fibre," *Optics express*, vol. 14, no. 4, pp. 1596–1603, Mar. 2006.

[2.14] W. G. Telford, F. V Subach, and V. V Verkhusha, “Supercontinuum white light lasers for flow cytometry,” *Cytometry. Part A : the journal of the International Society for Analytical Cytology*, vol. 75, no. 5, pp. 450–459, May 2009.

[2.15] B. Washburn, R. Fox, N. Newbury, J. Nicholson, K. Feder, P. Westbrook, and C. Jørgensen, “Fiber-laser-based frequency comb with a tunable repetition rate,” *Optics express*, vol. 12, no. 20, pp. 4999–5004, Oct. 2004.

[2.16] J. Knight and T. Birks, “All-silica single-mode optical fiber with photonic crystal cladding,” *Optics letters*, vol. 22, no. 7, pp. 484–485, Apr. 1996.

[2.17] J. K. Ranka, R. S. Windeler, and a J. Stentz, “Visible continuum generation in air-silica microstructure optical fibers with anomalous dispersion at 800 nm,” *Optics letters*, vol. 25, no. 1, pp. 25–27, Jan. 2000.

[2.18] T. A Birks, J. C. Knight, and P. S. Russell, “Endlessly single-mode photonic crystal fiber,” *Optics letters*, vol. 22, no. 13, pp. 961–963, Jul. 1997.

[2.19] F. Yu, “Low loss silica hollow core fibers for 3–4 micron spectral region,” *Optics Express*, vol. 20, no. 10, pp. 11153–11158, 2012.

[2.20] A. M. Jones, a V. V. Nampoothiri, A. Ratanavis, T. Fiedler, N. V Wheeler, F. Couny, R. Kadel, F. Benabid, B. R. Washburn, K. L. Corwin, and W. Rudolph, “Mid-infrared gas filled photonic crystal fiber laser based on population inversion,” *Optics express*, vol. 19, no. 3, pp. 2309–2316, Jan. 2011.

[2.21] L. W. Kornaszewski, N. Gayraud, J. M. Stone, W. N. Macpherson, a K. George, J. C. Knight, D. P. Hand, and D. T. Reid, “Mid-infrared methane detection in a photonic bandgap fiber using a broadband optical parametric oscillator,” *Optics express*, vol. 15, no. 18, pp. 11219–11224, Sep. 2007.

[2.22] Corning, “Corning SMF-28 Ultra Low Loss Optical Fibre,” *SMF-28 Data Sheet*, 2007. [Online]. Available: http://www.corning.com/docs/opticalfiber/pi1470.pdf. [Accessed: 08-Mar-2012].

[2.23] P. Roberts, F. Couny, H. Sabert, B. Mangan, D. Williams, L. Farr, M. Mason, a Tomlinson, T. Birks, J. Knight, and P. St J Russell, “Ultimate low loss of hollow-core photonic crystal fibres,” *Optics express*, vol. 13, no. 1, pp. 236–244, Jan. 2005.

[2.24] M. Nielsen, C. Jacobsen, N. Mortensen, J. Folkenberg, and H. Simonsen, “Low-loss photonic crystal fibers for transmission systems and their dispersion properties,” *Optics express*, vol. 12, no. 7, pp. 1372–1376, Apr. 2004.

[2.25] G. Kumar and R. Gupta, “Dispersion modelling of micro structured optical fibres for telecommunications deployment,” *Science Technology & Management forAISECT University*, Vol.2, Issue 3, March 2013, ISSN 2778-4187.

[2.26] F. Poli and A. Cucinotta, “Tailoring of flattened dispersion in highly nonlinear photonic crystal fibers,” *Photonics Technology Letters, IEEE*, vol. 16, no. 4, pp. 1065–1067, 2004.

[2.27] P. S. J. Russell, “Photonic-Crystal Fibers,” *Journal of Lightwave Technology*, vol. 24, no. 12, pp. 4729–4749, Dec. 2006.

[2.28] J. M. Dudley, L. Provino, N. Grossard, R. S. Windeler, and B. J. Eggleton, “Supercontinuum generation in air – silica microstructured fibers with nanosecond and femtosecond pulse pumping,” *America*, vol. 19, no. 4, pp. 765–771, 2002.

[2.29] J. C. Travers, A B. Rulkov, B. A Cumberland, S. V Popov, and J. R. Taylor, “Visible supercontinuum generation in photonic crystal fibers with a 400 W continuous wave fiber laser,” *Optics express*, vol. 16, no. 19, pp. 14435–14447, Sep. 2008.

[2.30] R. Song, J. Hou, S. Chen, W. Yang, and Q. Lu, “High power supercontinuum generation in a nonlinear ytterbium-doped fiber amplifier.,” *Optics letters*, vol. 37, no. 9, pp. 1529–1531, May 2012.

[2.31] B. A. Cumberland, J. C. Travers, S. V Popov, and J. R. Taylor, “29 W High power CW supercontinuum source,” *Optics express*, vol. 16, no. 8, pp. 5954–5962, Apr. 2008.

[2.32] J. Kutz, “Enhanced supercontinuum generation through dispersion-management,” *Optics Express*, vol. 13, no. 11, pp. 3989–3998, 2005.

[2.33] A. Kudlinski and A. Mussot, “Visible cw-pumped supercontinuum,” *Optics letters*, vol. 33, no. 20, pp. 2407–2409, Oct. 2008.

[2.34] A. Mussot, M. Beaugeois, M. Bouazaoui, and T. Sylvestre, “Tailoring CW supercontinuum generation in microstructured fibers with two-zero dispersion wavelengths,” *Optics express*, vol. 15, no. 18, pp. 11553–11563, Sep. 2007.

[2.35] T. A Birks, W. J. Wadsworth, and P. S. Russell, “Supercontinuum generation in tapered fibers,” *Optics letters*, vol. 25, no. 19, pp. 1415–1417, Oct. 2000.

[2.36] N. Leindecker and A. Marandi, “Octave-spanning ultrafast OPO with 2.6-6.1 μm instantaneous bandwidth pumped by femtosecond Tm-fiber laser,” *Optics express*, vol. 20, no. 7, pp. 7046-7053, March 2012.

[2.37] B. Ortaç, M. Baumgartl, J. Limpert, and A. Tünnermann, “Approaching microjoule-level pulse energy with mode-locked femtosecond fiber lasers.,” *Optics letters*, vol. 34, no. 10, pp. 1585–1587, May 2009.

[2.38] S. M. Kobtsev, S. V. Kukarin, S. V. Smirnov, and Y. S. Fedotov, “High-energy mode-locked all-fiber laser with ultralong resonator,” *Laser Physics*, vol. 20, no. 2, pp. 351–356, Feb. 2010.

[2.39] K. M. Gundu, M. Kolesik, J. V. Moloney, K. S. Lee "Ultra-flattened-dispersion selectievly liquid-filled photonic crystal fibres" *Optics Express*, vol. 14, no. 15, pp. 6870 - 6878, 2006

[2.40] J. H. V. Price, T. M. Monro, H. Ebendorff-Heidepriem, F. Poletti, P. Horak, V. Finazzi, J. Y. Y. Leong, P. Petropolous, J. C. Flanagan, G. Brambilla, X. Feng and D. J. Richardson, "Mid-IR Supercontinuum generation from nonsilica microstructured optical fibres" *IEEE Journal of Quantum Electronics*, vol. 13, no. 3, pp. 738 - 749, June 2009

[2.41] W. Yang, B. Zhang, K. Yin, X. Zhou and J. Hou, "High power all fibre mid-IR supercontnuum generation in a ZBLAN fibre pumped by a 2 μm MOPA system" *Optics Express*, vol. 2, no. 7, pp. 19732 - 19742, 2013

3. Mid-IR OPOs

Having concluded in Chapter 2 that fibre best continuum generation is not best suited to countermeasure applications; this chapter evaluates the suitability of more established OPO technology. This chapter explores the use of a degenerate PPLN OPO as a tool for the characterisation and pumping of ZGP or other mid-IR nonlinear materials which generate radiation above 8μm (where the atmospheric transmission is high – refer back to Figure 1.2). These materials cannot be directly pumped at 1064nm facilitating the requirement for the PPLN OPO. The need for line-narrowing is recognised and concludes with a demonstration of a degenerate OPO, line narrowed using an intracavity diffraction grating, which was then used to characterise a crystal of Zinc Germanium Phosphide (ZGP) over 200nm in the region of degeneracy.

3.1 Sources for the mid-IR

The attraction of the OPO is that it offers an effective way of accessing three wavelengths, two of which are tuneable, from the same laser with minimal additions. The BAE Systems Advanced Technology Centre, at which the EngD was based, specialises in using pulsed (Q-Switched and mode-locked), 1 μm pump sources with OPOs and up-conversion devices based on Periodically Poled Lithium Niobate (PPLN) for applications including infrared countermeasures and laser dazzle [3.1]. Down conversion in PPLN has been demonstrated up to 7.3 μm [3.2] (albeit at low power – 0.04mW at 7.25μm) which for some applications, such as spectroscopy in contrast to infrared countermeasures, may be adequate however it would be more useful to be able to access wavelengths beyond this. The further into the infrared that can be probed (out to e.g. 12μm), the more spectral details can be resolved making a more sensitive device for identifying different molecular fingerprints. As shown in Figure 3.1 there is a gap in the availability of conventional, direct-emission laser sources in the electromagnetic spectrum between 2 – 5 μm which is served by PPLN-based OPOs, whereas at longer wavelengths Quantum Cascade Lasers (QCLs) come into prominence.

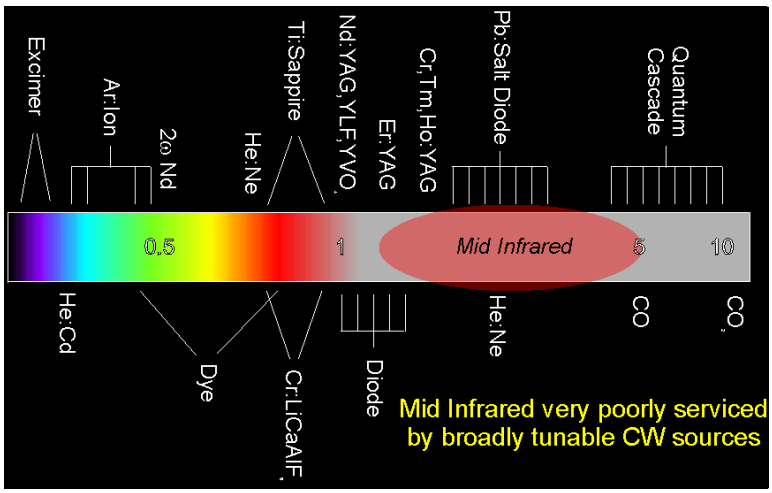

Figure 3.1: Conventional laser sources available across the electromagnetic spectrum

QCLs have developed rapidly since the early demonstrations which required cryogenic temperatures to supress thermal excitations within the sub-bands. Currently, powers of greater than 1W have been obtained at room temperature, with resolution down to <30MHz and a maximum tuning range of 430cm^{-1} [3.3]. It should be noted however that the best performance of QCLs in terms of power generated and overall efficiency have been obtained at temperatures far below room temperature.

Table 3.1 (below) compares the 3 nonlinear materials which will be discussed in this chapter.

	PPLN	ZGP	OP-GaAs
Nonlinearity (d_{eff} (pm/V))	14	72	90
Refractive Index (at the pump wavelength)	2.18	3.14	3.36
Transparency (nm)	400 – 4000 [3.46]	2000 – 8000 [3.41]	900 – 17000 [3.42]
Pump Wavelength (μm)	1.064	>2	1.9

Table 3.1: Summary of the key optical properties of the nonlinear materials discussed – PPLN, ZGP and OP-GaAs

The field of nonlinear optics is well described in number of texts and will be summarised here. Some materials have a nonlinear response to intense electric fields resulting in the transfer of energy from the original pump wavelength into a different

wavelength depending on the configuration of the nonlinear material – in this case we are concerned with down conversion of the pump wavelength into two lower energy fields. In order to capitalise on this interaction the material has to be phase matched, to ensure that the generated field sees gain along the length of the material. For the materials described in Table 3.1 the phase matching is either via poling/patterning of the structure (for PPLN/OP-GaAs) or through exploiting the natural birefringence of the material (ZGP).

For the case of birefringent materials, phase matching is achieved along the optic axis (where the o-ray and the e-ray are collinear) – illustrated in Figure 3.2. With respect to the crystal geometry, the exact angle (relative to crystal axes) for which this occurs varies depending on the wavelengths which are to be matched (this is discussed specifically for ZGP in Section 3.3).

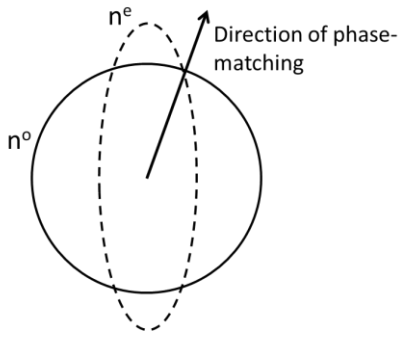

Figure 3.2: Optical indicatrix showing the phase matching direction for a positive uniaxial crystal

Quasi phase matching is obtained by reversing the sign of the nonlinear co-efficient after each coherence length (which varies according to the wavelengths which are to be generated ($l = \frac{1}{\Delta k}$ $where\ \Delta k = k_s + k_i - k_p$ $and\ k_n = \frac{2\pi n_n}{\lambda_n}$), to ensure that nonlinear gain is seen along the length of the crystal (illustrated in Figure 3.3 below) [3.47].

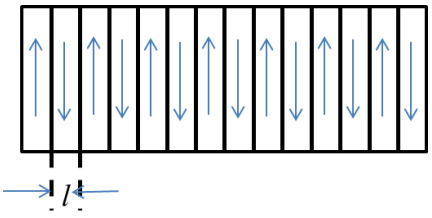

Figure 3.3: Illustration of the periodic structure of quasi phase matched material highlighting the coherence length

There are few materials commercially available for generating output beyond 5 μm where PPLN becomes increasingly absorbing with ZGP being the choice for this next section of work. The lower limit of transparency in ZGP is often quoted as 0.74 μm however there is still significant absorption below ~2.1 μm making shorter wavelengths impractical for practical devices. It is birefringently phase matched and requires a pump wavelength >1.9 μm due to material absorption. As the phase matching of the material is defined by its birefringence, a single crystal has a limited tuning range (angle, or temperature). Poled materials (e.g. PPLN) by contrast can be engineered to span a much wider range by, for example, having a fanned grating design. The first references to optical nonlinearity in Gallium Arsenide were in 1969 [3.4]. Despite its early promise as a nonlinear material, gallium arsenide cannot be poled in the same way as lithium niobate. A material can only be poled if it is ferroelectric. In the poling process, a large voltage is used to reverse the polarity of the material such that it is phase matched over the length of the crystal – Gallium Arsenide is not a ferroelectric material and therefore cannot undergo this process. In order to achieve phase matching in a length of Gallium Arsenide the phase matching domains have to be physically reversed, this was initially achieved by diffusion bonding – polishing, stacking and bonding thin layers of GaAs under pressure [3.38, 3.39]. This technique was of limited success for making samples which could be used for building an OPO due to significant losses at the interfaces due to surface roughness which would make the OPO threshold very high relative to the pump powers available at that time. More recently, it has been possible to realise a much lower loss domain reversed or 'orientation patterned' GaAs using methods developed for the microelectronics industry – Molecular Beam Epitaxy (MBE) or Hydride Vapour Phase Epitaxy (HVPE) [3.7].

OP-GaAs is transparent from 1.7 – 15 μm [3.42], much broader than the 2 – 8 μm [3.41] which is accessible from ZGP. In particular, this range allows direct pumping with a thulium laser, rather than having an additional frequency conversion stage to avoid ZGP absorption.

The equipment needed to manufacture devices with sufficiently low loss for practical purposes is expensive to purchase and maintain so collaborations were formed between parties with the relevant apparatus, namely Stanford and BAE Systems (Nashua, USA) for their MBE capability and AFRL/Thales for their GaAs HVPE capability. In 2002, collaborators from Stanford and Thales Research and Technology published the

nonlinear coefficient of OP-GaAs and demonstrated both difference frequency generation [3.5] and second harmonic generation [3.6] before the first demonstration of and OP-GaAs OPO in 2004 [3.7] following advances made in reducing the boundary losses using this new technique. BAE Systems, in 2009, constructed a GaAs HVPE growth facility to complement their existing MBE facility to further the development of OP-GaAs in a custom built reactor. This resulted in significantly lower losses which positioned BAE Systems as the provider of the lowest loss OP-GaAs devices with a loss of $<0.005 cm^{-1}$ reported in 2009 [3.8].

In summary, OP-GaAs is non-trivial to produce and not yet commercially available. Attempts were made to borrow some material from BAE Systems in the USA, however this endeavour was fraught with difficulty and did not result in any material for testing. Although a sample was obtained it could not be used due to ITAR (International Traffic in Arms) regulations. It became apparent in the autumn of 2010 that an alternative mid-IR crystal had to be sought for this project, and due to relative ease of procurement, ZGP was selected.

3.1.1 Comparing ZGP with OP-GaAs

Many of the standard advantages of poled material over birefringently phase matched material hold for ZGP and OP-GaAs. These include access to higher nonlinearities, longer interaction lengths (not always a good thing), tighter focussing and no walk-off. OP-GaAs samples are currently limited to a maximum thickness of 1mm, limiting power scaling. The challenge in growing thick samples is maintaining the integrity of the domain walls (and thus the efficiency of the phase matching), this is a process which can be refined with development work and essential in being able to increase the power handling of the OP-GaAs OPO. From a recent review of the literature, OP-GaAs research is currently directed towards expanding the nonlinear process with which OP-GaAs can be deployed, including frequency comb generation [3.9], widely tuneable difference frequency generation [3.10], terahertz wave generation [3.11] and supercontinuum generation [3.12].

The nonlinear figure of merit is used in order to compare materials, since a high refractive index reduces the efficiency of the conversion:

$$FOM = \frac{d_{eff}}{n^3} \tag{3.1}$$

Where d_{eff} is the effective nonlinear co-efficient of the material and n is its refractive index. The d_{eff} takes into account the nonlinear tensor components in addition to the phase matching conditions – for further details on how this is calculated the reader is referred to Chapter 5 of "Fundamentals of Optical Parametric Processes and Oscillators" (Tang and Cheng) [3.40]. For this, FOM_{ZGP} = 2.33 (n = 3.14, d_{eff} = 72) and $FOM_{OP\text{-}GaAs}$ = 2.37 (n = 3.36, d_{eff} = 90); so although the nonlinearity of GaAs is higher, its higher refractive index is a drawback. For comparison, FOM_{PPLN} = 1.78.

The availability of pump sources is also an important consideration in choosing a nonlinear material. The absorption in ZGP precludes direct pumping using mature sources, such as thulium fibre lasers, which are however suitable for OP-GaAs as the lower pumping limit is at 1.7 μm due to the onset of two photon absorption [3.13].

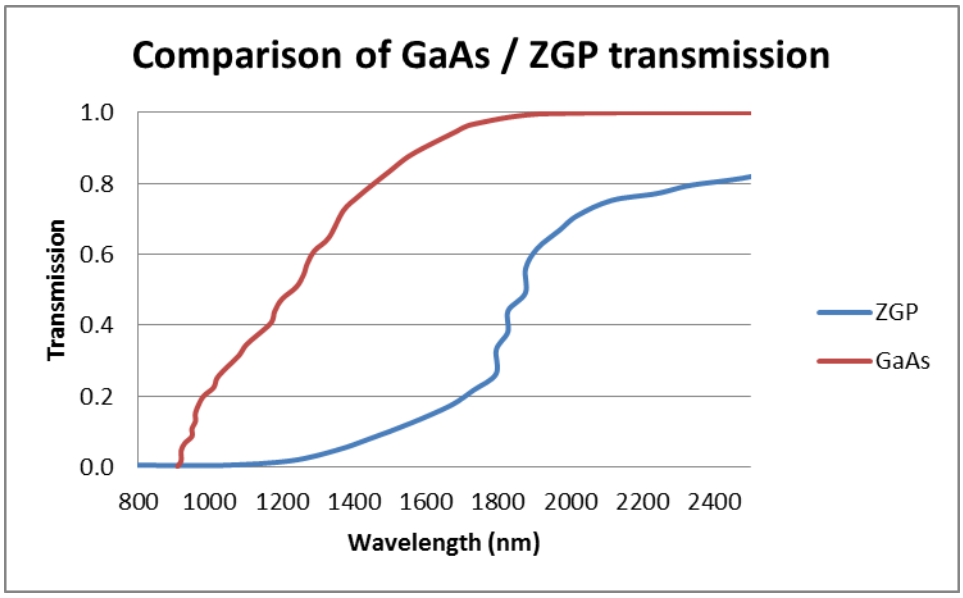

Figure 3.4: Comparison of transmission of Gallium Arsenide with ZGP (calculated from SNLO)

The higher thermal conductivity of OP-GaAs than ZGP (46W/mK [3.41] compared with 35W/mK [3.42] respectively) means that any thermal lensing which may be present is reduced which will be advantageous for power scaling. A thermal lens arises from a transverse refractive index change as a result of incident power on the material result. The varying nature of the lens strength with power could cause problems with

effective mode matching in the OPO. The acceptance linewidth of OP-GaAs is much smaller than that of ZGP [3.8], making the choice of pump source more critical to the efficiency of the OP-GaAs OPO – this will be modelled later in this chapter.

This chapter is focussed on mid IR generation between 2 – 6 μm aiming at multi-Watt average power levels. Although the levels achieved here do not meet this specification, the options for power scaling are considered and the redesign which would be required to make the work successful is specified. It should be noted that Dergashev [3.14] demonstrated a ZGP OPO which reached operational powers of 21W continuous wave and 37mJ pulses in a Q-Switched regime – this was using a fibre based pump system.

3.2 Pump source for OP-GaAs: the 2 μm degenerate PPLN OPO

The overall plan was to procure OP-GaAs and use it to demonstrate an OP-GaAs OPO in both the intra-cavity and extra-cavity configurations. Due to the lack of control with regards to the specifications of the material, the pump source had to be designed to be as flexible as possible – hence it was decided to build a PPLN OPO as a pump, although ultimately the plan was to use a VECSEL (with a centre wavelength of 2μm, power ~5W). PPLN is typically available commercially as a single crystal which has a number of poled regions of different grating periods, providing number of different phase matching solutions for a given pump source, with the additional option of temperature tuning. ZGP or OP-GaAs meanwhile are only available as crystals of specific phase matching design, be this the cut angle in the ZGP (to enable birefringent phase matching) or patterning period in OP-GaAs (quasi phase matching). It is for this reason that in the following sections the choice of pump source is an important consideration. In the Laser Coalition project, the ultimate aim was to realise a VECSEL pumped *intracavity* OPO based on OP-GaAs which extends the spectral coverage from that of PPLN, and the *extracavity* OP-GaAs OPO was supposed to be a stepping stone to this goal. The projected development goals, as defined at the start of the project, are shown in the flow diagram below:

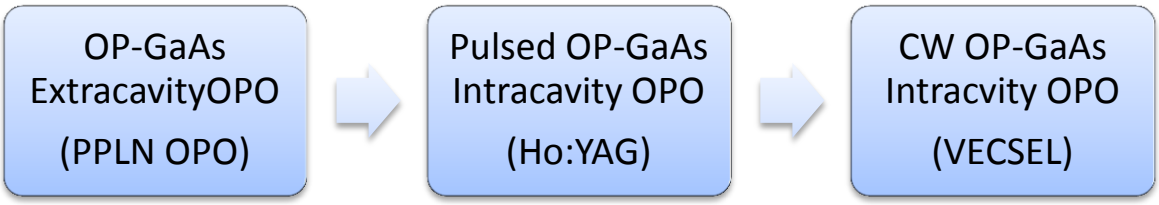

Figure 3.5: Flow diagram of original development work

The planned end result of this work was to realise a high power, stable, continuous wave, spectrally pure OP-GaAs OPO which extended the spectral coverage of PPLN. To complement the OPO development work there was a parallel project to investigate the power scalability of VECSELs (this met the same fate as the project described here).

A sample of OP-GaAs had been grown by Schunemann and it had been planned to make this available for this project. This sample had the following characteristics:

- 60.5 μm period
- 16.4 x 1.4 x 6mm dimensions
- AR coated at 2.1 μm and 3 – 5 μm

Such a sample would have the following OPO tuning curve as a function of pump wavelength at room temperature (using the Sellmeier coefficients obtained by Skauli [3.21]):

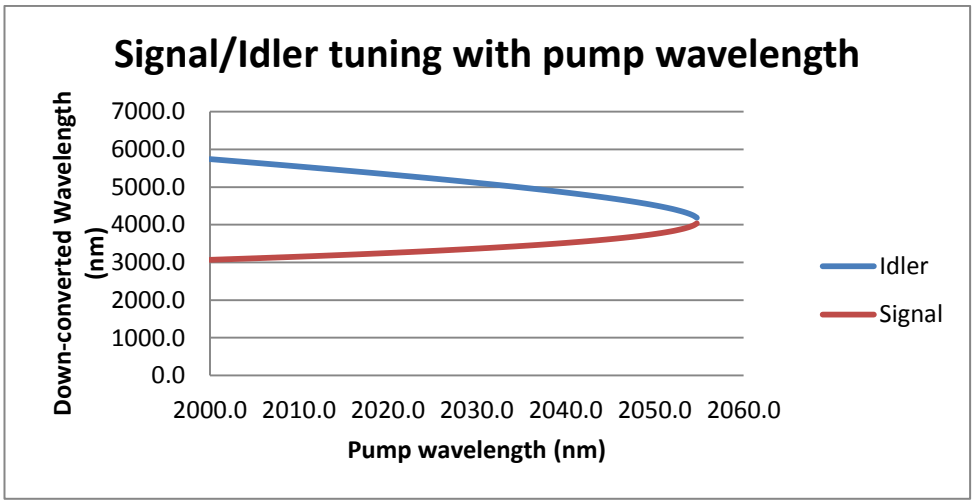

Figure 3.6: Pump tuning characteristics for OP-GaAs with a grating period of 60.5μm at room temperature (300K) (obtained using SNLO – [3.26])

This sample was grown for operation at 2.05 μm (and is assumed that the coating bandwidth was sufficiently broad to capture this under a specified 2.1 μm coating). The broad gain bandwidth which characterises VECSELs would comfortably allow a full investigation of this tuning range.

3.2.1 Linewidth Requirement for ZGP OPO

The linewidth of an OPO is defined by the crystal dispersion and the following relations allow the prediction of OPG threshold and the associated output linewidth of the PPLN OPO for a given set of pump, signal and idler wavelengths [3.15].

$$K\, I_{th} = \left[\frac{1}{2l}\ln\left(\frac{4\,\lambda s\, E_{th}}{h\, c}\right)\right]^2 \tag{3.2}$$

$$K = \frac{8\,\pi^2 d_{eff}^2}{\epsilon_o c\ \lambda_s \lambda_i\ n_s n_i n_p} \tag{3.3}$$

From the analysis detailed by Zayhowski [3.15], E_{th} is defined as the pump pulse energy, with a threshold defined as when the signal power reaches 1 μW, l is the crystal length, and the subscripts p, s and i represent the pump signal and idler waves. Applying this to the system designed here the single pass gain generated via Optical Parametric Amplification (OPA) should not be observed for pulses with an intensity less than 80MW/cm^2. The power density of the pulses is 19MW/cm^2, comfortably below the threshold for OPA, and the optical damage threshold of 100MW/cm^2 [3.46].

$$\left(P_{pk} = \frac{P_{avg}}{rep\ rate} = \frac{12}{30kHz} \approx 28kW\ ;A = \pi * (220 * 10^{-4})^2 = 1.52 * 10^{-3} cm^2\right)$$

The expression for the associated linewidth is shown below, where I_p is the pump intensity and Λ is the PPLN grating period.

$$\left|\left(\frac{np}{\lambda p} - \frac{ns}{\lambda s} - \frac{ni}{\lambda i} - \frac{1}{\Lambda}\right)^2 - \frac{K\ Ip}{\pi^2}\right| l^2 \leq 1 \tag{3.4}$$

This expression has been plotted (at degeneracy) against crystal length showing how the output linewidth increases with crystal length.

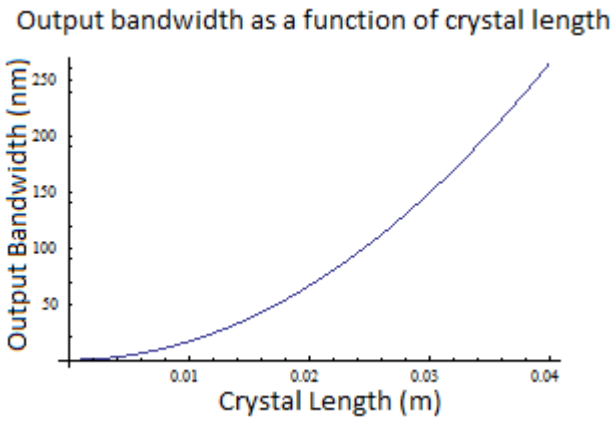

Figure 3.7: PPLN OPO output linewidth varying with crystal length

This is shown experimentally (Figure 3.8) by Perrett in his investigation into the application of line narrowing techniques with degenerate PPLN OPOs in order to pump ZGP [3.16].

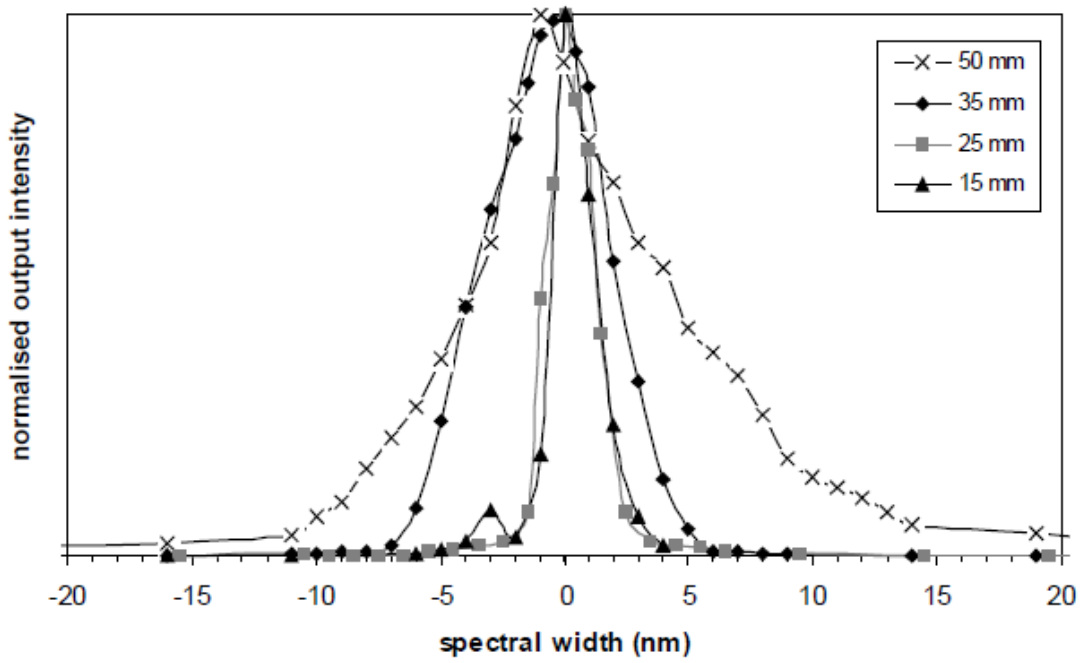

Figure 3.8: Dependence of spectral linewidth on PPLN crystal length for a grating narrowed degenerate PPLN OPO (Perrett [3.16]**)**

From Figure 3.8, a degenerate PPLN OPO can have a linewidth in excess of 100 nanometres which exceeds the linewidth which is required to pump a ZGP OPO. This

will be shown in the following analysis. The gain of an OPO depends on the phase mismatch of the interacting beams, which aims to be zero through phase matching. This is not exactly the case as the beams are focussed which introduces a non-zero Δk, so there is an associated bandwidth with the process. From the thesis of Britton [3.17], the pump acceptance bandwidth of an OPO (FWHM) is:

$$\Delta\lambda = \frac{4\pi\ 20.481}{l}\left(\frac{n_p}{\lambda_p^2} - \frac{n_s}{\lambda_s^2} - \frac{n_i}{\lambda_i^2} + \frac{1}{\lambda_p}\frac{dn_p}{d\lambda_p} - \frac{1}{\lambda_s}\frac{dn_s}{d\lambda_s} - \frac{1}{\lambda_i}\frac{dn_i}{d\lambda_i}\right) \qquad (3.5)$$

Where the factor of 20.481 originates analytically from the gain of the OPO with respect to the phase mismatch, *l* is the crystal length and the refractive indices (n) and their derivatives (dn/dλ) are obtained from the appropriate Sellmeier equations. Figure 3.9 shows the effect of increasing crystal length on the acceptance bandwidth of the ZGP OPO based on the Sellmeier equations developed by Zelmon (2001) [3.18] showing that for a 15 mm crystal of ZGP with signal and idler equal to 3.7 and 5 μm respectively, the acceptance bandwidth should be 6.77 nm. This is contrasted with the result from using the Ghosh 1998 [3.19] Sellmeier equations which suggest the acceptance bandwidth should be 5.6 nm. Such discrepancies between the anticipated acceptance bandwidth are common in the literature, with Henrikssson quoting a bandwidth of 5 nm.cm and Perrett, 7nm.cm, presumably due to the discrepancy in the Sellmeier co-efficients arising from the experimental method used to determine them. The Sellmeier equation is used to determine the refractive index of a material at a particular wavelength, the form of the equation is largely the same but the co-efficients used differ depending on the material. Generally, the refractive index of a material is measured over a range of wavelengths and the data points are fitted to a curve of the same form as the Sellmeier equation using a least squares fit [3.43]. As it is an experimental procedure there is always some amount of error associated with the measurement.

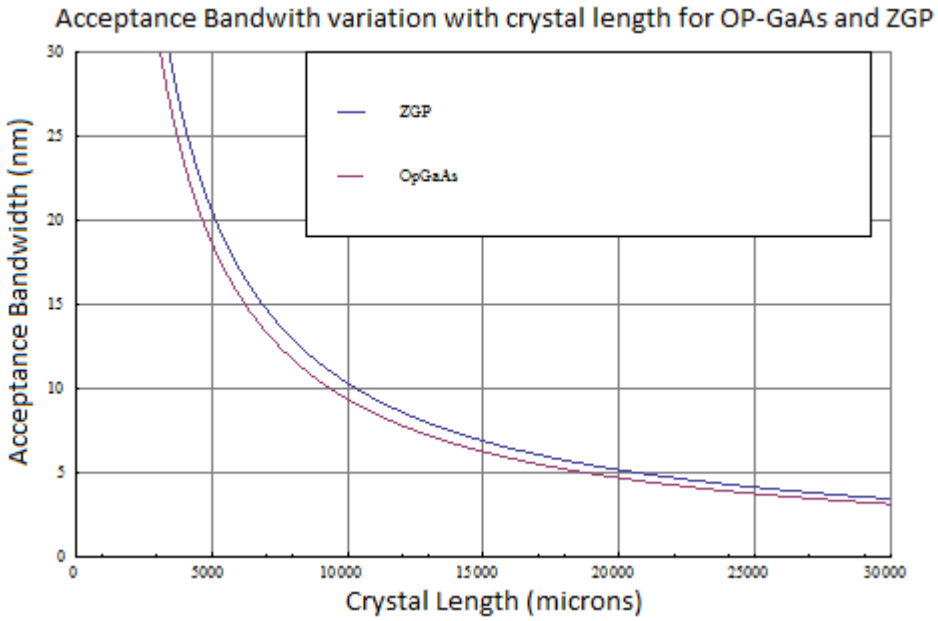

Figure 3.9: Modelled acceptance bandwidth for ZGP and OP-GaAs shown as crystal length increases using expressions from [3.21]

Henriksson *et al* [3.20] obtained an acceptance bandwidth of 4.2nm for a 24mm crystal of ZGP which is consistent with the model which has been employed above.

As mentioned above, a PPLN OPO at degeneracy has a wavelength span far in excess of the acceptance bandwidth of ZGP, thus requiring significant spectral line narrowing, typically achieved using etalons and diffraction gratings with alternative methods using volume Bragg gratings. The spectral acceptance bandwidth for OP-GaAs is also shown for comparison in Figure 3.9, using the result from [3.21] for calculating the refractive indices. In the absence of line narrowing, the incident power is distributed in a larger spectral range, with only the portion which is 'in-band' being available for nonlinear conversion.

3.2.2 Grating requirement for line-narrowing

Diffraction gratings are effective at line narrowing as they only retro-reflect light of a specific wavelength, the linewidth of which is defined by the grating characteristics. Any light which does not meet the condition for reflection is lost from the cavity. In using a grating, the blaze angle must be calculated, and for narrowing the required acceptance bandwidth needs to be accommodated.

The blaze angle is dependent on the groove spacing and wavelength being reflected:

$$\theta_{blaze} = \sin^{-1}\left(\frac{m\lambda_s}{2a}\right) \tag{3.5}$$

where m is the diffraction order (m = 1) and a is the groove spacing (830 lines/mm). For the laser parameters required, this returns an angle of 62 degrees.

The grating acceptance bandwidth can be calculated from [3.22]:

$$\Delta\lambda_G = \frac{1}{2}[0.83\frac{\lambda_s}{\tan(\theta_{blaze})\,\pi\,\omega_o}] \tag{3.6}$$

where ω_o is the spot size on the grating. From the expression, the only design variable is the beam size on the grating – the larger the spot size on the grating, the narrower the linewidth. For a spot size of 200 μm, a linewidth of 3.2nm can be expected – this should be sufficient to realise the OPO based on ZGP.

In this work, the grating was a plane ruled reflection grating with 30° nominal blaze angle and 830 lines/mm obtained from Richardson Gratings. The efficiency curve is shown in Figure 3.10.

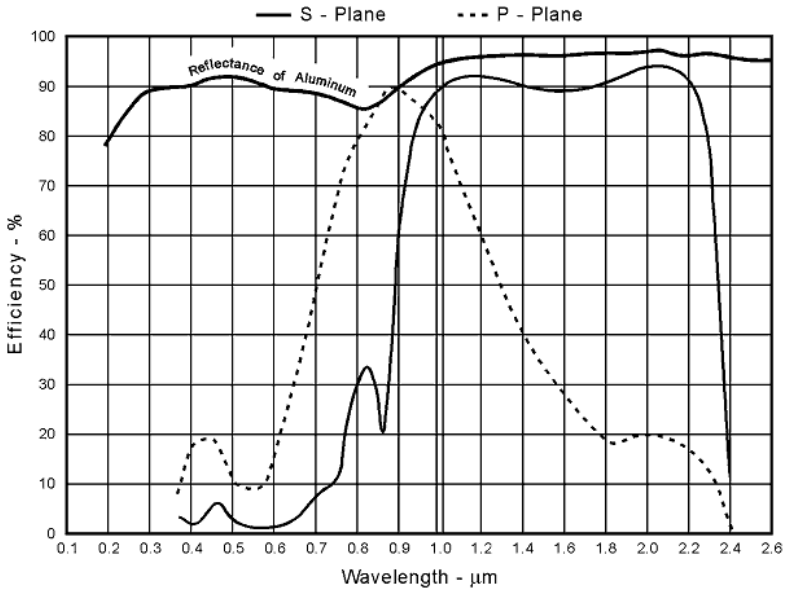

Figure 3.10: Diffraction grating efficiency (Richardson Gratings – [3.44])

3.2.2.1 *Cavity Design*

Having highlighted the requirement for a line narrowing element in the cavity it was decided, to avoid damage of the diffraction grating, to design the cavity such that the

grating, used in the Littrow configuration, has minimal interaction with the high pump fields (as shown in Figure 3.11). The grating increases the loss for wavelengths that do not satisfy the criterion described by expression 3.6. The pump source was a Coherent PRISMA which had a repetition rate between 20 – 100 kHz, and a maximum average output power of 12W. The power was controlled prior to the PPLN OPO by using a variable attenuator comprising a half wave plate and a polarising beam splitter cube.

The PPLN which is referred to throughout this thesis is doped with Magnesium Oxide. Without this doping the material suffers from a lower threshold for photorefractive damage, typically undoped PPLN should be operated at temperatures above 100°C to avoid this effect. Photorefractive damage occurs when electrons become mobilised in regions of high intensity leading to changes in refractive index which are visible as beam distortions [3.23]. In this demonstration, the tuning periods which are required to phase-match to the degenerate wavelength are only available by elevating the temperature. The PPLN used was 40mm long with a poling period aperture of 0.5 x 0.5 mm, the period used was 31.6 μm, which was heated to 185°C to reach the degeneracy (2.13 μm) for the mid-IR ZGP OPO.

Two main cavity options were explored and shown in Figure 3.1.

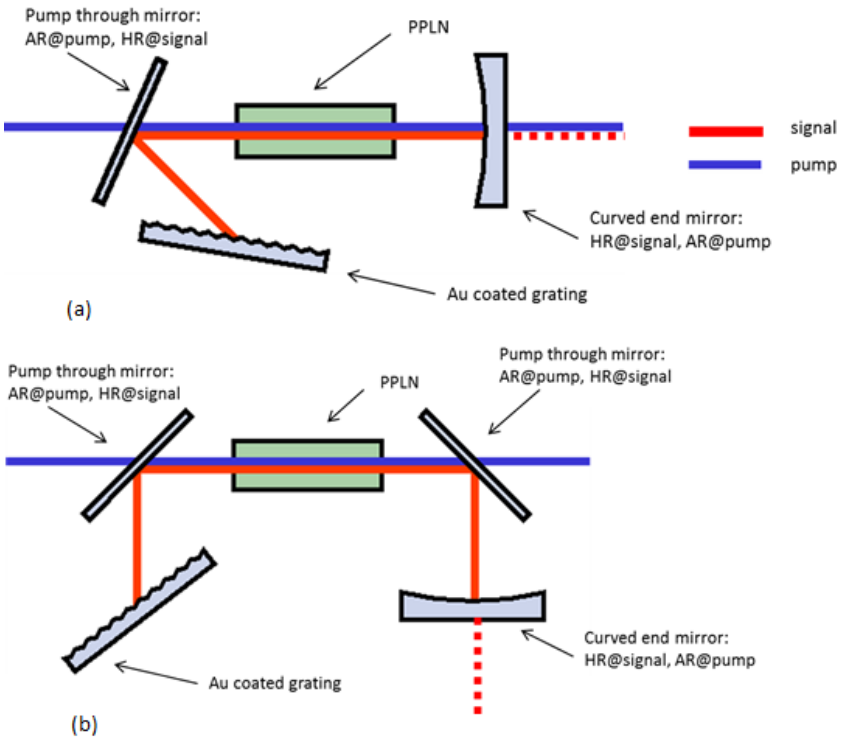

Figure 3.11: (a) Cavity Design for grating-narrowed PPLN OPO; (b) Cavity design using 45° mirrors

In designing an OPO cavity, there are different ‘rules’ depending on the pulse duration of the pump laser. In the case of the nanosecond pulse discussed here, losses are much less of a problem than they are for continuous wave sources, and because the physical length of the pulse is 4.2m long, the requirement to carefully control the cavity length to maximise gain in the OPO crystal is negated. As mentioned earlier, there is a requirement to line narrow the PPLN OPO to meet the bandwidth requirements, for which a diffraction grating was employed. Ultimately, the decision on cavity design was made due to budget restrictions. The preference was to proceed with the design shown in Figure 3.11 (b) due to the additional arm in which an etalon could be placed; however 45° mirrors were beyond the scope of the budget.

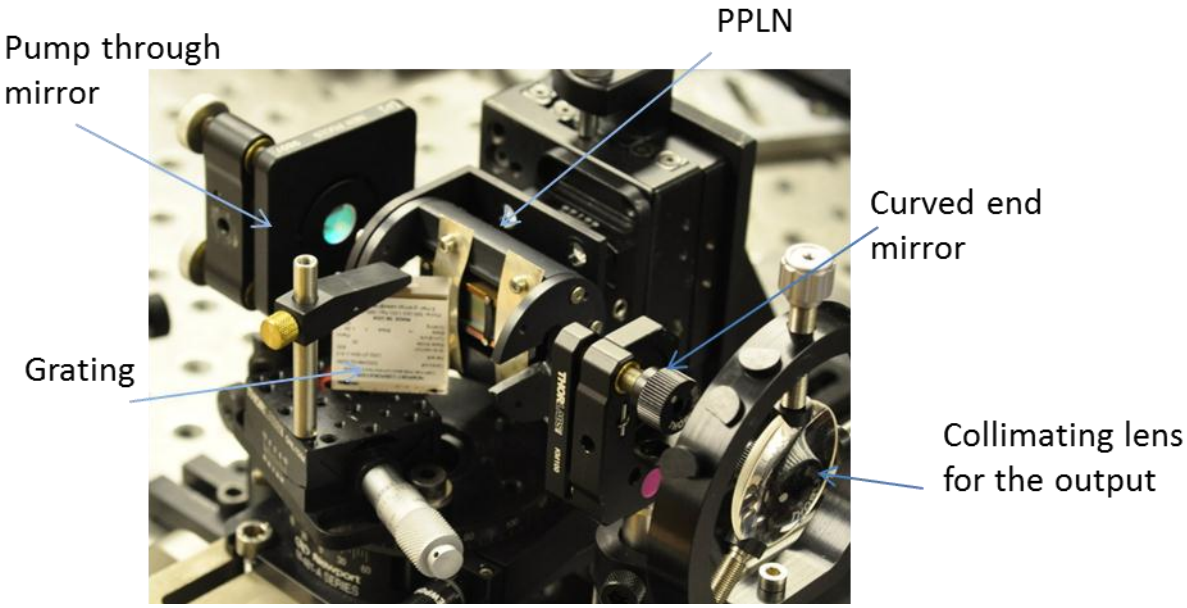

Figure 3.12: Grating-narrowed PPLN OPO

Prior to discussing system performance, the key characteristics are summarised (and shown in Figure 3.13 below):

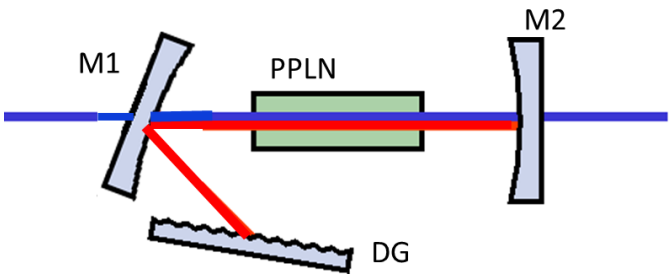

Figure 3.13: Finalised cavity design for degenerate PPLN OPO

- Pump source: Coherent PRISMA – 14ns pulses, 30kHz rep rate, 12W average power (0.4mJ)
- The total cavity length was 140mm, which includes a 43mm 'dog-leg' for the grating
- M1 and M2 have a 75mm radius of curvature, forming a signal waist of 160 μm in the PPLN overlapping with a pump waist of 220 μm
- The mirror coatings are R<1.5% at 1064nm and R<1% at 1400 – 1800nm (no data was given across the degenerate range [3.45])
- The PPLN grating period is 31.6μm at room temperature, and is held at 185°C for phase matching to degeneracy (2.128 μm)
- The diffraction grating has a blaze angle of 30° with 830lines/mm

3.2.2.2 Performance analysis – theory vs. experiment

The PPLN OPO was evaluated to assess its quality as a pump source for the second stage device. This section examines the PPLN OPO thresholds, both predicted and from experiment, the optimum output coupling for highest power, temperature tuning and the effectiveness of the line narrowing described previously.

The predicted threshold of the device was calculated from the equations developed by Brosnan and Byer for nanosecond OPOs [3.25]:

$$J_T = \frac{2.25}{\gamma g_s \xi^2}\tau\left[\frac{l}{2\tau c}\ln\frac{P_{th}}{P_n} + 2\alpha l + \ln\frac{1}{\sqrt{R}} + \ln 2\right]^2 \qquad (3.7)$$

Where $\gamma = \frac{2\omega_2\omega_1 d_{eff}^2}{n_3 n_2 n_1 \varepsilon_o c^3}$ and $g_s = \frac{\sigma_3^2}{\sigma_3^2+\sigma_2^2}$; the subscripts 1, 2 and 3 denote the idler, signal and pump fields respectively for frequency, ω, and beam waists, σ. In the paper the threshold is defined as the signal field being observable – 100 μJ ($\ln\frac{P_{th}}{P_n} = 33$). If this is converted to power, 100μJ corresponds to a power of 3W average, 7kW peak, which is not realistic for the system described here, therefore the threshold is redefined to be 4mW (0.1μJ) thus $\ln\frac{P_{th}}{P_n} = 25$. The value of ζ in this equation is equal to the length of the crystal as there are no walk-off effects in PPLN. It is important to note that this approach is only approximate as it assumes no pump focussing. The pulse width, τ, is defined as the $1/e^2$ halfwidth rather than the FWHM.

The appropriate substitutions into this expression yield a threshold fluence of 0.25J/m^2 which corresponds to a threshold of 0.94W, which is very low when there is a maximum available field of 12W. In order to optimise the output coupling from the

PPLN OPO, a number of output couplers with the following reflectances were tried; High Reflector (HR), 80%, 60%, 40% and 10% (these will be referred to as e.g. 0.4R for an output coupler which is 40% reflecting). The power obtained from these is plotted in Figure 3.14 together with the values for the cavity with the grating in place, and the modelled values. From this it is expected that optimum output coupling would occur for an output coupler of approximately 20% reflectivity for the signal.

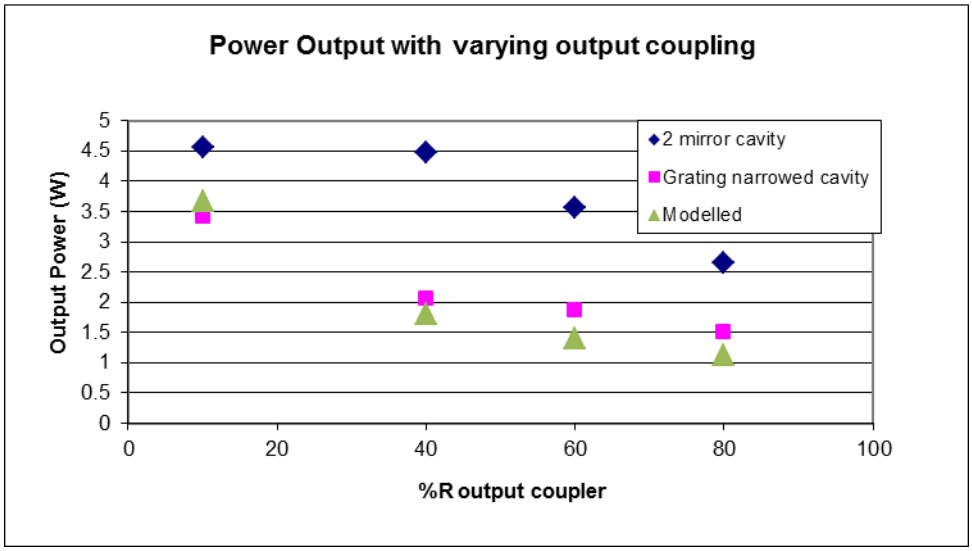

Figure 3.14: Variation in output power with output coupling of the PPLN OPO in the grating narrowed and un-narrowed configurations alongside the modelled (grating narrowed) results

The discrepancy between the model and the measured values is due partly to the assumptions made in the model with regards cavity losses, Gaussian vs. plane wave approximation, focussing (or not focussing) into the OPO, pulsed or continuous wave operation of the pump. To reduce the complexity of the model, a number of simplifying assumptions are made which ends up effectively reducing the intensity which is being focussed in the OPO crystal – this would lead to an artificially high value for threshold, thus making the discrepancy in Figure 3.14 less surprising.

In the case of the 0.1R output coupler, the graph of slope efficiency measured a threshold far lower than what was obtained by extrapolating the curve at higher pump powers, indicating that there is significant single pass gain generating a measurable signal. The significance of this shall be discussed later in the chapter. It was decided to proceed with the 0.1R output coupler as it yielded the higher output power, and also avoided beam distortion through thermal lensing.

In order to fully characterise the PPLN OPO and find the temperature for the degenerate point, a temperature tuning curve was obtained before the grating was installed in the cavity. The signal wavelengths were varied by adjusting the oven temperature and measured with a wavemeter (the idler wavelengths inferred via conservation of energy). This is shown in Figure 3.14 overlaid with data from SNLO:

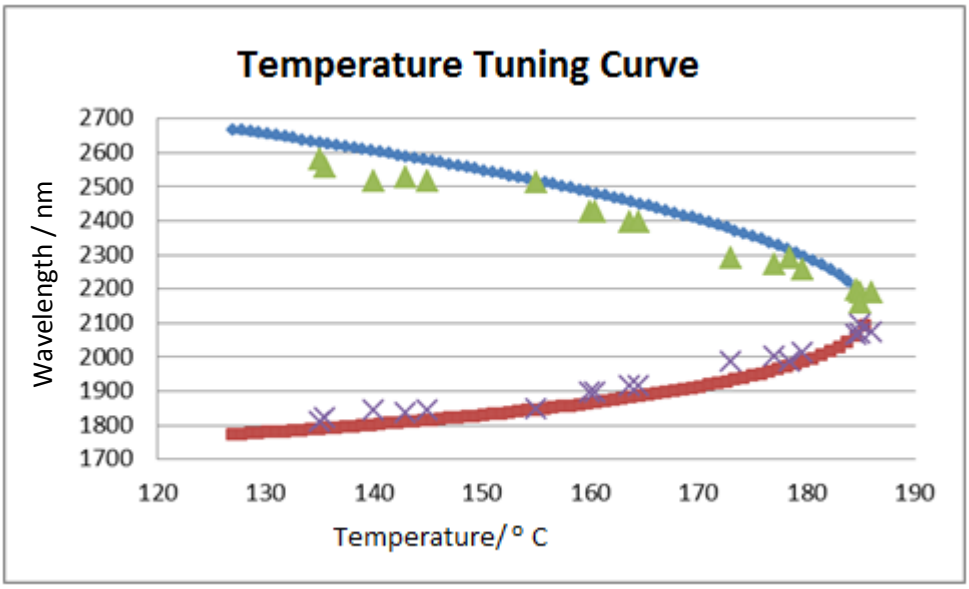

Figure 3.15: Theoretical curves obtained using SNLO Nonlinear Optics Code (red and blue) (available from A. V. Smith, AS-Photonics, Albuquerque, NM) [3.26]**, for a grating of 31.6 µm overlaid with experimental data (green triangles / purple crosses)**

Using the Bristol Instruments Spectrum Analyser, the following spectra were taken of the degenerate output; with and without the diffraction grating in place (Figure 3.16). The noise in the degenerate (no diffraction grating) is due to the low spectral density across into the meter which has been exacerbated by the normalisation.

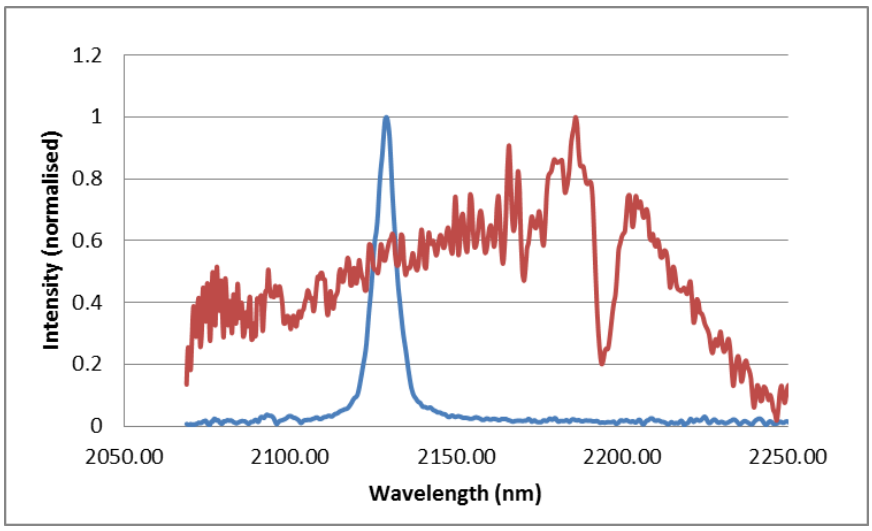

Figure 3.16: Effectiveness of line narrowing using a diffraction grating (blue – diffraction grating; red – no diffraction grating)

There is a clear benefit in using a diffraction grating to reduce the spectral linewidth of the PPLN OPO from the degenerate, un-narrowed linewidth of 100nm (FWHM) to the narrowed linewidth width of 10nm (FWHM) as shown from Figure 3.16. Although this is larger than the predicted linewidth of 3.2nm, the analysis to follow will indicate that this should be sufficient narrowing for the second stage – the ZGP OPO.

The overall wavelength tuning range obtained by varying the angle of the grating was 200nm. The tuning was measured directly from a wavemeter, rather than from the angular rotation of the grating on its mount. 2050 – 2250nm is an excellent range over which to examine the ZGP as it covers the main pump wavelengths of interest – the VECSEL (2.05 μm), Ho:YAG (2.09μm) and the degenerate PPLN OPO (2.13 μm). The application of this tuning range is detailed in the next section.

In conclusion to this sub-section, the final design of the PPLN OPO which was used to pump the ZGP OPO has the power transfer curve and mode profile shown in Figure 3.17 and 3.18 with a slope efficiency of 26%, a maximum combined power out of ~3.4W (real) and a spectral linewidth of 5nm.

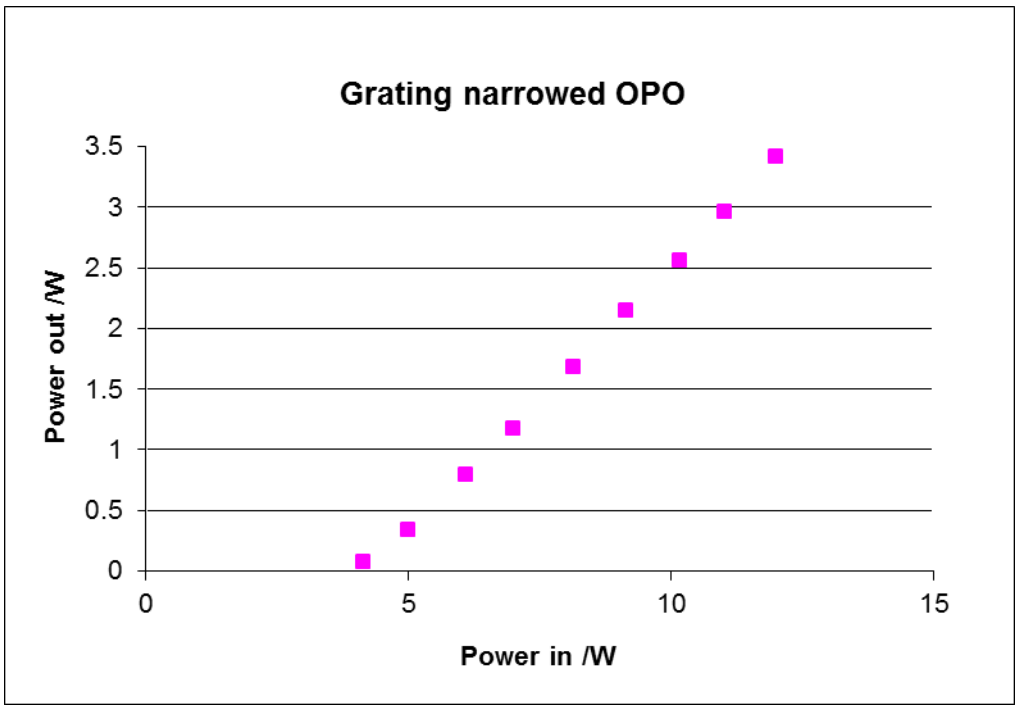

Figure 3.17: Efficiency curve of grating narrowed OPO

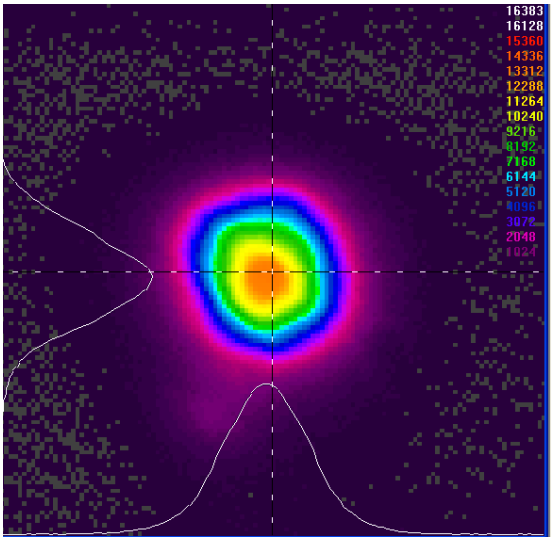

Figure 3.18: Mode intensity profile of line-narrowed output measured at 2.2W

3.3 2 µm pumped OPOs using ZGP/OP-GaAs

Following the resourcing issues which led to the substitution of OP-GaAs with ZGP late in the project, the ZGP crystal had to be flexible enough to fit the range of experiments that were intended for the OP-GaAs. Ultimately *due to being over constrained* the ZGP OPO did not reach threshold, therefore this section will analyse the design in detail in

order to highlight the possible oversights in order to ensure that a follow up experiment would be successful.

The decision making process for choosing the ZGP is analysed first of all, before going on to examine the expressions used to calculate thresholds and going over the possible oversights that were made. Following this, conclusions will be drawn with regards to experimental re-design to ensure a more favourable outcome in the future.

3.3.1 Procurement process for ZGP

As described above, ZGP was not the intended nonlinear material for this work. As a result of this compromises were needed and decisions made in terms of the crystal design which were, in part, responsible for the final result. As with most nonlinear crystals, the signal and idler wavelengths are set by the crystal design, which in a birefringent material is the crystal cut angle which defines the path over which the three interacting beams experience minimal walk-off such that they can interact. Mirrors had already been procured for an OPO based on OP-GaAs which was intended to have a grating period of 60.5 μm resulting in phase matching between 3.6 and 4.5 μm (calculated from SNLO – shown in Figure 3.19) using a pump wavelength of 2.05 μm, which is the more common wavelength for pumping this material using a fibre pumped holmium laser.

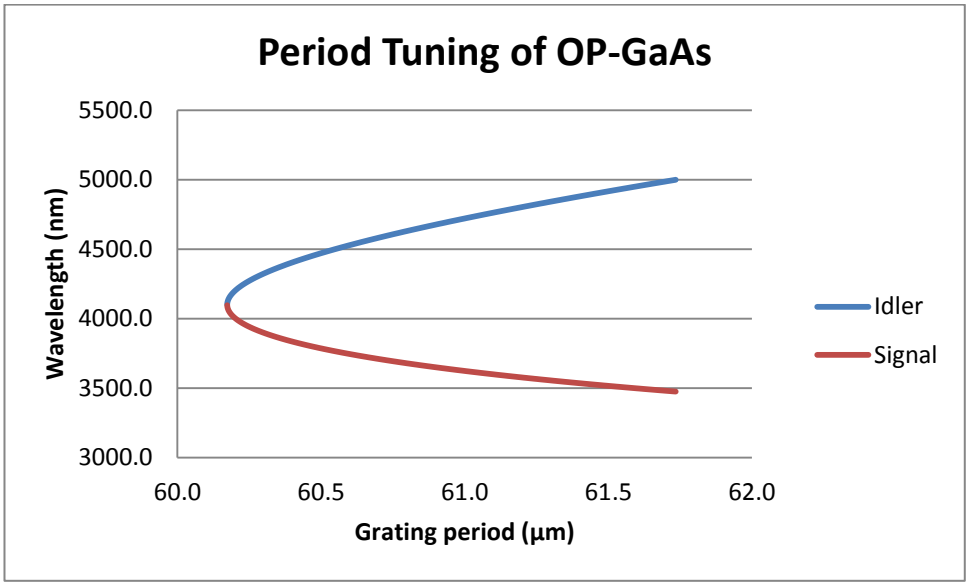

Figure 3.19: OP-GaAs period tuning curve, calculated using SNLO for a pump wavelength of 2.05μm

This resulted in a coating specification of AR at 2.13 μm and HR over the signal and idler wavelengths (the wide range was chosen to optimise the range over which the OP-

GaAs should phase match). It was decided that the ZGP OPO should be doubly resonant (DRO) in order to minimise threshold and optimise the chance of success.

At the time of procurement, the intention was to use the ZGP in the extra-cavity configuration, before potentially employing a VECSEL pump in the intracavity configuration. However this did not proceed due to a lack of mirrors with appropriate coatings. As the mirrors had already been specified, the initial aim was to maximise the utility of the ZGP for the pump sources that were available. Table shows the generated signal and idler wavelengths for a range of ZGP cut angles, using the formula shown below [3.27], across a range of possible pump wavelengths, including the holmium laser and the VECSEL (in collaboration with University of Strathclyde).

$$\theta pm_{ooe} = \tan^{-1}\left(\sqrt{\frac{1-U}{U-S}}\right) \tag{3.8}$$

where $U = \frac{(A+B)^2}{C^2}$ and $S = \frac{(A+B)^2}{(D+E)^2}$ and $A = \frac{no(\lambda i)}{\lambda i}$, $B = \frac{no(\lambda s)}{\lambda s}$, $C = \frac{no(\lambda p)}{\lambda p}$, $D = \frac{ne(\lambda i)}{\lambda i}$

and $= \frac{ne(\lambda s)}{\lambda s}$.

Fundamentally, the OPO will only provide gain at the signal wavelength if there is sufficient overlap of the modes within the crystal. This is more difficult to achieve in birefringent crystals due to potential walk-off between the pump and signal modes. This equation calculates the phase matching angle, taking into account the refractive index seen by each of the wavelengths, this is shown in Table 3.2 for a the pump wavelengths which were initially available.

Pump source and wavelength (μm)	OPO λ's	ZGP cut angle (°)						
		53	**53.5**	54	54.3	54.5	55	55.2
VECSEL (2.05)	λ_{signal}	3.066	3.164	3.279	3.361	3.425	3.639	3.78
	λ_{idler}	6.186	5.822	5.469	5.256	5.106	4.695	4.479

Ho:YAG (2.09)	λ_{signal}	3.296	3.447	3.665	3.904			
	λ_{idler}	5.712	5.309	4.863	4.498			
Degen PPLN (2.13)	λ_{signal}	3.64	4.091					
	λ_{idler}	5.135	4.444					

Table 3.2: Phase matched wavelengths for ZGP using various pump sources and cut angles (using Ghosh Sellmeiers) – illustrated in Figure 3.20. Shaded values show the combinations where OPO mirrors were available.

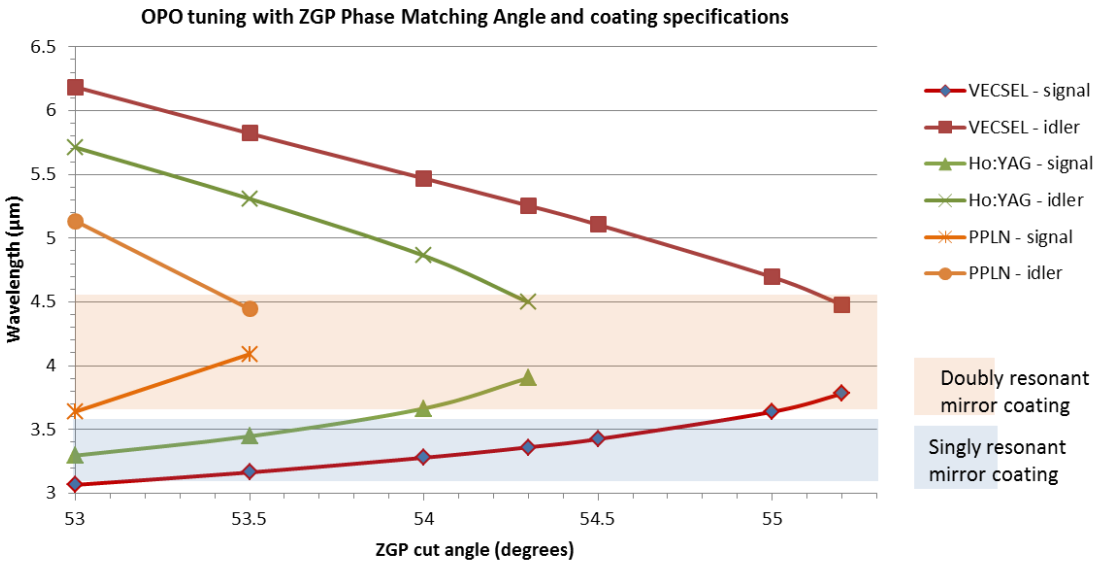

Figure 3.20: OPO tuning with pump wavelength showing where the generated signal and idler are compatible with the mirrors in the shaded areas

From Table , only the angles which are shaded have solutions which fit the DRO mirrors, the other solutions could be realised in a single resonant configuration using other optics which were available (HT 2130nm, HR 3100 – 3600nm)- illustrated in Figure 3.20 for clarity. The doubly resonant solution for the degenerate PPLN OPO was deemed most likely to succeed as a DRO has lower losses than an SRO resulting in a reduced threshold for the ZGP OPO. In addition to this, the phase matched solutions for the VECSEL and Ho:YAG laser also fall within the coating bandwidths of the SRO mirrors. With all this in mind, the ZGP cut angle was chosen to be 53.5°.

The crystal was procured from Ingcrys Laser Systems Ltd with the following specifications and tolerances:

$ZnGeP_2$ crystal
5*3*15mm, cut / polished suitable for laser application.
(5mm side is in plane of angle tuning)
Type 1, $\theta = 53.5°$, $\varphi = 0°$
Cut angle tolerance: +/- 0.5 deg
Absorption: < $0.05cm^{-1}$ @ 2.1um
Parallelism: 30 arc sec.

3.3.2 Use of OPO to Characterise the ZGP

Having built the PPLN OPO, the first useful task was to characterise the transmission of the ZGP prior to building an OPO around it. This was achieved by temperature tuning across the wavelengths accessible to the PPLN grating period (using the spectrum analyser to confirm), and using sharp band-pass filters at 2128nm to cover the maximum range: the experimental set-up used is shown in Figure 3.21 and results are shown in Figure 3.22.

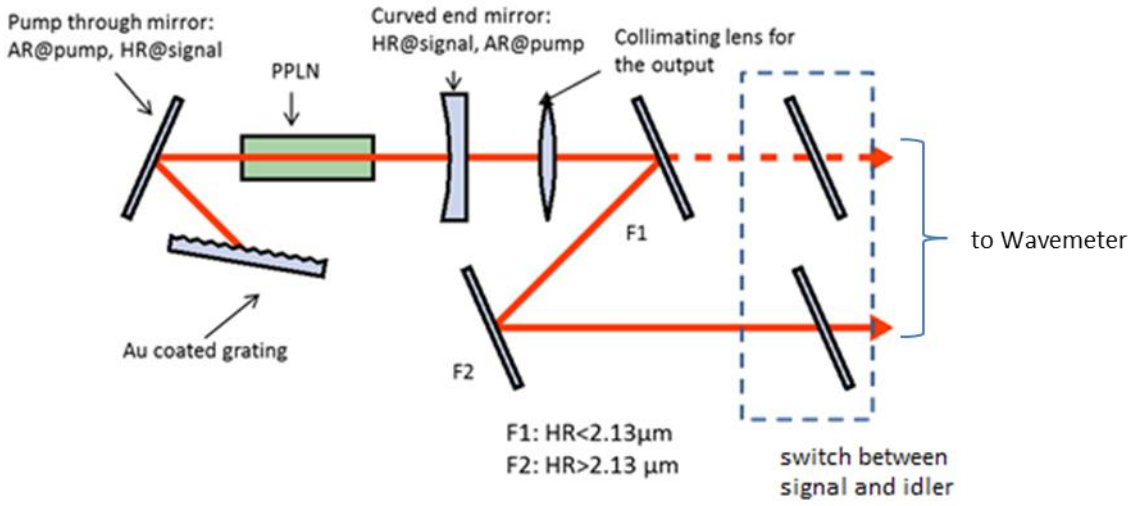

Figure 3.21: Experimental set-up for isolating wavelengths for ZGP characterisation

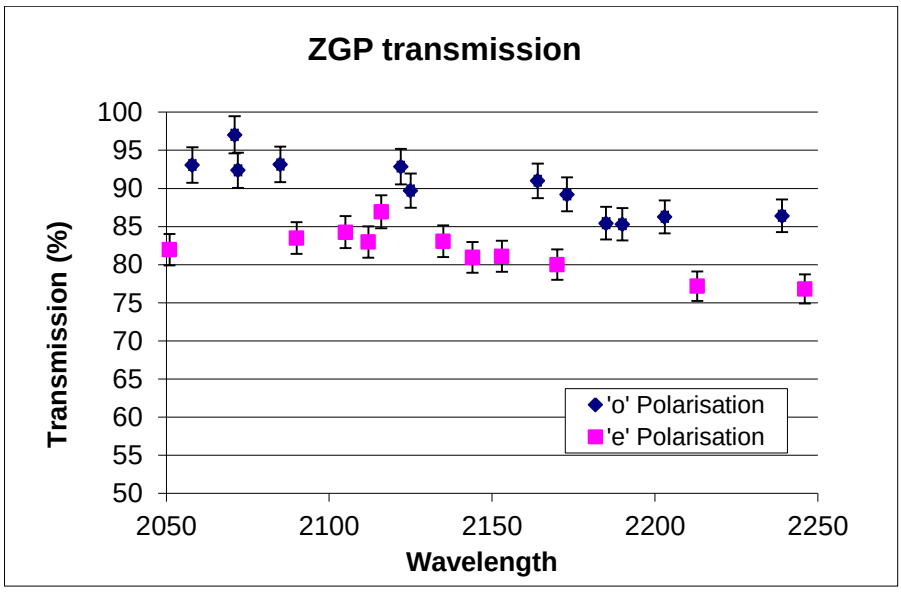

Figure 3.22: ZGP Transmission for 'o' and 'e' polarisations

Although the transmission of both polarisations is shown above, it is the interaction of the o-ray which is of greatest interest as this is the polarisation which is required for phase matching in the ZGP OPO. This measurement falls short of the quoted specification of the crystal (<0.05cm^{-1} at 2.1 μm), but due to time limitations on the project this was not investigated further. The error bars show ±2.5% arising from the combination of power drift with time from the PPLN OPO and power metre measurement error. Taking these into account, the transmission is less sensitive with wavelength than the data points would suggest. This ZGP data has not been compared directly with the SNLO data shown in Figure 3.4 as the SNLO data is for an uncoated ZGP and thus rendering the comparison invalid.

3.4.3 Cavity design and projected ZGP performance

For optimum gain, the confocal parameter (b) should be equal to the crystal length and the beam waist (ω_o) located at the centre of the crystal [3.28], i.e. $b = \frac{2\pi\omega_0^2}{\lambda}$ This corresponds to a pump waist of 71 μm, and 98 μm for the signal for a 15mm long crystal. Given this spot size, damage thresholds have to be considered alongside the effects of walk-off. Given a damage threshold of 60MW/cm^2 from the supplier (Ingcrys [3.29]) (14ns pulse duration, 30kHz repetition rate), the maximum average power is 1.26W which is less than the 3.4W available from the first stage OPO. In relaxing the spot size to comfortably avoid the damage limit, a waist of 160 μm is preferred.

3.3.2.1 Focussing constraints and damage threshold

As described earlier in the case for PPLN, the threshold is minimised for shorter cavity lengths. Mounts were therefore designed to be low profile to enable them to be positioned closest to the ZGP for the mirror radii that were selected. As already mentioned, the mirrors for this system had been procured prior to the ZGP being selected as the nonlinear material, so plane mirrors were used instead. It would have been preferable to use mirrors with a short radius of curvature to provide a tight focus in the crystal for the signal which would have resulted in a better pump/signal overlap in the cavity. As it stands, the pump beam was focussed into the ZGP using a 175mm focal length lens as shown in Figure 3.23 to form a focus spot size of 160 µm radius

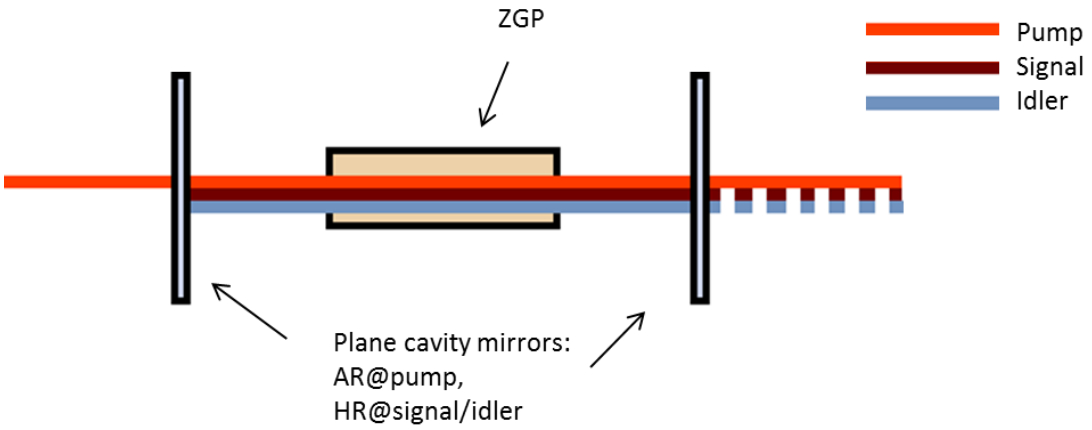

Figure 3.23: Cavity design for the ZGP OPO

The use of plane mirrors to demonstrate such OPO operation is widely reported in the literature [3.20], [3.30] and [3.31]. An ABCD analysis of a plane mirror cavity indicated that the cavity should be unstable, however, it is well documented that the effect of gain in the cavity stabilises it.

Having completed a thorough analysis of the ZGP cavity design requirements, calculating thresholds that looked achievable, it was surprising to find that the OPO did not reach threshold. A review was carried out, further investigating the parameters of the PPLN OPO as well as checking again the mirror transmissions and ZGP cavity design. This process is described in the following sections.

3.3.3 Review of ZGP design

OPOs have a finite acceptance bandwidth which is determined by the phase matching of the nonlinear material which often results in an output which is spectrally broader than a

laser. The decision to use an OPO to pump the ZGP was primarily driven by the need for flexibility in pump wavelengths which meant that the issue of line narrowing the output had to be addressed. There are a number of examples where fibre lasers have been used as pump source for ZGP and OP-GaAs as they naturally have a very narrow linewidth, for example, Ding *et al* reported a <0.05nm output from a gain switched thulium laser [3.32] which can then be used to pump a Holmium solid state laser to generate wavelengths which are not absorbed by the nonlinear material. Ideally, mature 1 μm laser technology could be used for everything however ZGP exhibits strong defect related absorption below 2 μm [3.33] which necessitates more complex pump sources.

In addition to the use of fibre lasers, the tandem OPO configuration has been cited repeatedly using a number of nonlinear materials including PPLN [3.16] and PPKTP [3.34], [3.35]. As well as being highly absorbing below 2.1 μm, it has a small pump acceptance bandwidth (calculated about to be in the region of 6nm for a 15mm crystal) which conflicts greatly with the dynamics of an OPO especially at degeneracy where it tends to span up to ~100nm. A summary of various ZGP pump geometries are shown in Table with cavity layouts shown in Figure 3.24:

	Henriksson [3.30] PPKTP	Elder [3.36] Ho:YAG	Perrett [3.16] PPLN	Lancaster [3.35] KTP
ZGP length	14.3mm	15mm	11mm	2 x 8mm*
Pulse description	4ns, 10Hz	38ns, 25kHz	27ns, 10kHz	22ns
Max avail for pumping	250μJ	27.3W	25mm – 0.49mJ; 50mm – 0.62mJ	2.2W
Threshold	50μJ	6W	25mm – 80μJ; 50mm – 270μJ	0.23W

Table 3.3: Examples of ZGP OPOs *these 2 crystals were employed in a walk-off compensated scheme

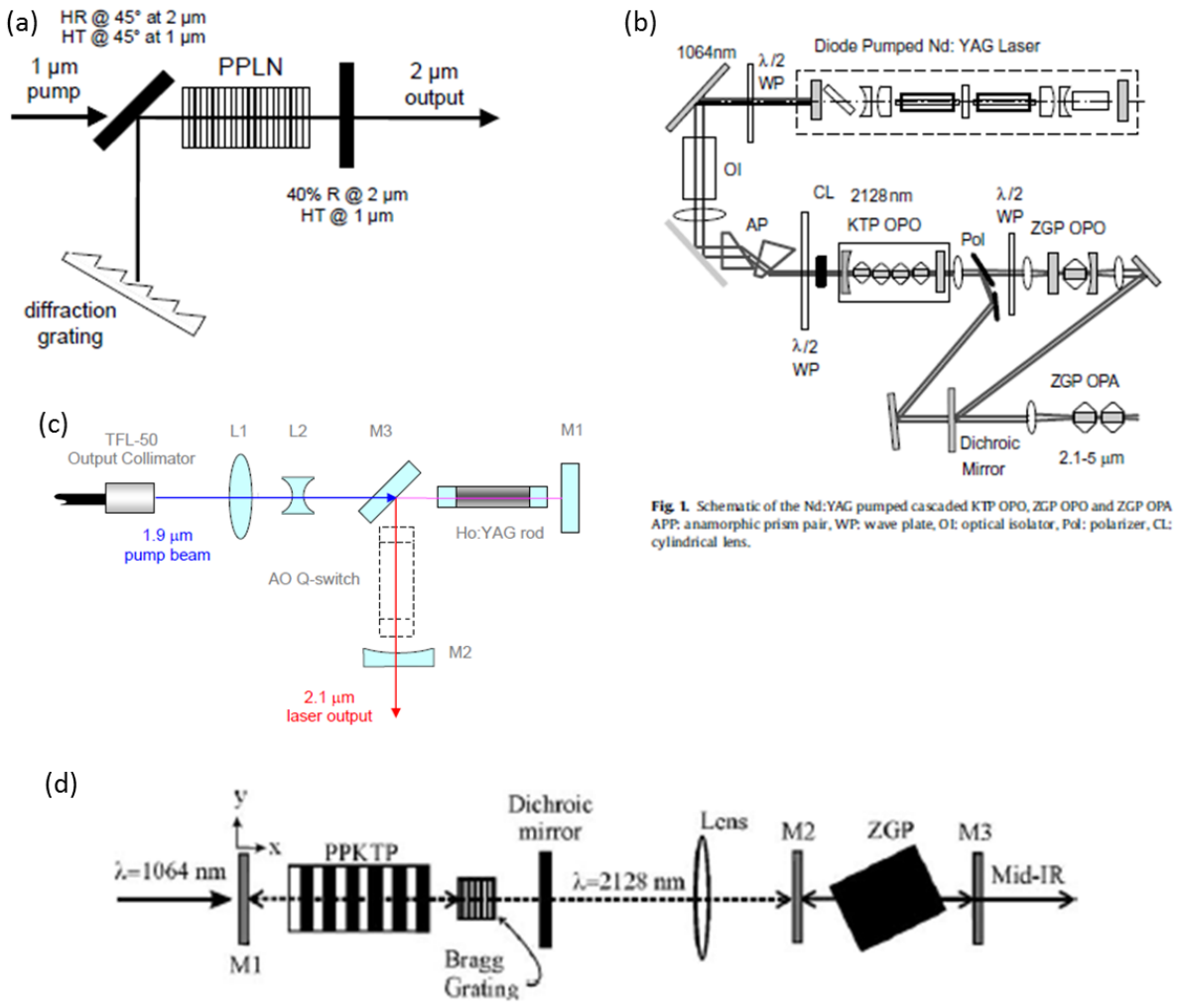

Fig. 1. Schematic of the Nd:YAG pumped cascaded KTP OPO, ZGP OPO and ZGP OPA APP: anamorphic prism pair, WP: wave plate, OI: optical isolator, Pol: polarizer, CL: cylindrical lens.

Figure 3.24; Cavity Configurations for results in Table 3.3 (a) Perrett [2.16]; (b) Lancaster [3.35]; (c) Elder and (d) Henriksson [3.30]

The most relevant reference to the work carried out here is that by Perrett and co-workers in acknowledging the presence of a high single pass gain, or Optical Parametric Generation (OPG) in the PPLN stage which does not experience any line narrowing [3.16]. This is the most likely cause of non-optimal performance of the OPO that was attempted here. There was 2.4W of OPG in the 3.4W of output generated by the PPLN OPO described above, measured by blocking the off axis arm of the cavity. There was no indication of pedestal broadening on the trace from the laser spectrum analyser; however this is most likely due to the lack of resolution and large dynamic range which would be required to see both the narrowed feature and the pedestal. The effect of increasing pump power on spectral width is shown in Figure 3.25.

Figure 3.25 shows the effect of increasing pump power on the spectral linewidth of the grating narrowed PPLN OPO, the FWHM and $1/e^2$ linewidth are noted in Table :

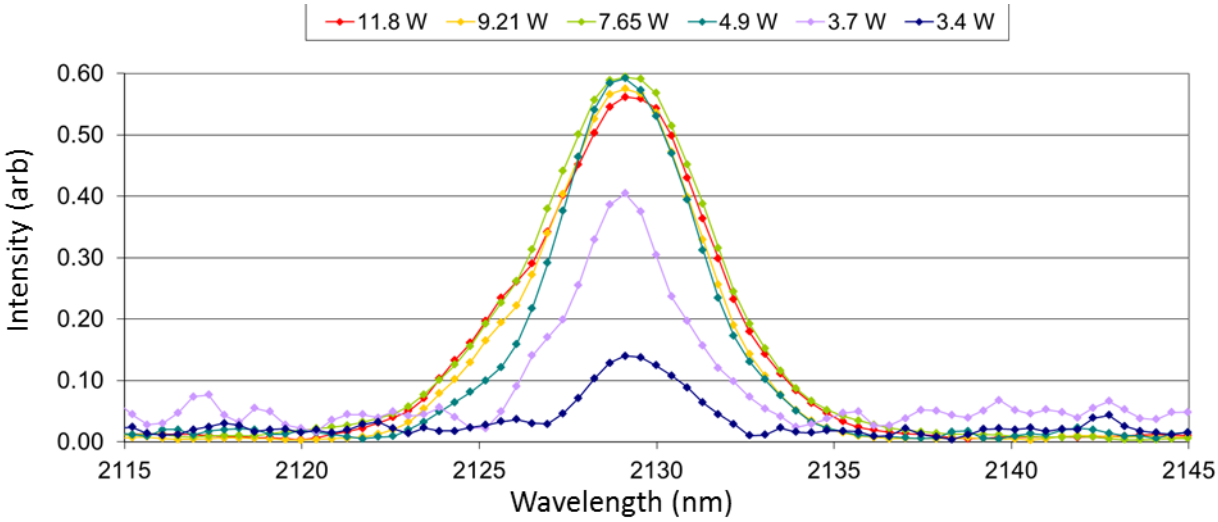

Figure 3.25: Effect of increasing linewidth on power

Input Power to PPLN OPO (W)	FWHM of degenerate output (nm)	$1/e^2$ of degenerate output (nm)
3.2	3.41	-*
3.7	3.39	8.67 (5.75)
4.9	4.43	10.5 (7.52)
7.65	5.48	9.60 (9.30)
9.21	4.95	10.54 (8.40)
11.8	5.46	12.2 (9.27)

Table 3.4: variation of linewidths of narrowed output with increasing input power *there is too much low level noise to be able to define the $1/e^2$ width for this point. Values in brackets show the expected $1/e^2$ width based on the FWHM

If the spectra were Gaussian in nature, the $1/e^2$ widths would be the same as those denoted in the brackets in the same right hand column of the table (these values are calculated via the conversion equation: $2\omega = \frac{\sqrt{2}FWHM}{\sqrt{\ln 2}}$). The fact that they are not

suggests that the line narrowing was not as effective as it should have been, possibly due to OPG. Again, the calculated linewidth for the narrowed output was 3.2nm which would have accommodated the ZGP acceptance bandwidth, but the measured spectra (power dependant 3.4 – 5.5nm) are too broad.

3.3.3.1 Threshold of the device

From the previous section the final linewidth achievable from the OPO was ~10nm FWHM, and the maximum power available was ~3.4W at degeneracy.

In calculating the thresholds that are expected for such a device, the analysis has to take into account any walk-off effects in ZGP due to its birefringence. The factor of ζ is calculated from the following:

$$\xi = l_w erf\left(\frac{\sqrt{\pi}}{2}\frac{l}{l_w}\right) \tag{3.9}$$

And

$$l_w = \frac{\sqrt{\pi}}{2}\frac{\sigma_3}{\rho}\sqrt{\frac{w_3^2 + w_2^2}{w_3^2 + 0.5w_2^2}} \tag{3.10}$$

where the symbols are as previously defined, and ρ is the double refraction angle (which in the case of the OPO is ~ 10^{-4} as the cut angle has been chosen such that the walk off is negligible in order to achieve phase matching; for pump and signal spot sizes of 330 μm, the walk-off length is 3.37m.

In an attempt to validate the model, results published by Elder *et al* were used. Here, 12.6W of combined mid-IR output was demonstrated using a Ho:YAG laser pumped by a fibre laser with 52% efficiency and a threshold of ~6W [3.36], which is in agreement with predictions of the model described here. It follows that, for the parameters of the ZGP OPO built at BAE, the expected threshold is ~3W. As the maximum power available to the ZGP OPO from the PPLN OPO is 3.5W, it is likely to be difficult to attain threshold given the losses that will be present in the ZGP OPO cavity.

The transmission spectra of the mirrors were measured, (shown below in Figure 3.26 and Figure 3.7); these indicate that that the HR coating is close to ideal. However, the

AR coating for the pump wavelength is clearly not ideal with a transmission of only ~86%. If this is combined with the pump absorption which was measured (shown in Figure 3.2) to be ~90% on the power available for down-conversion is reduced by ~23% to 2.7W, below the predicted threshold.

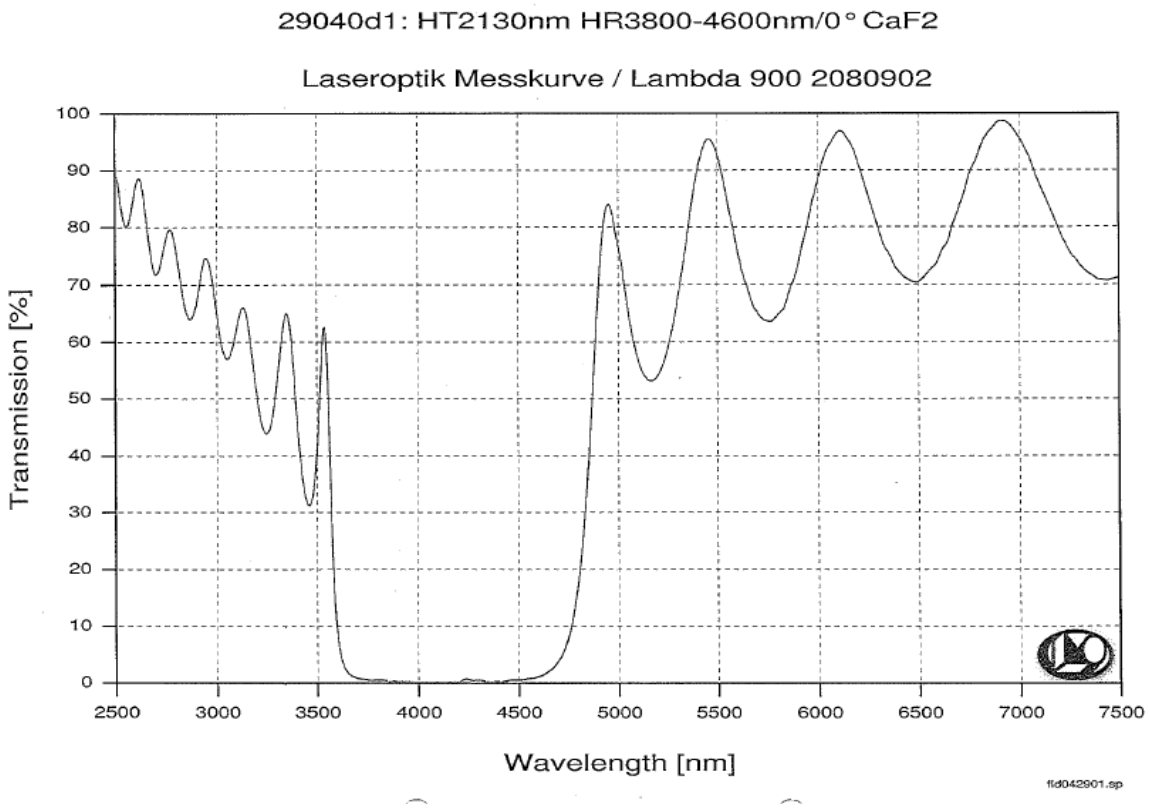

Figure 3.26: Mirror transmission spectrum (signal/idler) for use with ZGP OPO

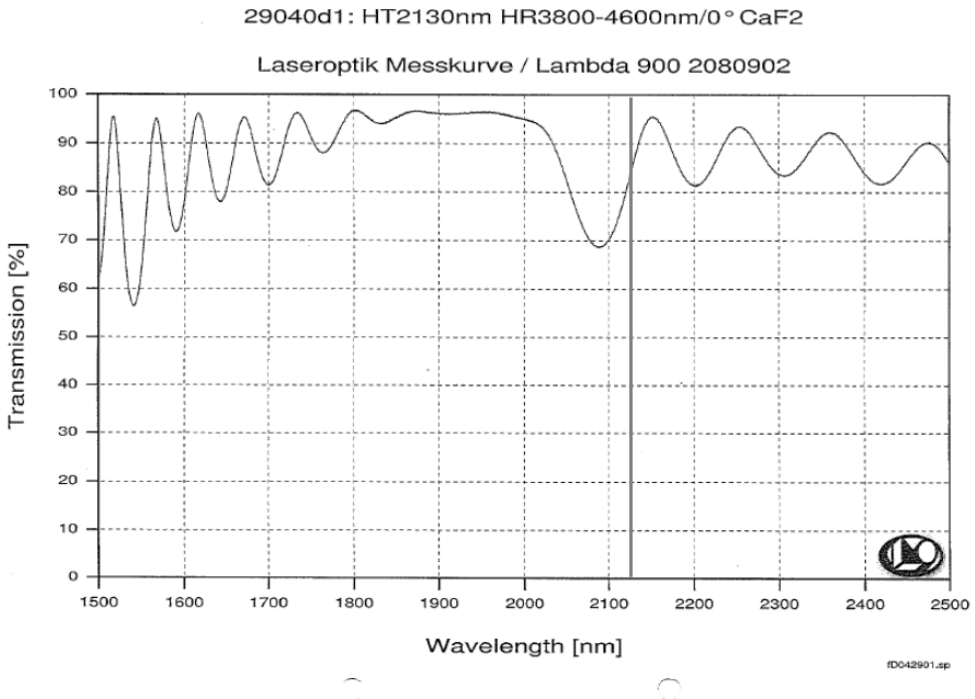

Figure 3.27: Mirror transmission spectrum with the pump wavelength marked at 2130nm (for ZGP OPO)

3.4 Conclusion

In this chapter the design and build of a nanosecond, line narrowed degenerate MgO:PPLN OPO is described. This OPO was intended to pump a ZGP OPO. Due to large amounts of single pass gain in the OPO, and higher than anticipated ZGP transmission losses and mirror coatings the line narrowing was not sufficient to bring the ZGP OPO above threshold.

Having found the PPLN OPO to be spectrally too broad for pumping the ZGP, a more feasible route forward would be to use the Ho:YAG – fibre laser approach (see Table for the phase matching wavelengths). The narrow linewidth would have easily brought the ZGP OPO above threshold as has been demonstrated by Elder [3.36], and would have also been effective in demonstrating an OP-GaAs OPO with an appropriate period. The ability to use a range of sources to fully characterise and pump these OPOs (ZGP/OP-GaAs) would allow both a range of wavelengths to characterise the material (narrowed PPLN OPO) and a narrow linewidth source to evaluate the OPO (Ho:YAG).

If the acceptance bandwidth for OP-GaAs is compared with that of ZGP, we find that Vodopyanov quotes an approximate OP-GaAs acceptance bandwidth of 6 cm^{-1} [3.7], which corresponds to ~3nm, narrower than was required for the ZGP OPO. Thus for either of these systems to work, the linewidth of the source must be reduced.

It is shown in Figures 3.7 and 3.8 (from equation (3.4)) that the output linewidth of an OPO increases with crystal length suggesting that it would be beneficial to repeat the experiment with a shorter crystal (this was not done at the time due to the available PPLN crystals with an appropriate grating period). This manoeuvre would result in a narrower linewidth, but would not get rid of the suspected OPG, thus it would be beneficial to use a pump source which had lower pulse energy. This could be achieved by increasing the repetition rate of the source, or moving to shorter pulse lengths. Improvements to the ZGP cavity would include the output mirror being HR at the pump wavelength to enable double passing which would have brought down the threshold.

A line narrowed, high power, degenerate PPLN OPO has been demonstrated with a maximum available output power of 3.4W and linewidth of 10nm. This was then used to characterise the transmission of ZGP. The project highlighted the complexities of working with critically phase matched materials such as ZGP and thus grew the capability of the BAE Systems Advanced Technology Centre, further accentuating the benefits of moving to non-critically phase matched materials such as OP-GaAs for generation of wavelengths greater than 6 μm.

3.5 References

[3.1] D. Graham-Rowe, “New laser to dazzle pirates on the high seas,” *New Scientist (Tech)*, 2011. [Online]. Available: http://www.newscientist.com/article/dn19930-new-laser-to-dazzle-pirates-on-the-high-seas.html. [Accessed: 07-Sep-2012].

[3.2] M. Watson, M. O'Connor, P. Lloyd, D. Shepherd, D. Hanna, C. Gawith, L. Ming, P. Smith, and O. Balachninaite, "Extended operation of synchronously pumped optical parametric oscillators to longer idler wavelengths," *Opt. Lett.* vol. 27, no. 23, pp. 2106-2108 (2002).

[3.3] Y. Yao, A. J. Hoffman, and C. F. Gmachl, “Mid-infrared quantum cascade lasers,” *Nature Photonics*, vol. 6, no. 7, pp. 432–439, Jun. 2012.

[3.4] W. J. Jr and I. Kaminow, “Contributions to optical nonlinearity in GaAs as determined from Raman scattering efficiencies,” *Physical Review*, vol. 1, no. 3, 1969.

[3.5] O. Levi, T. Pinguet, and T. Skauli, “Difference frequency generation of 8-μm radiation in orientation-patterned GaAs,” *Optics letters*, vol. 27, no. 23, pp. 2091–2093, 2002.

[3.6] T. Skauli, K. L. Vodopyanov, T. J. Pinguet, a Schober, O. Levi, L. a Eyres, M. M. Fejer, J. S. Harris, B. Gerard, L. Becouarn, E. Lallier, and G. Arisholm, “Measurement of the nonlinear coefficient of orientation-patterned GaAs and demonstration of highly efficient second-harmonic generation.,” *Optics letters*, vol. 27, no. 8, pp. 628–630, Apr. 2002.

[3.7] K. L. Vodopyanov, O. Levi, P. S. Kuo, T. J. Pinguet, J. S. Harris, M. M. Fejer, B. Gerard, L. Becouarn, and E. Lallier, “Optical parametric oscillation in quasi-phase-matched GaAs.,” *Optics letters*, vol. 29, no. 16, pp. 1912–1914, Aug. 2004.

[3.8] P. Schunemann and L. Pomeranz, “Recent advances in all-epitaxial growth and properties of orientation-patterned gallium arsenide (OP-GaAs),” in *CLEO*, 2009, pp. 200–201.

[3.9] I. Vodopyannov, K., Sorokin, E., Schunemann, P., Sorokina, “4.4 - 5.4 micron frequency comb from a subharmonic OP-GaAs OPO pumped by a femtosecond Cr:ZnSe laser,” in *Advances in Optical Materials, OSA Technical Digest (CD) (Optical Society of America, 2011)*, paper AME2

[3.10] C. Phillips, J. Jiang, C. Mohr, and A. Lin, “Widely tunable midinfrared difference frequency generation in orientation-patterned GaAs pumped with a femtosecond Tm-fiber system,” *Optics Letters*, vol. 37, no. 14, pp. 2928–2930, Jul. 2012.

[3.11] G. Imeshev, M. E. Fermann, K. L. Vodopyanov, M. M. Fejer, X. Yu, J. S. Harris, D. Bliss, and C. Lynch, "High-power source of THz radiation based on orientation-patterned GaAs pumped by a fiber laser.," *Optics express*, vol. 14, no. 10, pp. 4439–4444, May 2006.

[3.12] P. S. Kuo, K. L. Vodopyanov, M. M. Fejer, D. M. Simanovskii, X. Yu, J. S. Harris, D. Bliss, and D. Weyburne, "Optical parametric generation of a mid-infrared continuum in orientation-patterned GaAs.," *Optics letters*, vol. 31, no. 1, pp. 71–73, Jan. 2006.

[3.13] W. C. Hurlbut, Y.-S. Lee, K. L. Vodopyanov, P. S. Kuo, and M. M. Fejer, "Multiphoton absorption and nonlinear refraction of GaAs in the mid-infrared.," *Optics letters*, vol. 32, no. 6, pp. 668–670, Mar. 2007.

[3.14] P. F. Dergachev, A., Moulton, "High-power, High-energy Diode-pumped Tm:YLF-Ho:YLF ZGP laser system," in *Advanced Solid State Photonics*, Vol. 83, p.137, February 2003.

[3.15] J. J. Zayhowski, "Periodically poled lithium niobate optical parametric amplifiers pumped by high-power passively Q-switched microchip lasers.," *Optics letters*, vol. 22, no. 3, pp. 169–171, Feb. 1997.

[3.16] B. J. Perrett, "Spectral line narrowing in PPLN OPO devices for 1-μm wavelength doubling," *Proceedings of SPIE*, vol. 5620, no. May 2011, pp. 275–283, 2004.

[3.17] P. E. Britton, "Fibre Laser pumped PPLN Nonlinear Devices," University of Southampton, 2000.

[3.18] D. Zelmon, E. Hanning, and P. Schunemann, "Measurements and Sellmeier coefficients for zinc germanium phosphide from 2 to 9 μm with implications for phase matching in optical frequency-conversion devices," *JOSA B*, vol. 18, no. 9, pp. 1307–1310, 2001.

[3.19] G. Ghosh, "Sellmeier coefficients for ZGP," *Applied optics*, vol. 37, no. 7, pp. 1205–1212, 1998.

[3.20] M. Henriksson, L. Sjöqvist, G. Strömqvist, V. Pasiskevicius, and F. Laurell, "Tandem PPKTP and ZGP OPO for mid-infrared generation," in *Proceedings of SPIE*, 2008, vol. 7115, pp. 71150O1–71150O10, 2008.

[3.21] T. Skauli, P. S. Kuo, K. L. Vodopyanov, T. J. Pinguet, O. Levi, L. a. Eyres, J. S. Harris, M. M. Fejer, B. Gerard, L. Becouarn, and E. Lallier, "Improved dispersion relations for GaAs and applications to nonlinear optics," *Journal of Applied Physics*, vol. 94, no. 10, pp. 6447, 2003.

[3.22] K. Puech, L. Lefort, and D. Hanna, "Broad tuning around degeneracy in a singly resonant synchronously pumped parametric oscillator by means of a diffraction grating," *JOSA B*, vol. 16, no. 9, pp. 1533–1538, 1999.

[3.23] Covesion, “Magnesium-doped PPLN crystals.” [Online]. Available: http://www.covesion.com/products/magnesium-doped-ppln-mgoppln-crystals/. [Accessed: 15-Jun-2013].

[3.24] B. D. Giles, A.G., Sinclair, “Photonics Simulation Software for Teaching.” http://www.st-andrews.ac.uk/~psst [downloaded February 2009]

[3.25] R. L. Brosnan, S.J., R.A., Byer, “Papers Optical Parametric Oscillator Threshold and Linewidth Studies,” *IEEE Journal of Quantum Elecronics*, vol. QE-15, no. 6, pp. 432–444, 1979.

[3.26] A. Smith, “SNLO Nonlinear Optics Code.” http://www.as-photonics.com/snlo

[3.27] V. G. et al Dmitriev, “Calculation of Phase Matching Angles in Uniaxial Crystals,” in in *Handbook of Nonlinear Optical Crystals*, Springer, 1999, p. 14.

[3.28] G. D. Boyd, “Parametric Interaction of Focused Gaussian Light Beams,” *Journal of Applied Physics*, vol. 39, no. 8, p. 3597, 1968.

[3.29] Ingcrys, “ZGP invoice.” 2010.

[3.30] M. Henriksson, M. Tiihonen, V. Pasiskevicius, and F. Laurell, “Mid-infrared ZGP OPO pumped by near-degenerate narrowband type-I PPKTP parametric oscillator,” *Applied Physics B*, vol. 88, no. 1, pp. 37–41, May 2007.

[3.31] K. L. Vodopyanov, F. Ganikhanov, J. P. Maffetone, I. Zwieback, and W. Ruderman, “ZnGeP2 Optical Parametric Oscillator with 3 . 8 – 12 . 4-micron tunability,” *Optics letters*, vol. 25, no. 11, pp. 841–843, 2000.

[3.32] Ding, J, Sampson, B., Carter, A., et al “A monolithic thulium doped single mode fiber laser with 1.5ns pulsewidth and 8kW peak power,” in Proc. *SPIE 7914, Fiber Lasers VIII: Technology, Systems, and Applications*, 7914X, February 2011.

[3.33]P. D. Mason and L. F. Michaille, “Review of the development of nonlinear materials for mid-IR generation,” *Proceedings of SPIE*, vol. 7115, p. 71150N–71150N–10, 2008.

[3.34] P. B. Phua, B. S. Tan, R. F. Wu, K. S. Lai, L. Chia, and E. Lau, “High-average-power mid-infrared ZnGeP2 optical parametric oscillator with a wavelength-dependent polarization rotator.,” *Optics letters*, vol. 31, no. 4, pp. 489–491, Feb. 2006.

[3.35] D. G. Lancaster, “Efficient Nd:YAG pumped mid-IR laser based on cascaded KTP and ZGP optical parametric oscillators and a ZGP parametric amplifier,” *Optics Communications*, vol. 282, no. 2, pp. 272–275, Jan. 2009.

[3.36] I. Elder, “Thulium fibre laser pumped mid-IR laser,” *Proceedings of SPIE*, vol. 7115, pp. 711505–711505–11, 2008.

[3.37] D. Bamford, "OP-GaAs," *PSI Corp webpage*, 2013. [Online]. Available: http://www.psicorp.com/product_service/products/opgaas.html. [Accessed: 28-Jul-2013].

[3.38] Jin Li ; David B. Fenner ; Krongtip Termkoa ; Mark G. Allen ; Peter F. Moulton ; Candace Lynch ; David F. Bliss ; William D. Goodhue; Wafer-fused orientation-patterned GaAs. Proc. SPIE 6875, Nonlinear Frequency Generation and Conversion: Materials, Devices, and Applications VII, 68750H (February 13, 2008); doi:10.1117/12.762315.

[3.39] Byer, R. L. "Diffusion-bonded nonlinear materials for practical quasi phase-matched mid IR devices" Ginzton Laboratory Report #54091, April 1996

[3.40] Tang, C. L. and Chen, L. K. "Fundamentals of Optical Parametric Processes and Oscillators" Chapter 5, p. 59, Hardwood Academic Publishers, 1995

[3.41] Thermal conductivity of ZGP (data sheet) – online http://inradoptics.com/pdfs/Inrad_WP_ZGP.pdf accessed on 22/3/14

[3.42] Thermal conductivity of GaAs (data sheet) – online http://www.janis.com/Libraries/Window_Transmissions/GalliumArsenide_GaAs_TransmissionCurveDataSheet.sflb.ashx accessed on 22/03/14

[3.43] Sellmeier Formula – RP Photonics http://www.rp-photonics.com/sellmeier_formula.html accessed on 23/03/14

[3.44] Richardson Gratings data sheet http://www.gratinglab.com/Products/Product_Tables/Efficiency/Efficiency.aspx?catalog=53-*-525R online accessed 23/03/14

[3.45] Covesion data sheet for part # MOPO1-1-40 - online http://www.covesion.com/products/magnesium-doped-ppln-mgoppln-crystals/mgo-ppln-for-optical-parametric-generation-oscillation.html accessed 23/03/14

[3.46] Covesion – online http://www.covesion.com/support/material-properties-of-lithium-niobate.html accessed 23/03/14

[3.47] R. W. Boyd, "Nonlinear Optics", Academic Press, 2nd Edition, 2003

4 Introducing the Intracavity PPLN OPO based on VECSELs

In Chapter 3, the ultimate aim was to enable a source of mid-IR (3 - 5μm) with reasonably high powers (> 1W) where an extracavity OPO is the only practical option. In this chapter the emphasis is on compact, efficient low power sources for spectroscopy of, for example, volatile hydrocarbons.

In order to detect the smallest concentrations of a hydrocarbon it is necessary to have the highest resolution source possible to pick out subtle differences between the spectra and hence identify gases more accurately. This would be achievable using a Continuous Wave (CW) source, tuneable over a range of wavelengths as this is operating at the fundamental time/bandwidth limit. For spectroscopy, only low infrared powers are required making the intracavity OPO (ICOPO) preferable over its extracavity counterpart, as discussed below. For CW OPOs higher powers are required to bring the OPO above threshold which, when the mid-IR power requirement is low (and the OPO is not operating far above threshold) results in a less efficient system. By moving to an intracavity scheme, the OPO is positioned within the 1064nm laser, enabling access to the high circulating fields, bringing the OPO to threshold for a much lower diode pump power.

Continuous wave intracavity OPOs (CW IC-OPOs) based on Nd materials have, for a long time, had their progress hampered by relaxation oscillations which arise from the long upper state lifetime of the Neodymium atom in the laser gain material which can result in amplitude fluctuations [4.2]. These amplitude (power) fluctuations means that they are unsuitable as tunable spectroscopic sources [4.3]. Recent solutions to the problem of relaxation oscillations in CW IC-OPOs have included the use of an upconversion crystal within the laser cavity to dampen these oscillations [4.3] and the use of a VECSEL (Vertical, External Cavity Surface Emitting Laser) as the parent laser [4.2]. The former has enabled single frequency oscillation with minimal additional frequency selective components, whilst the latter should avoid the issue of relaxation oscillations altogether as the upper state lifetime of the VECSEL is significantly shorter. It is this latter solution which will be investigated within the following chapters, building on the work described by Stothard *et al* in [4.2]. It had been thought that the key obstacle in enabling a continuous wave IC-OPO was the problem of relaxation oscillations. However having succeeded in eliminating relaxation oscillations by using a

VECSEL, reliable single frequency operation has not yet been observed in the case of the VECSEL IC-OPO.

This chapter begins with a short review of the literature relating to previous demonstrations of single frequency IC-OPOs as a reference to build upon when looking at the VECSEL-based system. This is followed by a discussion of the VECSEL as a stand-alone laser with particular reference to its excellent frequency characteristics and its potential as a parent laser to host an IC-OPO. The integration of the IC-OPO into the VECSEL cavity is examined in Chapter 6.

4.1 Intracavity OPOs

The first single frequency intracavity OPO was demonstrated in 1979 [4.10] and since then the host lasers have changed in line with progress in laser gain material development, but the concept has stayed the same. The host lasers reported vary from dye-lasers in the 80's [4.10], [4.17] through to the solid state systems in the current configurations [4.3]. The nonlinear elements have varied from critically phase matched materials such as ADA [4.11] and ZGP in the mid-IR regime [4.12] to poled materials such as PPLN [4.13]. It is useful therefore to review the developments; particularly in *single frequency* intracavity OPO schemes to gain insight into what has been achieved in other systems to enable single frequency operation and whether this can be applied in the VECSEL system. Single frequency operation has been observed in dye [4.11] and solid state [4.14], [4.15], [4.16] lasers. Important system parameters include the tendency to exhibit relaxation oscillations, the gain bandwidth of the pump laser, spatial hole burning and polarisation sensitivity.

4.1.1 Dye ICOPOs

With homogeneously broadened lasers such as the dye laser, spatial hole burning in the standing wave cavity can make it difficult to obtain single frequency operation. This is due to the gain being extracted by the main mode at the anti-nodes of the standing wave, allowing additional longitudinal modes to extract the remaining gain. This causes particular problems in cavities where the gain is not at the end of the cavity – like the dye laser. Intracavity frequency doubled dye lasers were first demonstrated in 1978 by Wagstaff and Dunn [4.10], drawing on the experience of Schroder *et al* [4.17] in using a ring in preference to a standing wave resonator to mitigate these effects. In this example (Wagstaff, 1978) in order to obtain single frequency operation of a frequency doubled

dye laser with a longitudinal mode spacing of 165 MHz, a 0.5mm thick etalon (quartz, R = 30% coatings) was used in addition to a 3-plate birefringent filter (quartz with optic axis at 25 degrees to the plate). There were 14 Brewster surfaces in the cavity, ensuring significant loss to the unwanted polarisation to ensure efficient frequency doubling. The dye laser itself is similar to the VECSEL in that the laser emission does not have a preferential polarisation direction and gain is available for an unpolarised pump. Since the nonlinear material (ADP) used is polarisation sensitive, to enable effective OPO operation Brewster surfaces were used to define the circulating polarisation in the laser cavity. Without the 14 Brewster surfaces, the laser polarisation would rotate to that of least loss and the OPO would be switched off, making them essential to the successful operation of the ICOPO.

In order to obtain single frequency operation, birefringent tuners and etalons were used. By adding multiple birefringent tuners the laser linewidth is reduced (by designing the thickness of the plates) and the wavelength can be tuned (by rotating them).

4.1.2 Titanium Sapphire

The use of titanium sapphire (Ti:S) laser gain material in a frequency conversion device was first reported by Edwards *et al* in 1998 [4.13]. Most often the Ti:S laser is associated with mode-locking due to its large gain bandwidth however this wide tuning range was also used to tune the signal and idler for a fixed nonlinear crystal. The Ti:S laser is normally pumped by a green linearly polarised laser. The focus in the gain medium tends to be very small, therefore the material is Brewster cut (rather than using AR coatings) to avoid damage due to high circulating fields, hence the laser here is linearly polarised. Birefringent filters are used as an effective tuning mechanism over a large bandwidth. This is preferable to the use of etalons over a large tuning range as the tilting of the etalon to tune the wavelength results in a walk-off loss which increases with the etalon thickness.

4.1.3 Nd-based ICOPOs

Nd-based solid state lasers, as well as suffering from spatial hole burning, also suffer from relaxation oscillations. These occur because the upper state lifetime of the laser gain material is longer than the cavity damping time. The amplitude fluctuations which result from relaxation oscillations make the sources unsuitable as spectroscopic tools, as discussed earlier. This is a key area of research in the nonlinear optics group (at St

Andrews) and a number of ways to solve this problem have now been shown by this group. These include using a high repetition rate Q-switched pump laser to obtain maximum average power without having peak powers which are likely to induce damage on the OPO crystal (here, the repetition rate ties into the cavity damping time such that the oscillations do not become self-sustaining) [4.18]. Most relevant to the case of continuous wave single frequency sources, is the use of second harmonic generation to increase the damping time of the relaxation oscillations such that they have no effect on the amplitude stability of the laser [4.20]. Nd-based systems operate with horizontal polarisation, so polarisation defining elements are not required. As this is a standing wave cavity, there are a finite number of spatially hole burnt modes which have a spacing which is defined by the cavity length (~250GHz) therefore there are only a few modes which overlap with the Nd:YVO_4 crystal. To reduce the modes of oscillation down to one, a single etalon (of prescribed thickness and finesse) can be used thus ensuring that once the relaxation oscillations have been eliminated the laser and therefore idler will operate on a single longitudinal mode.

There is an example of an active stabilisation technique in which the frequency behaviour of the cavity is tied to that of an external source (known as a pump-enhanced IC-OPO) which avoids the need for intracavity frequency selection elements [4.21]. Although this technique was an important development in IC-OPOs, enabling the first Nd-based single continuous wave IC-OPO, it has not been pursued here as one of the main drivers in this project is to keep the cavity as simple as possible. Also, the application of active stabilisation to the VECSEL cavity does not constitute anything new, merely the extension of a known technique to a new problem.

4.2 VECSELs

The key thing that differentiates Vertical, External Cavity Surface Emitting Lasers (VECSELs), (also known as Semiconductor Diode Lasers (SDLs) or Optically Pumped Semiconductor Lasers (OPSLs)) from other semiconductor lasers such as edge emitting diodes or diode bars is that the external cavity and optical pumping enables a low divergence, circular, near diffraction limited, high quality output beam. The combination of the favourable beam quality, short upper state lifetime (eliminating relaxation oscillations), large gain bandwidth (broad tunability range) and the negligible effect of thermal lensing in the gain material makes the VECSEL a promising host for an IC-OPO which can be used for high resolution spectroscopy. The components of a

VECSEL are shown in Figure 4.1 for reference, with the internal structure shown in Figure 1(b).

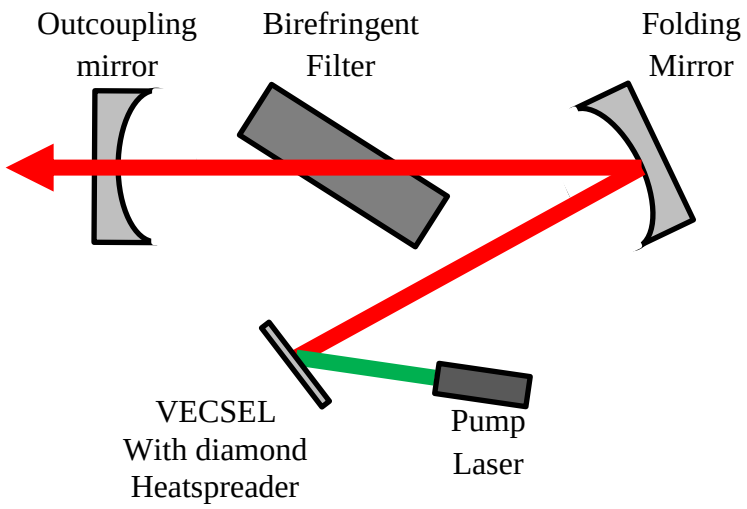

Figure 4.1: VECSEL cavity layout

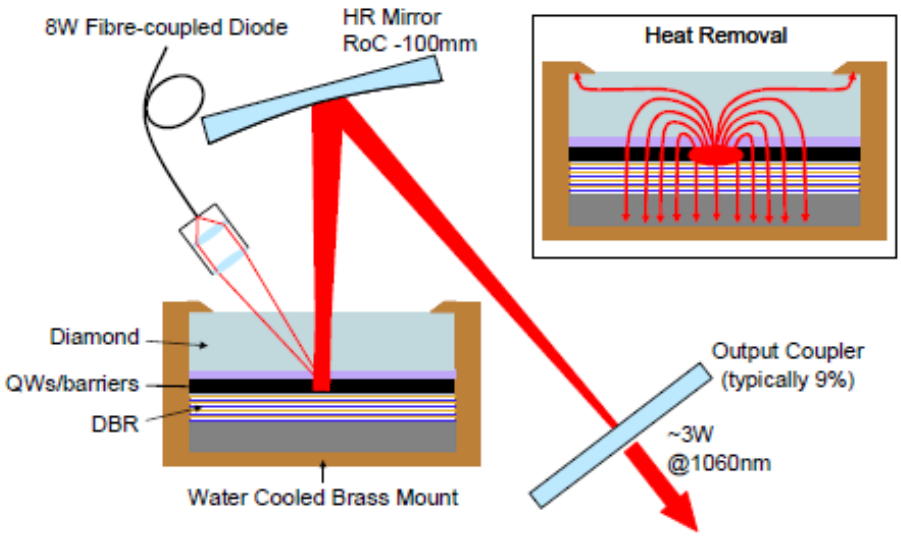

Figure 4.1 (b): VECSEL with intracavity heatspreader (inset shows heat removal paths) [4.19]

The gain structure is grown upon a Bragg mirror with a wide reflectivity range (for the laser discussed later in the chapter this is from ~1040 – 1060nm). The main challenge for building an efficient VECSEL is removing the heat from the chip itself. This is achieved for the VECSEL used here by mounting a diamond heatspreader onto the front face of the chip, and having the whole assembly mounted within a water cooled brass block (as shown in Figure 4.1 (b)).

There have been problems using Nd based materials due to the long upper state lifetime of the Nd atom leading to prolonged bursts of relaxation oscillations in the CW regime. In contrast, the very short upper state lifetime of the VECSEL provides a highly stable amplitude. Furthermore, the thin gain region promotes effective cooling and thus removes any significant thermal lensing in the laser medium which is also systemic in Nd-based lasers. The tuning bandwidth is very broad (tuned via the birefringent filter shown in Figure 4.1) which adds flexibility and, for example, has enabled the generation of THz waves by difference frequency generation [4.4]. VECSELs preferentially operate on a single longitudinal mode which is in some part due to the design of the quantum wells within the VECSEL chip. By placing the quantum wells at the antinodes of the standing wave of the electric field pattern established by the Bragg mirror, gain extraction is maximised and spatial hole burning is avoided [4.5].

An important part of the VECSEL design is the incorporation of a thin (~500μm) sheet of diamond which serves a dual function due to its combination of high thermal conductivity and high optical transmission. Its primary function is to dissipate heat from the diode pump laser but less favourably it also behaves as an intracavity etalon which inhibits smooth tuning across the gain bandwidth. Without effective heat dissipation, the VECSEL output power will be reduced as the quantum well gain falls as the temperature rises. Within the gain region, an increase in temperature will shift the position of the quantum well gain peak relative to the position of the resonance of oscillation, further reducing the gain. If the laser overheats due to excess diode pump, these effects will walk out of alignment and the laser will switch off [4.5].

To date, an IC-OPO based on VECSEL pumping has been demonstrated, but no detailed study of the frequency characteristics of the scheme has been carried out [4.2]. A number of reasons that the VECSEL IC-OPO should have superior frequency stability characteristics compared with a Nd-based system have been described, however inserting a nonlinear crystal is a considerable challenge. A nonlinear crystal behaves like a nonlinear loss in the cavity with down-conversion being an additional output coupling mechanism of the pump. The lack of specificity of the polarisation of the VECSEL beyond the use of a Birefringent Filter/Tuner (BRF) inserted at Brewster's angle results in an interaction between polarisation loss and nonlinear loss. This is shown in Figure 4.2, where (a) shows the dips in power resulting from the occasions where the nonlinear loss due to the OPO is less than the polarisation loss due to the

Brewster surfaces in the cavity, and (b) shows what happens spectrally at these points. In Figure 4.2 (b), the blue trace shows the natural lasing wavelength of the VECSEL with red showing the spectral distortion that occurs when the OPO is in alignment – this results in the OPO being less efficient resulting in the power drops seen in (a). The black trace in (b) shows the effect of adding the BRF – the pump power is depleted resulting in efficient down conversion.

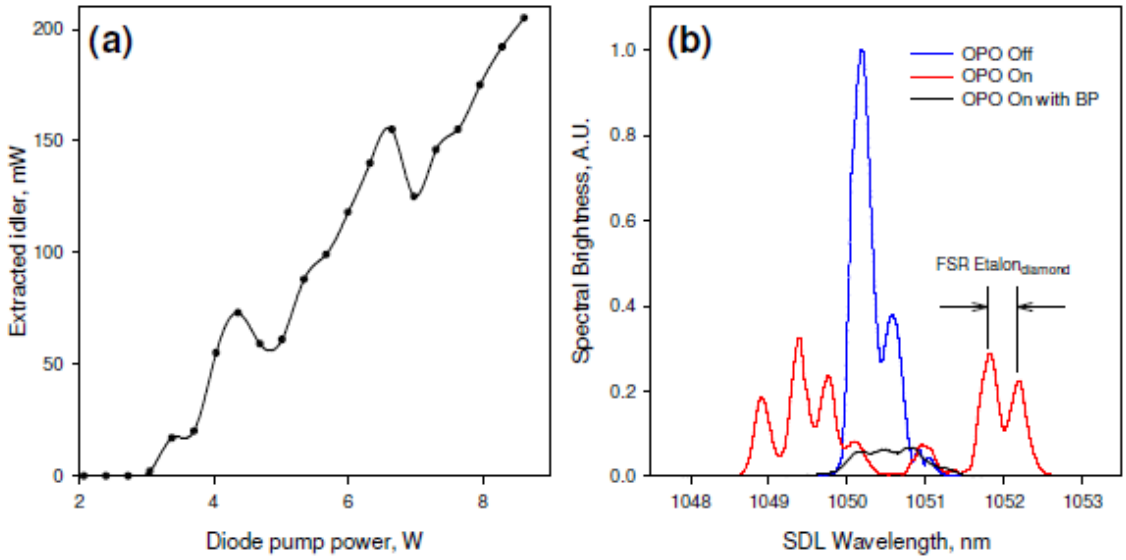

Figure 4.2: (a) Idler output as a function of pump power (with no BRF) and (b) illustration of the wavelength distortion resulting from insufficient polarisation definition [4.2] **(BP = Birefringent Plate)**

If linearly polarised light is incident on a BRF at the first surface the polarisation is switched from linear to elliptical polarisation, and then on exit from the plate only the wavelengths which see an integer number of rotations will have lossless escape from the material, with the remaining wavelengths seeing Brewster loss [4.6]. The addition of more Brewster surfaces increases this polarisation dependent loss, such that the laser operates more effectively by tolerating the nonlinear loss and resulting in more efficient down conversion.

4.2.1 VECSEL frequency behaviour

To provide a base-level for comparison of the VECSEL dynamic, the frequency spectra of the free running VECSEL without the BRF was measured for a range of power levels (see Figure 4.3 (a – c). This shows that at low circulating fields, only a few modes are present and with increasing field additional modes are excited closer to the peak of the VECSEL gain curve at 1050nm. The spacing of these discrete modes arises from the convolution of the diamond heat-spreader which acts as an intracavity etalon with the

cavity modes. Without the BRF to provide extinction, the number of modes increases as the pump power increases, with all active modes around the centre of the VECSEL gain peak of 1050nm but a bandwidth exceeding 20nm from 1040 to 1060nm. The bandgap of the semiconductor, which defines the lasing wavelength, is temperature sensitive so when the pump power is increased a red shift in wavelength is seen in the spectra.

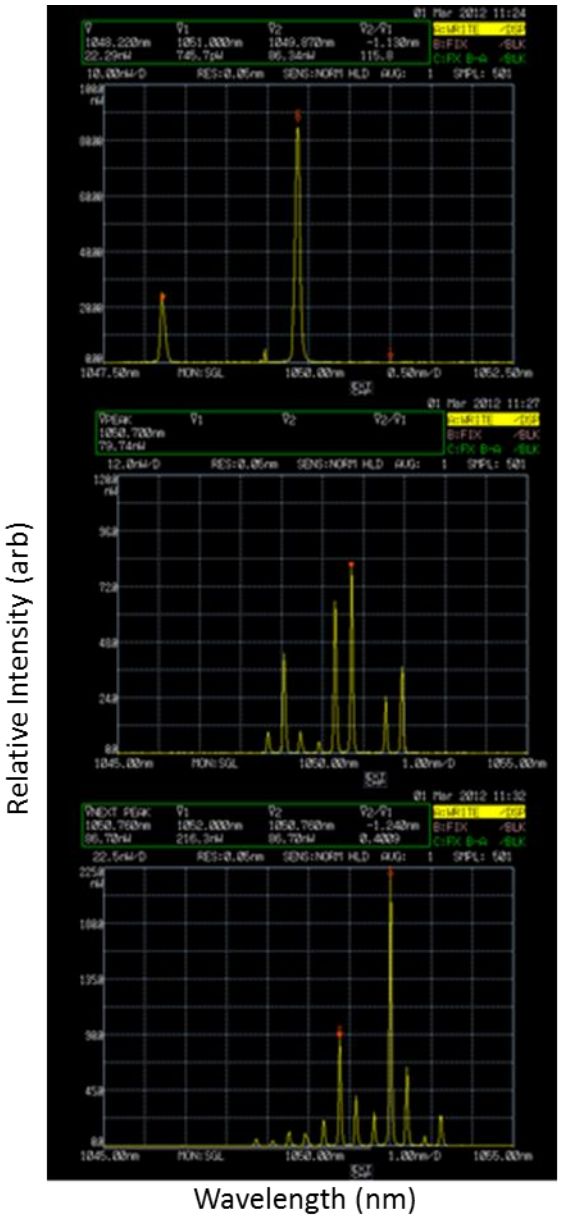

Figure 4.3: VECSEL spectra (cavity without a BRF) measured using an Optical Spectrum Analyser (OSA) when pumped with a diode pump power of (a) 2, (b) 4.8 and (c) 8.6W (x- axis range is from 1045 – 1065nm)

By adding a BRF to the cavity (with no nonlinear element) the laser operates on a single longitudinal mode. The linewidth of the peaks shown in Figure 4.3 is 0.1 nm which is close to the limit of the instrument resolution (0.05nm). Therefore the OSA cannot be relied upon for an accurate linewidth and confirmation of single frequency operation. In

addition to the OSA, a scanning Fabry Perot Interferometer (FPI) with a free spectral range of 2 GHz is used to obtain fine spectral resolution (a sample trace is shown in Figure 4.4). These techniques need to be executed in parallel in order to observe when the laser is running on a single frequency as there could be overlapping modes shown as a single mode on the FPI from adjacent diamond modes.

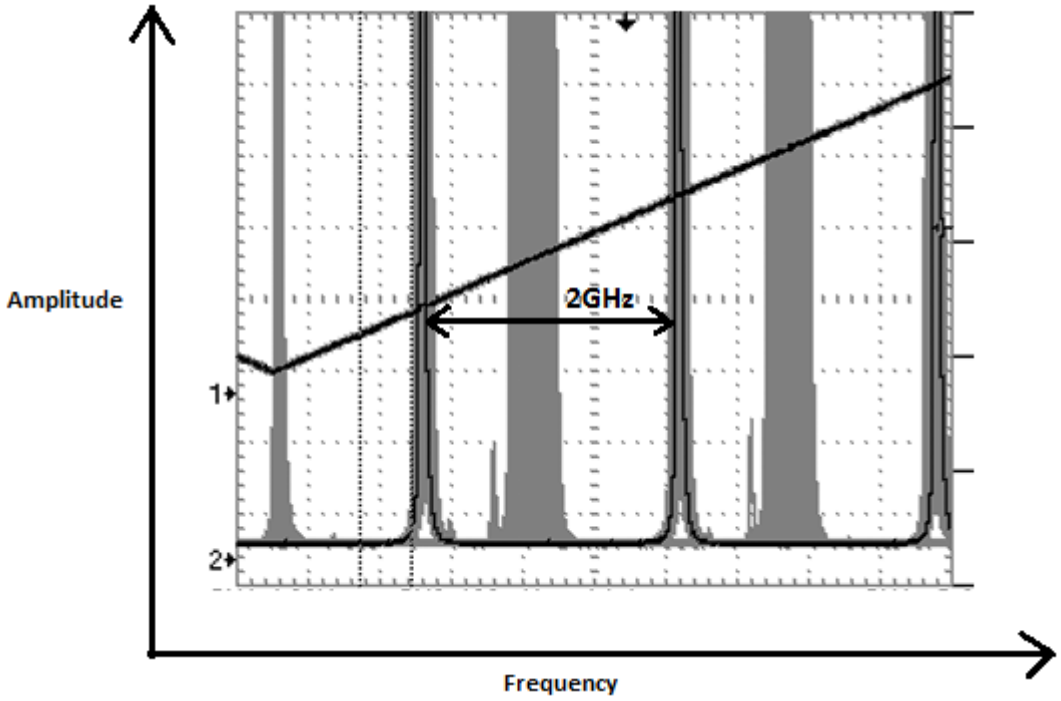

Figure 4.4: 2GHz Scanning Fabry Perot Interferometer trace showing the occasional mode hop (grey regions)

Using the BRF, the wavelength can be systematically hopped between diamond modes over the range 1039 – 1060 nm shown in Figure 4.5 which is limited by the reflectivity of the Bragg grating that is integrated in the VECSEL structure (each of the wavelength peaks in the Figure is associated with a single longitudinal mode, but using the 'hold' function of the OSA this image was built up over the full tuning range).

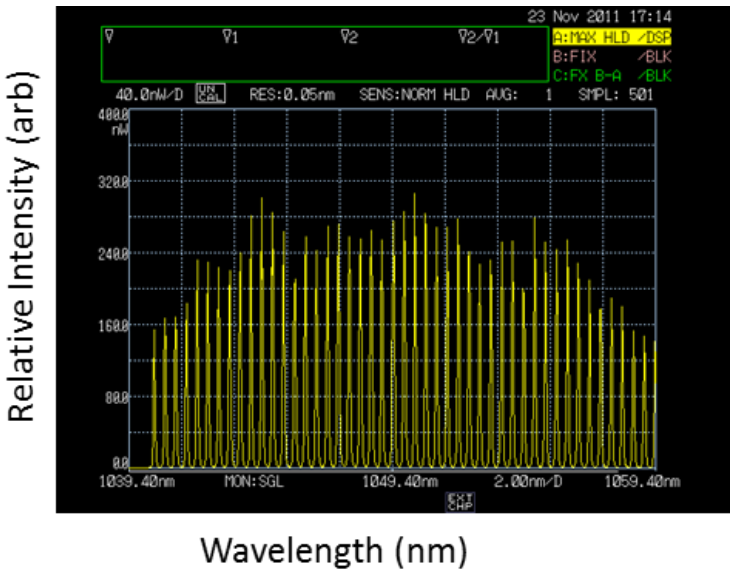

Figure 4.5: OSA trace showing the cumulative modes available when mode hopping across the tuning range of the VECSEL (1039 – 1059nm). The 'hold' function of the OSA was used to build up this image.

This frequency stability was observed over a range of cavity lengths (although mode hops were found to be more frequent at longer cavity lengths due to increased sensitivity to mechanical perturbations via mechanical instability, or air currents). The circulating field was unchanged for all cavity lengths tested, confirming that the laser is single frequency as a result of frequency selection rather than being due to a low circulating field (this observation becomes important in later comparative work). If the frequency selective components of the cavity are modelled, it becomes evident that the single frequency operation is not predicted.

4.2.2 Modelling of frequency selective elements

Having observed experimentally that the birefringent filter (BRF) is sufficient to enable stable single frequency operation for the VECSEL, a model was developed by the author based on the results of Preuss [4.7] and used for verification and further development of the cavity design. The behaviour of BRF used in the VECSEL cavity was probed externally using a linearly polarised HeNe laser and a polariser to determine the transmission of the BRF at different angles of rotation (as shown in Figure 4.6) and compared with the matrices developed by Preuss [4.7].

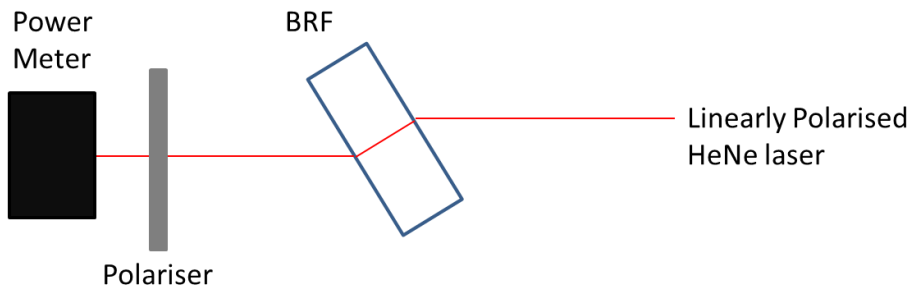

Figure 4.6: Set-up used for determining the transmission of the BRF as it is rotated (BRF fixed at Brewsters angle and rotated around the plane of the beam)

In order to validate the method of characterising the BRFs a known 1mm thick etalon was characterised – a comparison between the model and the experiment is shown in Figure 4.7.

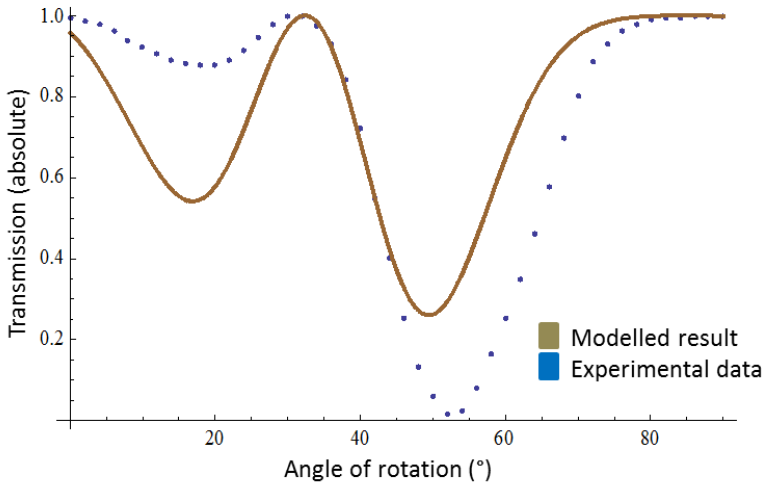

Figure 4.7: Comparison of the model with the experimental result for a 1mm thick quartz BRF (characterised using a 633nm HeNe laser)

There is a discrepancy in the magnitudes of the transmission between the model and the experimental results shown in Figure 4.7 however the trends in the transmission are sound.

Having validated the method, the transmission of the BRF was measured as a function of angle. This is plotted in Figure 4.8, together with the expected (modelled) transmission.

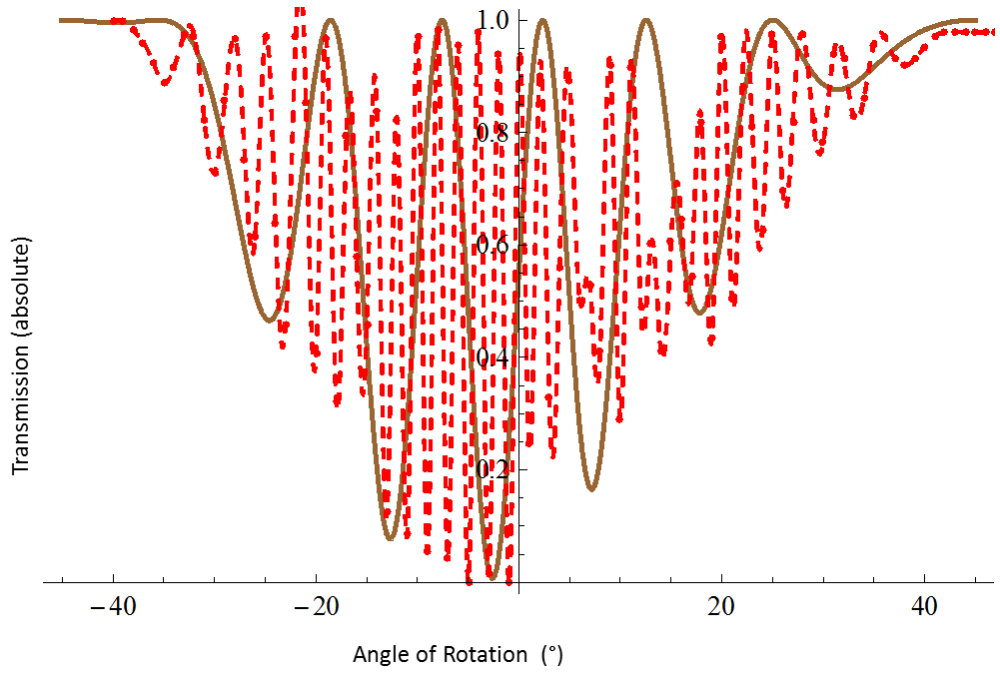

Figure 4.8: Solid line: Modelled BRF result using Preuss analysis for 5mm thick BRF, Dashed line: Experimental result

From Figure 4.8, it is clear that the model for a 5mm thick BRF, which assumed that the optic axis is along the surface of the plate is not an accurate representation of the observed behaviour. Another model which was examined, by Zhu (1999) [4.8], included terms which allowed the optic axis to be outwith that plane, however, the only way to arrive at a solution for this particular BRF (in the absence of a data sheet) would be to use an iterative approach, which would provide only limited insight. From the measured data, the BRF which was supplied with the VECSEL was more selective than a plate of the same dimensions with the plane along the surface of the optic. It was concluded that from an engineering perspective, the measured increased selectivity was more important in this case than understanding exactly the cut angle of the material and the efforts to understand this particular filter were terminated here.

Other methods of increasing the spectral selectivity include using multiple filters – this is modelled in the following section. The variation in spectral selectivity afforded by varying the thickness of the material is considered in Figure 4.9 which looks at the effect of stacking BRFs to reduce the spectral bandwidth of the laser similar to the methods that were employed for single frequency dye lasers [4.10].

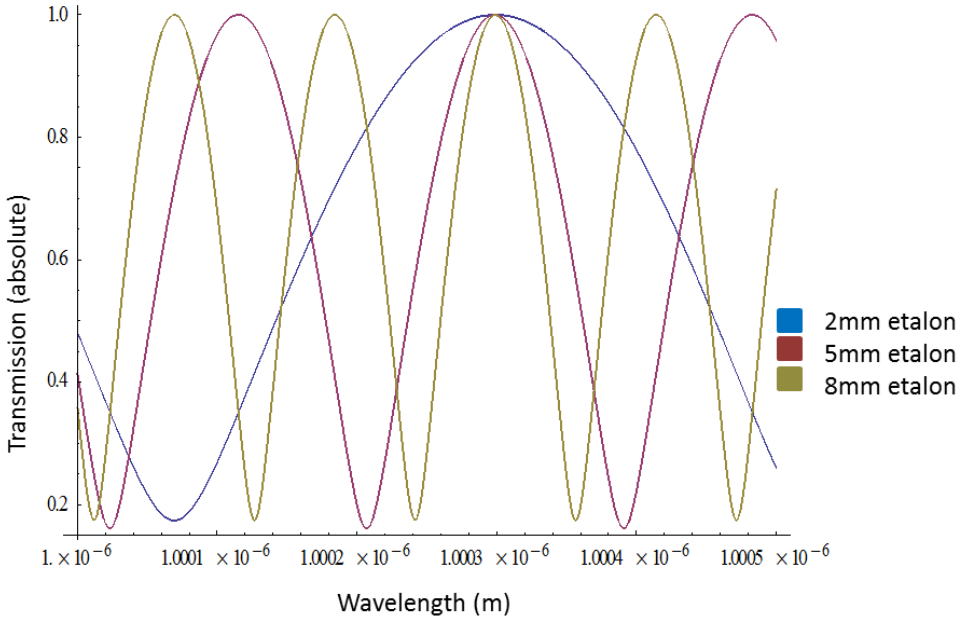

Figure 4.9: Modelled transmission spectra of 3 BRF plates (2mm, 5mm and 8mm) overlapped to show the plates working together to narrow the linewidth

Having examined at the effect of adding multiple BRFs of various thicknesses to increase spectral line narrowing, the addition of etalons will now be considered in the context of the cavity as a whole. The Free Spectral Range (FSR) of an etalon is $\frac{c}{2nL}$ where n is the refractive index and L is the thickness of the etalon, the values of FSR for the different optical components must be considered when looking for the most useful element to reduce the laser to single frequency operation. The intrinsic elements which have been used so far are summarised in Table , and illustrated in Figure 4.10.

Table 4.1: Free Spectral Range/Bandwidths of the cavity elements

Cavity element	**FSR/bandwidth**
Cavity axial modes (350mm cavity)	430MHz FSR
BRF	20GHz Bandwidth
Diamond etalon	110GHz FSR

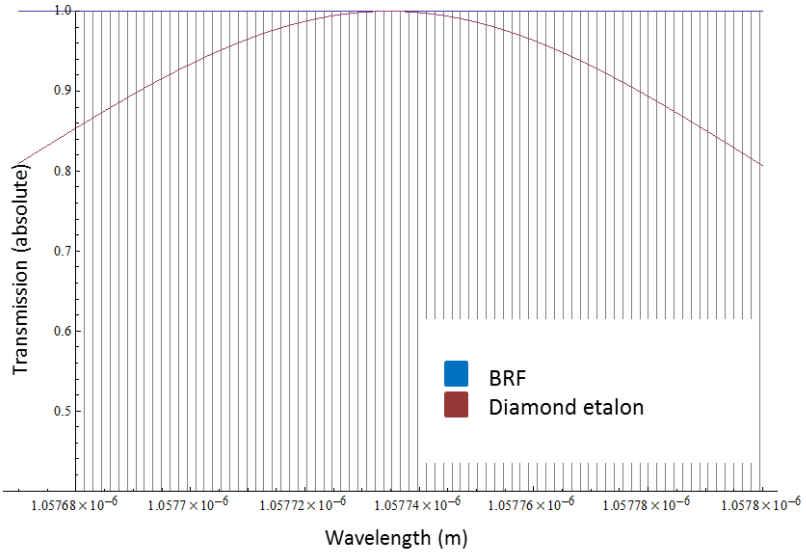

Figure 4.10: Modelled transmission of the intrinsic frequency selective components of the VECSEL cavity (as described in Table)

From Figure 4.10 it is clear that there are a large number of cavity modes which see high transmission with only the diamond etalon and the BRF in place. What follows is a theoretical analysis of 2 additional off-the-shelf etalons (described in Table), as the 1mm BRF described in Figure 4.7 has insufficient discrimination to be useful, which could potentially be implemented to force the number of lasing cavity modes down to one.

Table 4.2: FSR and finesse of off-the-shelf etalons for use in the VECSEL cavity

Material (label)	Etalon FSR (GHz)	Thickness (mm)	Finesse
Quartz	10GHz	10	15
YAG	820GHz	0.1	1

Due to the contrast between the FSR of the cavity modes and the bandwidths of the frequency selective elements making the plots difficult to read, the cavity modes have been removed when investigating the addition of the off-the-shelf etalons. In Figure 4.11, the BRF transmission is plotted alongside the YAG and the diamond etalon and in Figure 4.12, the cavity modes are added on a much reduced wavelength scale. Conventionally, these graphs are plotted against frequency due to the reciprocal nature

of frequency and wavelength, however over such a small range (5nm) this is not deemed to be a problem.

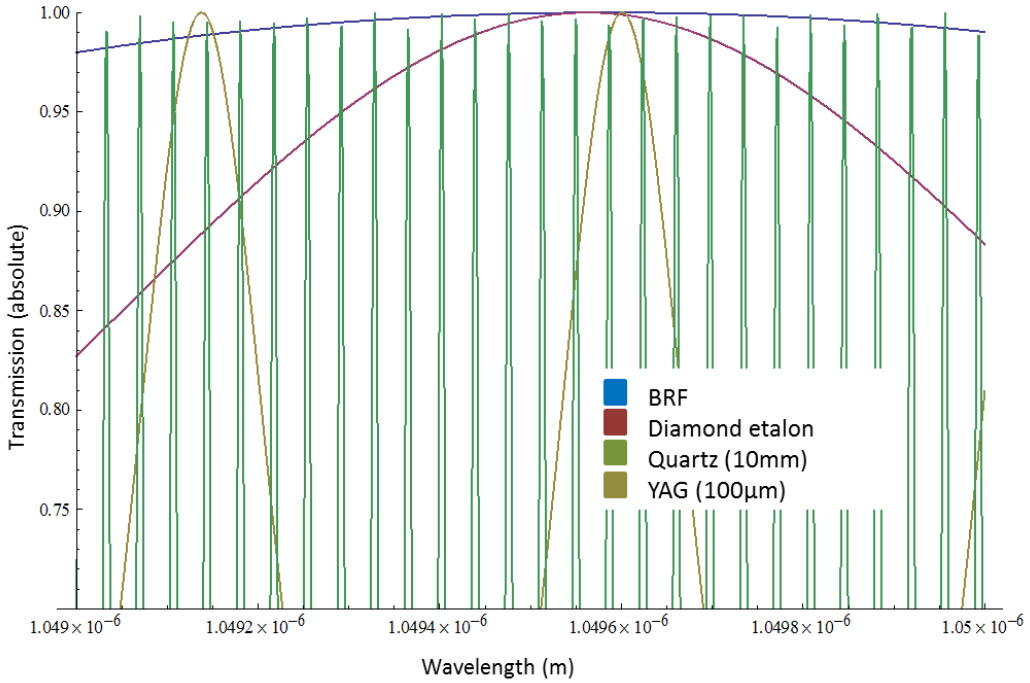

Figure 4.11: Modelled frequency spectra (over 1nm) of VECSEL cavity elements with additional off-the-shelf etalons

The coarse spectrum modelled in Figure 4.11 indicates that the addition of both the 10mm quartz etalon and the 100µm YAG etalon in the cavity discriminate to a very narrow wavelength region. Further detail of how the axial modes fit into this model is shown in Figure 4.12 showing that this combination would successfully result in a single lasing cavity mode.

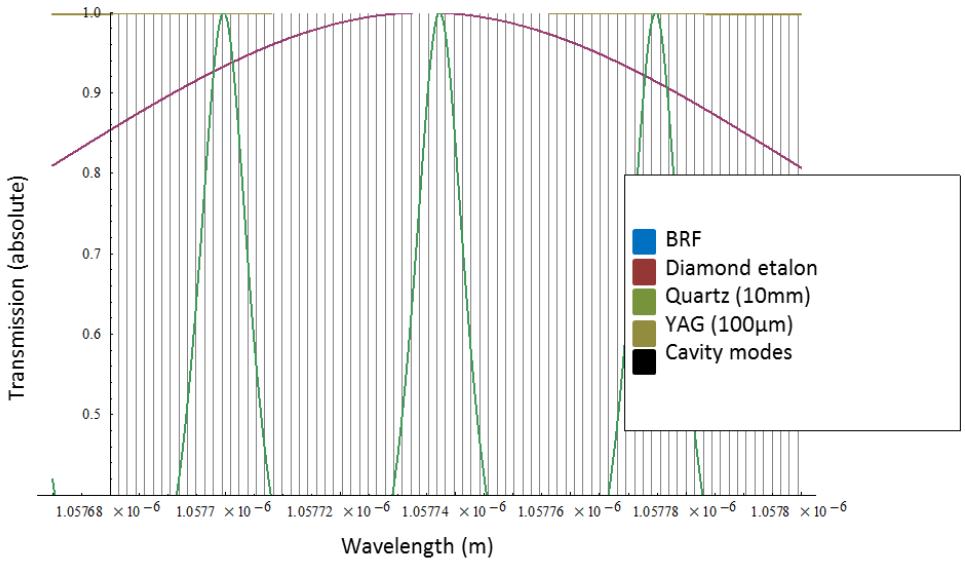

Figure 4.12: Axial mode selectivity of the BRF, diamond, quartz and YAG etalons (BRF is flat over this range)

From this, you can see that in close detail, that a number of elements are required to reduce the number of lasing cavity modes to one, and when examined closely on the scale shown (<1nm) the BRF and the YAG etalon barely influence the spectra. This analysis coupled with the observed single frequency behaviour of the VECSEL suggests that there may still be something subtle in the design of the VECSEL which is integral in enabling single frequency operation. The lack of selectivity down to the single axial mode supports the theory that the frequency instability could be due to increased sensitivity to any cavity feedback. The single frequency operation of the VECSEL is challenging if it is to be maintained over long periods of time and has been the subject of at least one PhD thesis [2006 - [4.9]].

4.3 Summary

It has been shown that given the excellent beam quality, thermal management, the lack of spatial hole burning and most importantly the short upper state lifetime of the VECSEL makes it a good candidate for hosting an IC-OPO. Additionally, a review of ICOPO over a range of laser gain media was carried out, detailing any frequency selection mechanisms which were successful. From the examples in section 4.1 there are no obvious indicators that the addition of PPLN should cause a problem. Although it has already been mentioned that a CW, relaxation-oscillation free system has been realised in a Nd-based system, the VECSEL solution potentially offers a more compact footprint (by a factor of ~2) with tunability of the pump wavelength. In order to obtain a continuously tunable IC-OPO, a PPLN with fanned (rather than fixed) grating period

has been used [4.18], by fixing the grating and exploiting the tunability of the VECSEL a simpler, and cheaper architecture can be realised.

In the following chapter the implications of adding nonlinear components to this cavity will be examined, in particular their effect on the frequency characteristics of the parent laser.

4.4 References

[4.1] W. R. Bosenberg, a Drobshoff, J. I. Alexander, L. E. Myers, and R. L. Byer, "Continuous-wave singly resonant optical parametric oscillator based on periodically poled $LiNbO_3$," *Optics letters*, vol. 21, no. 10, pp. 713–715, May 1996.

[4.2] D. J. M. Stothard, J. Hopkins, D. Burns, and M. H. Dunn, "Intracavity Optical Parametric Oscillator pumped by a Semiconductor Disk Laser (VECSEL)," *Optics Express*, vol. 17, no. 13, pp. 10648–10658, 2009.

[4.3] D. J. M. Stothard and M. H. Dunn, "Relaxation oscillation suppression in continuous-wave intracavity optical parametric oscillators.," *Optics express*, vol. 18, no. 2, pp. 1336–1348, Jan. 2010.

[4.4] M. Scheller, J. Yarborough, J. Moloney, M. Fallahi, M. Koch, and S. Koch, "Intracavity Generation of Continuous Wave Terahertz Radiation in the Milliwatt Regime," in *CLEO:2011 - Laser Applications to Photonic Applications, OSA Technical Digest (CD) (Optical Society of America, 2011)*, paper CMFF1.

[4.5] M. D. Calvez, S., Hastie, J. E., Kemp, A. J., Laurand, N., Dawson, "Chapter 2," in *Semiconductor Disk Lasers*, 1st ed., O. G. Okhotnikov, Ed. Wiley VCH, pp. 74–94, 2010.

[4.6] = [4.10]

[4.7] D. R. Preuss and J. L. Gole, "Three-stage birefringent filter tuning smoothly over the visible region : theoretical treatment and experimental design," *Applied Optics*, vol. 19, no. 5, pp. 702 - 710, 1980.

[4.8] S. Zhu, "Birefringent filter with tilted optic axis for tuning dye lasers: theory and design.," *Applied optics*, vol. 29, no. 3, pp. 410–415, Jan. 1990.

[4.9] K. Gardner, "Single Frequency VECSELs," University of Strathclyde, 2006.

[4.10] C. Wagstaff, "A second-harmonic, ring dye laser for the generation of continuous-wave, single-frequency UV radiation," *Journal of Physics D: Applied Physics*, vol. 355, pp. 355 - 368 1979.

[4.11] A. Ferguson and M. Dunn, "A tunable, frequency-doubled, continuous-wave dye laser using ADA," *Optics Communications*, vol. 23, no. 2, pp. 177–182, 1977.

[4.12] L. H. Tan and P. B. Phua, "Generation of watt level mid-infrared wavelengths using intra-cavity ZnGeP2 OPO within a 2.1μm Ho:YAG laser," *Proc. SPIE 7917, Nonlinear Frequency Generation and Conversion: Materials, Devices, and Applications X*, 79170O (February 21, 2011).

[4.13] T. J. Edwards, G. a Turnbull, M. H. Dunn, M. Ebrahimzadeh, H. Karlsson, G. Arvidsson, and F. Laurell, "Continuous-wave singly resonant optical parametric

oscillator based on periodically poled RbTiOAsO(4).," *Optics letters*, vol. 23, no. 11, pp. 837–839, Jun. 1998.

[4.14] W. R. Bosenberg and D. R. Guyer, "Broadly tunable, single-frequency optical parametric frequency-conversion system," *Journal of the Optical Society of America B*, vol. 10, no. 9, p. 1716, Sep. 1993.

[4.15] G. Robertson, M. J. Padgett, and M. H. Dunn, "Continuous-wave singly resonant pump-enhanced type II LiB_3O_5 optical parametric oscillator.," *Optics letters*, vol. 19, no. 21, pp. 1735–1737, Nov. 1994.

[4.16] K. Schneider, P. Kramper, S. Schiller, and J. Mlynek, "Toward an optical synthesizer: a single-frequency parametric oscillator using periodically poled $LiNbO_3$," *Optics letters*, vol. 22, no. 17, pp. 1293–1295, Sep. 1997.

[4.17] H. W.Schroder, L. Stein, D. Frolich, B. Fugger and H. Welling , "A high-power single-mode cw dye laser," *Applied Physics A*, vol. 14, no. 4, pp. 377–380, 1977.

[4.18] D. J. M. Stothard, C. F. Rae, and M. H. Dunn, "An Intracavity Optical Parametric Oscillator With Very High Repetition Rate and Broad Tunability Based Upon Room Temperature Periodically Poled MgO : $LiNbO_3$ With Fanned Grating Design," *IEEE Journal of Quantum Electronics*, vol. 45, no. 3, pp. 256–263, 2009.

[4.19] F. v. Loon, A.J. Kemp,A.J. Maclean, S. Calvez, J.-M. Hopkins, J. E. Hastie, M. D. Dawson, D. Burns, "Intracavity diamond heatspreaders in lasers: the effects of birefringence" *Optics Express*, vol. 14, no. 20, pp 9250-9260, October 2006

[4.20] D. J. M. Stothard and M. H. Dunn, " Relaxation oscillation suppression in continuous-wave intracavity optical parametric oscillators" *Optics Express*, vol. 18, no. 2, pp. 1336-1348, 2010

[4.21] D. J. M. Stothard, I. D. Lindsay and M. H. Dunn, "Continuous-wave pump-enhanced optical parametric oscillator with ring resonator for wide and continuous tuning of single frequency radiation" *Optics Express*, vol. 12, no. 3, pp. 502-511, 2004

5 VECSEL IC-OPO – towards the single frequency source for spectroscopy

The key objective for this chapter is to bring the knowledge described in Chapter 4, and apply it to the VECSEL IC-OPO with the aim of enabling single frequency operation. The VECSEL IC-OPO set-up is shown in Figure 5.1. If this is compared to the VECSEL described in the previous chapter, the differences are that (i) the cavity is linear, to make it easier to accommodate intracavity elements; (ii) the end mirror is now curved; and (iii) the cavity has been extended to allow insertion of an additional lens and the nonlinear crystal.

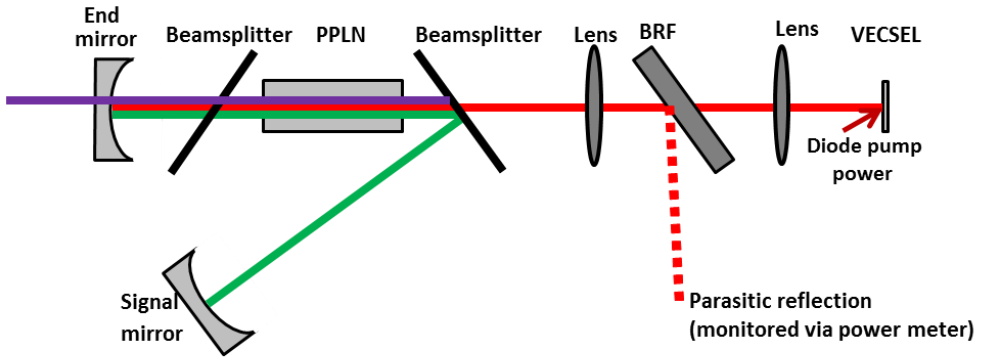

Figure 5.1 : Layout for VECSEL ICOPO showing all intracavity elements (red – pump; green – signal; purple – idler) and the parasitic pump reflection used for diagnostics

The VECSEL IC-OPO did not run single frequency naturally, therefore further investigation was required. The first part of this chapter describes the tests which were carried out in order to ascertain the factor(s) that may be inhibiting single frequency operation and hence develop the most likely hypotheses for the frequency instability. The chapter then goes on to describe the results of these measurements.

5.1 Towards the Single Frequency VECSEL IC-OPO

Having gathered evidence to suggest that the VECSEL is a reasonably stable single frequency laser (with no active stabilisation) in chapter 4, it had been anticipated that when the PPLN was inserted into the laser cavity, the laser would continue to perform in the same way. However, the observed frequency stability was compromised, showing rapid and random frequency fluctuations and only occasionally and briefly (≤ 1 second) operating close to single frequency.

The initial hypothesis to explain this behaviour was the effect of parasitic cavities forming between the elements in the cavity. To test this hypothesis the PPLN was tilted off-axis to remove at least one of the parasitic cavities and hence improve the frequency stability. This worked as expected, however the OPO action ceased. An alternative solution was to expand the cavity length to allow the insertion of a second beamsplitter between the PPLN and the end mirror allowing the OPO cavity to be completely decoupled from the parent laser cavity, as shown in Figure 5.2. This resulted in a severe reduction in the circulating field and therefore the OPO barely operated above its threshold, hence any improvement in single frequency operation could also have been a result of the reduction in the circulating field due to increased cavity loss.

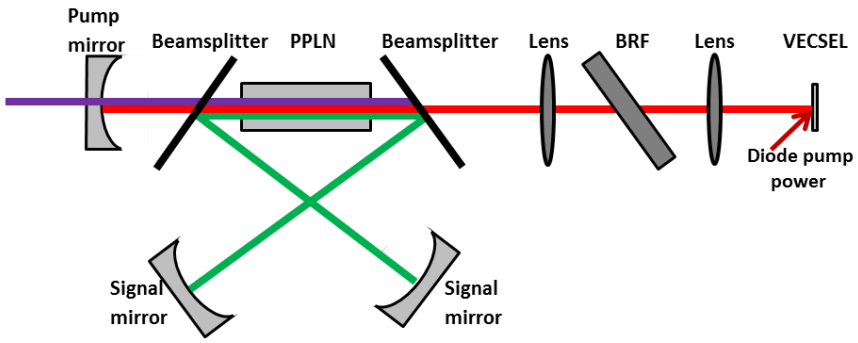

Figure 5.2 : PPLN IC-OPO with signal cavity decoupled from pump laser (VECSEL) cavity (pump – red; signal – green; idler – purple)

A number of nonlinear crystals were tested in the laser cavity without the addition of signal cavity mirrors, to determine whether there was something in the nonlinear response of the material which was causing instabilities rather than the problem being mechanical. A number of different types of PPLN were tested (limited by availability) and the behaviour was subtly different in each. The full history of each of these samples is unknown, but detailed to the best of the authors' knowledge:

- Samples A – C were obtained and coated by HC Photonics
- The fanned PPLN grating period was from 27.0 – 32.5μm (as described in [5.4]
- Samples A and B – dimensions: 0.5 x 15 x 40mm
- None of the samples were from the same batch
- Sample D
    - From Covesion (for room temperature SHG)
    - facets wedged in x and y
    - Dimensions 1 x 10 x 15mm

Sample	Description	AR coating wavelengths
Sample A	Fanned MgO:PPLN for OPO	AR@1064nm, signal and idler
Sample B	Fanned MgO:PPLN for OPO	
Sample C	Unpoled LN for THz generation	AR@1064nm
Sample D	Wedged MgO:PPLN for SHG (6.96μm period)	AR@1064/532nm

Table 5.1: Summary of materials tested intracavity for their effects on frequency stability

Unfortunately, due to the qualitative nature of the observations it was not possible to quantify the extent of any improvements and conclusions had to be made based on trends between the available crystals.

The frequency behaviour of the laser including the samples listed in Table was examined using the Fabry-Perot interferometer (via the parasitic reflection shown in Figure 5.3) and the intracavity field monitored via the intracavity beamsplitter with the lithium niobate both on and off-axis as shown in Figure 5.3.

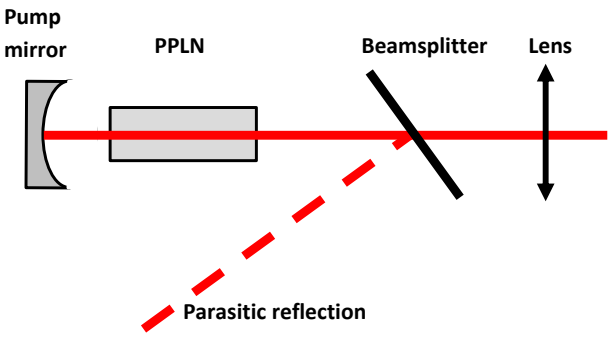

(a)

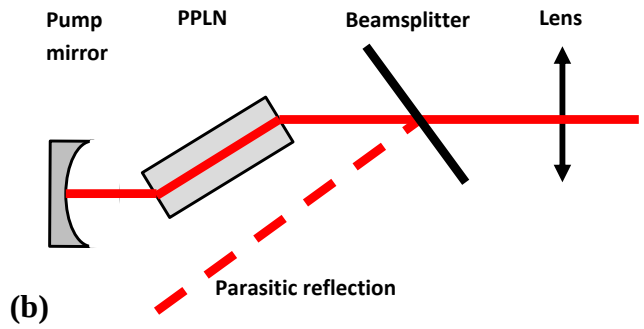

Figure 5.3: Configuration of the end section of the VECSEL used for characterising the reduction in circulating field (via the parasitic reflection from the beamsplitter) due to the PPLN. In (b) the offset angle is exaggerated for clarity. The parasitic reflection is monitored by a power meter for diagnostic purposes (the pump field is shown by the red line)

With sample A an improvement was observed when the crystal was tilted off axis relative to the optic axis without significant compromise to circulating field; by improvement it is meant that the single frequency occurrences were more frequent and lasted slightly longer. This led to the hypothesis that back reflections from the crystal coatings were causing coupled cavities between the crystal facets and other optical elements in the cavity. This sample was retired as it showed signs of coating damage across the tuning range. With sample B there was a slight improvement when it was tilted off-axis (as shown in Figure 5.3(b)), but with considerable reduction in the available field. In the original sample (A), it was possible to identify when the crystal was on-axis due to the significant change in frequency behaviour. Given that A and B are nominally identical this difference in behaviour was unexpected and at best provides an indication of the variability of PPLN from different batches with different coating runs. Further testing was carried out by substituting a piece of unpoled lithium niobate (Sample C) which was designed for IC-OPO based THz generation and therefore coated at 1064nm [5.5]. This showed clear improvements in that single frequency operation of the laser could be observed for seconds at a time. Finally, the cavity was tested with the wedged PPLN designed for SHG (Sample D). This was not an ideal comparison, as the crystal length, coatings and parallelism of the facets were all different. However, this was the only wedged crystal sample available and it did show significant improvement compared to the fanned OPO crystals. It was based on this observation that the decision was made to modify one of the plane-parallel PPLN crystals by polishing the end faces to create a 2° wedge.

In order to generate the high circulating field necessary to achieve OPO threshold, the cavities constructed use highly reflective mirrors to create a high finesse cavity. To

characterise the total loss (as it was not possible to differentiate between coating loss and material loss) of the PPLN crystals, a method of monitoring the circulating field is required. This was done via the parasitic reflection from an angled intracavity element (beamsplitter). The intracavity field was initially calibrated by replacing the end mirror of the laser cavity (which contained the same intracavity elements, with the exception of the nonlinear crystal) with a 10% output coupler, and measuring the output power from the laser and the parasitic reflection from the beamsplitters (the set-up used is shown in Figure 5.4). The value of the parasitic reflection can then be used to infer the circulating field in the cavity, when the output coupler is replaced by the high reflector, and hence evaluate the intracavity losses introduced by the various crystals.

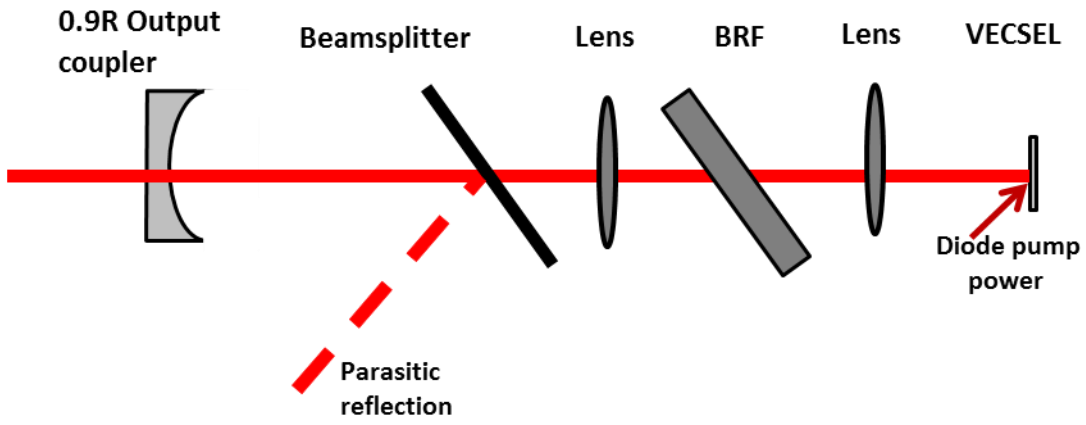

Figure 5.4: Set-up used to calibrate circulating field via parasitic reflection (to power meter; red – pump field)

Figure 5.5 (below) shows a typical chaotic frequency trace. Here the 'infinite persist' function of the oscilloscope is used to give an indication of the temporal instability.

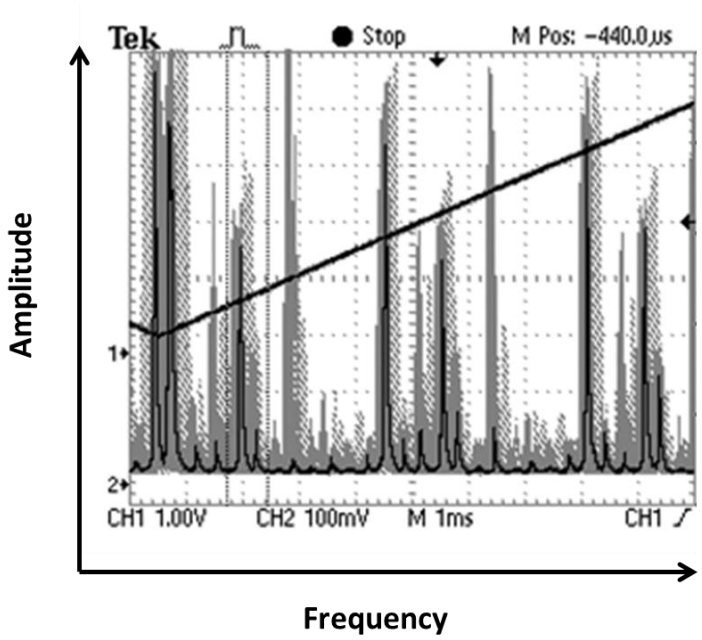

Figure 5.5 : Chaotic frequency behavious shown on a Fabry Perot Interferometer using the persist function to show time variance for sample A

The wedged PPLN designed for SHG (sample D) showed a discernible improvement in providing frequency stability with single frequency operation being observable for seconds at a time (followed by mode-hopping). Unfortunately this sample was different to the OPO crystals in that it was shorter, designed for SHG and was wedged in both the horizontal and vertical axes of the crystal, so the improved performance cannot be explicitly attributed to an improvement in coatings or to the eradication of interference from the crystal facets due to the wedge.

From the observations listed so far, the evidence suggests that PPLN OPO crystals specifically display a feedback problem, however the behaviour observed between the crystals was not consistent. When the specimens studied are compared by type, the crystals with the coatings that cover a narrower wavelength range (AR 1064/532nm for SHG compared with tr-band OPO broad bandwidth OPO coatings) provided greater confidence that single frequency operation was achievable in the IC-OPO configuration. Over the small trial range, the single wavelength AR coating had a lower reflectivity than the SHG crystal (dual wavelength coated) or the OPO crystals which not only are tri-band coated, but with a specified bandwidth over the signal and idler tuning ranges. This lead to the conclusion that a single frequency IC-OPO would be more feasible if the bandwidth over the signal and idler wavelengths was compromised in favour of minimising the losses. Referring back to the comparison between samples A and B

(with OPO coatings), as there are multiple coating layers these may have larger sample-to-sample variations accounting for the differing frequency effects. An additional problem is that the crystal coatings were originally designed for 1064nm when the peak of the VECSEL gain curve is at 1050nm. The loss of the coated PPLN (sample A), measured in transmission using a 1W VECSEL laser, is shown in Figure 5.6.

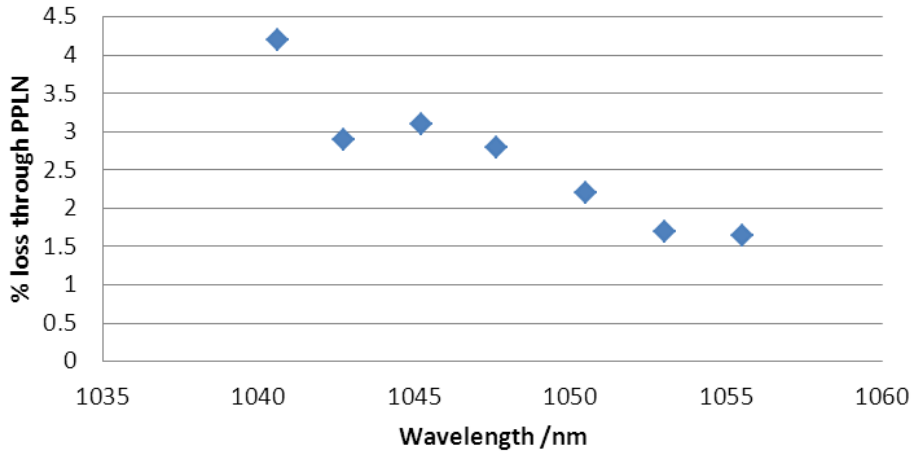

Figure 5.6: Transmission loss through PPLN

It is clear that although the coating performs reasonably well at 1050nm, it was not optimised for this wavelength.

Given the results described above, i.e. the frequency response of the VECSEL cavity containing different LN crystals, and the evidence of non-optimal OPO PPLN coatings, it was concluded that the 2 PPLN crystals designed for OPO operation should be reworked. Both were provided with improved AR coatings (see 5.2 below) and one was wedged on both the entry and exit facets to enable a direct comparison between the wedged and planar crystals with exactly the same coating, plus enabling a comparison to be made with the samples that have already been described. The results from this experimental comparison are described in section 5.5.

Another hypothesis is that there is simply insufficient selectivity in the cavity to reduce operation to a single mode. This was tested using two etalons of differing free spectral range (FSR)/finesse, and is described in section 6.3.

5.2 Re-design of crystal and coating

The standard nonlinear crystal used by the Nonlinear Optics group in St Andrews (where these experiments were carried out) has a fanned grating to enable potentially

seamless tuning over a wide range of wavelengths from a fixed pump source with appropriate motorised stages and cavity length control to prevent mode hopping. This provides challenges for the antireflection coating design because it has to cover all possible signal and idler wavelengths. There is the additional challenge here of covering a range of different pump wavelengths, given the tuning range of the VECSEL. The process of choosing an appropriate coating is discussed below and the rationale for the coating selection is described.

5.2.1 PPLN Coatings

Multi-layer dielectric coatings use layers of different refractive index, either $\lambda/4$ or $\lambda/2$ thick, deposited onto a substrate. If the coating is only required to be optimised for a single wavelength, it can be relatively simple consisting of only a few dielectric layers and hence inexpensive; however as the required bandwidth increases the coating design becomes more complex. Additionally, coatings in the infrared are challenging due to the increased thickness of the layers, and thus the overall thickness of the coating becomes greater which may lead to delamination due to surface stress [5.1]. Usually an anti-reflection coating has 2 – 4 layers, whereas the specifications for the OPO crystal involve at least 7 layers. The capability limit of the IR coatings was shown in Chapter 4 in the case of the ZGP mirror coatings which had a ~15% reflective coating on the rear surface that could not be minimised further due to absorption of the materials used to make the coating.

Laseroptik are the coating company which was used to design and apply the coating, the coating methods they use are Ion Beam Sputtering (IBS) and Electron Beam deposition (e-beam). The former has the lowest scattering and absorption losses and the e-beam technique is less precise for the mid IR wavelengths required here. The method used depends on the quality of the coating that is required and, to a certain extent, the available budget. Each additional coating layer adds complexity and expense.

For an OPO based on fanned grating PPLN to operate successfully, a good quality AR coating (R<1%) is required across the pump wavelengths and the full range of signal and idler wavelengths. This was impossible for the coating company to achieve with the techniques available and the limitation in the materials which can be used. The compromise between the quality of AR coating and the specified bandwidths is shown in Figure 5.7 (the data from the coating simulation provided by Laseroptik has been

extracted and re-plotted in this graph over the pump/signal wavelength range). This figure illustrates the significant improvement in the AR coating as the bandwidth is reduced in the signal wavelength region from 250nm (1450 – 1900nm) to 150nm (1470 – 1720nm). In the red trace both the signal bandwidth was reduced and a smaller bandwidth at the pump was requested. The hypothesis that the frequency instability is a result of feedback from the coatings in the VECSEL cavity led to the decision to pursue the best AR coating possible at the expense of bandwidth in order to improve the performance.

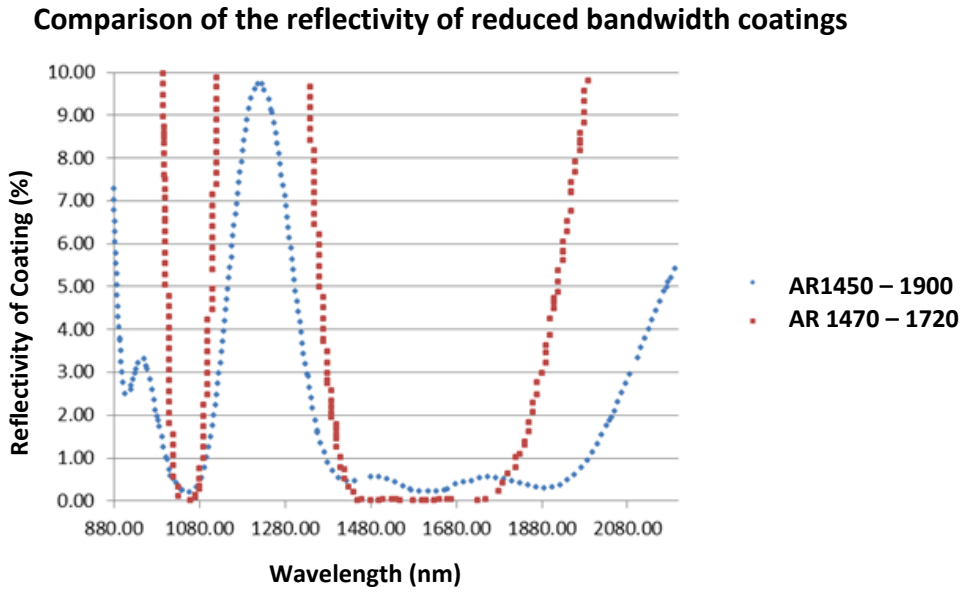

Figure 5.7 : Calculated coating reflectivity of wavelength AR1450 - 1900 (blue) and AR1470 – 1720 (red) coating designed for reduced bandwidth requirement (Data supplied by Laseroptik)

Figure 5.8 and Figure 5.9 show the reflectivity spectra of the same coatings as Figure 7, but with the x-axis extended to include the idler wavelengths (again, these Figures are the coating simulations provided by Laseroptik). Having seen in Figure 5.7 that the reduction in bandwidth in the pump and signal regions leads to a design which has significantly reduced reflectivity, there is also a marked reduction in the reflectivity of the idler wavelengths (shown in Figure 5.8 when compared with Figure 5.9). While it is difficult to get a good AR coating in all three wavelength bands, any improvement at the idler wavelength reduces any possibility of parasitic double resonance of the idler wave.

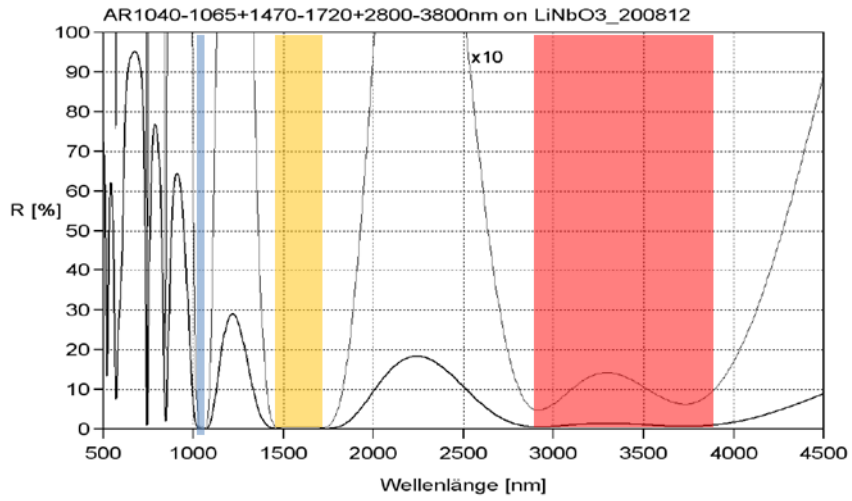

Figure 5.8 : Reduced bandwidth coating simulation by Laseroptik - AR1040-1065 (blue) +1470-1720 (yellow) +2800-3800 (red), showing in grey the x10 magification of the reflectivity on the same wavelength scale (narrow coating bandwidths compared with Figure 5.9)

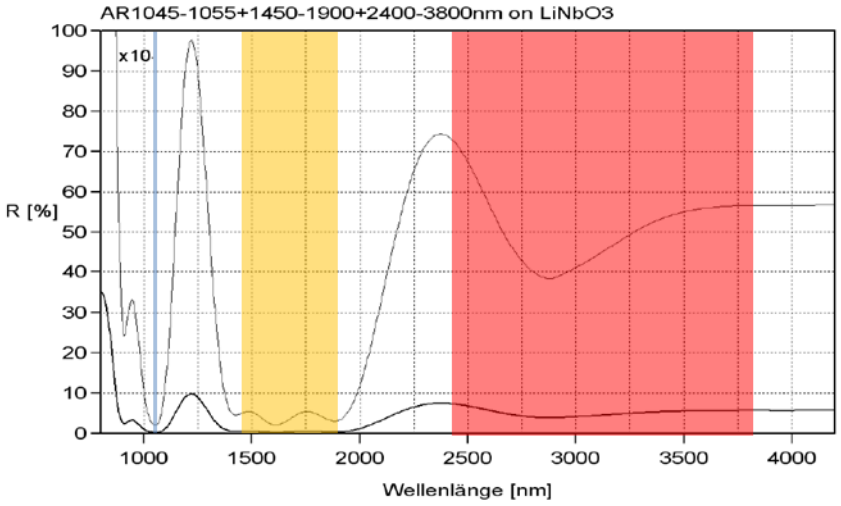

Figure 5.9 : Broader bandwidth coating simulation by Laseroptik - AR1045-1065 (blue) +1450-1900 (yellow) +2400-3800 (red), showing in grey the x10 magification of the reflectivity on the same wavelength scale

The optics used in the ICOPO were not all coated in the same coating run. The optics in the pump-only section of the cavity are standard 1064nm coated lenses whilst the VECSEL itself has a built in Bragg reflector which is highly reflecting over the range 1040 -1060nm. The OPO mirrors and beamsplitter are coated from the same batch, and the PPLN has been re-coated by Laseroptik using the reduced bandwidth coating shown in Figure 5.8.

5.2.2 Optics Coatings

Having examined the PPLN coatings and how best to improve them, testing the effect of tuning the OPO across the full coating range was carried out by tuning across the signal range by (i) fixing the grating period of the PPLN and tuning the VECSEL wavelength and (ii) fixing the VECSEL wavelength and tuning the PPLN across its fanned grating. The key variables which are of interest include (i) the idler output, (ii) circulating field, and (iii) OPO threshold. If the coatings were identical and reflectivity unchanged across the tuning ranges the clamped field would be uniform across the full VECSEL tuning range, with only a small reduction near the edges of its gain bandwidth which in turn would result in near constant idler power across the same range. The OPO threshold would be the same since the cavity losses would be the same and the calibration factor used to calculate the value of circulating field would also be constant. Figure 5.10 shows how these 3 variables vary with pump wavelength in reality and confirms that the coatings of the optics / PPLN are far from uniform. Here it is clear that the peak idler is generated at a pump wavelength of 1048nm whereas the maximum circulating field is at 1055nm, indicating an improved PPLN coating at this wavelength. The clamped field (OPO threshold) is approximately constant over this range, suggesting that the OPO cavity loss is constant over the signal range.

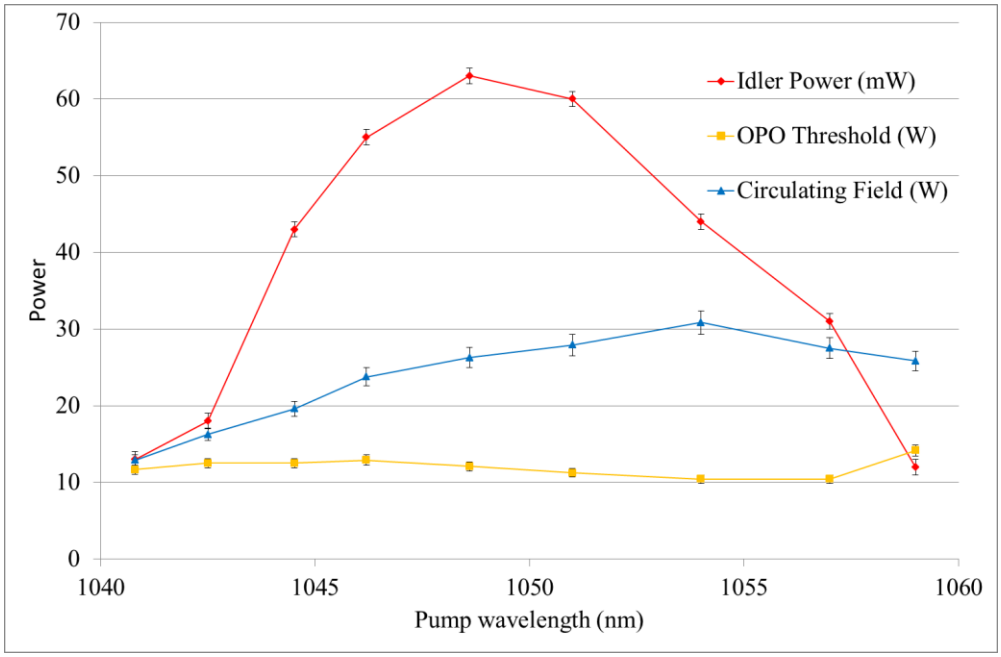

Figure 5.10 : Effect of signal tuning using the VECSEL on idler output, OPO clamped wavelength and circulating field

The data presented in Figure 5.10 were all taken using the same part of the PPLN, which means that as the pump wavelength is changed the signal and idler tune. In order to ascertain where the anomaly in the coating is, a second set of data were taken whilst the pump wavelength was kept constant. In this case the signal was tuned by translating the PPLN such that the grating period changed – this is shown in Figure 5.11.

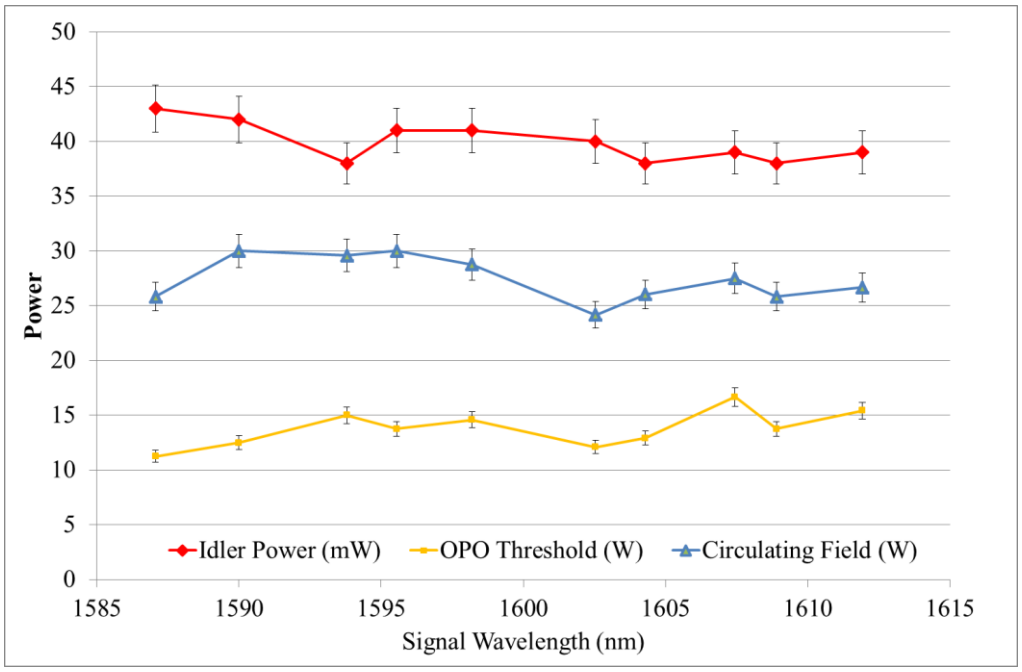

Figure 5.11 : Effect of signal tuning using crystal translation (fixed pump) on Idler power, OPO threshold and Circulating field (idler wavelengths ranging from 3146nm (1585nm signal) to 3034nm (1615nm signal))

It can be seen in this plot that the idler power decreases only slightly over the signal tuning range, with the clamped field (OPO threshold) increasing slightly over the same range. An increase in threshold with roughly the same circulating field will result in lower idler power.

Having determined how the OPO performs whilst tuning the pump wavelengths, it was decided that although pump tuning is an attractive idea it would require a new set of optics which are coated over the pump range. Since this was not the primary goal of this work the decision was made to fix the pump wavelength to that where idler output is highest – 1054nm, and a signal wavelength of 1585nm.

5.2.3 Experimental results from using PPLN with angled facets

The hypothesis that the VECSEL is highly sensitive to feedback meant that it was appropriate to test a PPLN crystal with angled entry and exit facets, in which there could be no back-coupling by design. The addition of a 2° wedge was calculated to

ensure sufficient walk-off between the resonant wave and any parasitic reflections whilst being advised by Laseroptik that this should not affect the performance of the dielectic coating. The re-worked PPLN crystals with new, identical coatings will be referred to herein as Sample W (wedge) for the piece which has angled facets, and Sample P (parallel) for the piece which has facets which are normal to the incident beam.

On insertion of Sample W, a significant reduction in circulating field of >50% was observed. This prompted a comparison of the angle-dependent losses of Sample P with the earlier Sample A (original PPLN crystal) to ascertain whether the loss could be related to the coating or perhaps there were problems with the crystal surface quality prior to coating. The results of this comparison are shown in Figure 5.12 (both data sets taken using the same experimental set-up), confirming that a tilt angle of 2° results in a 50% reduction in circulating field.

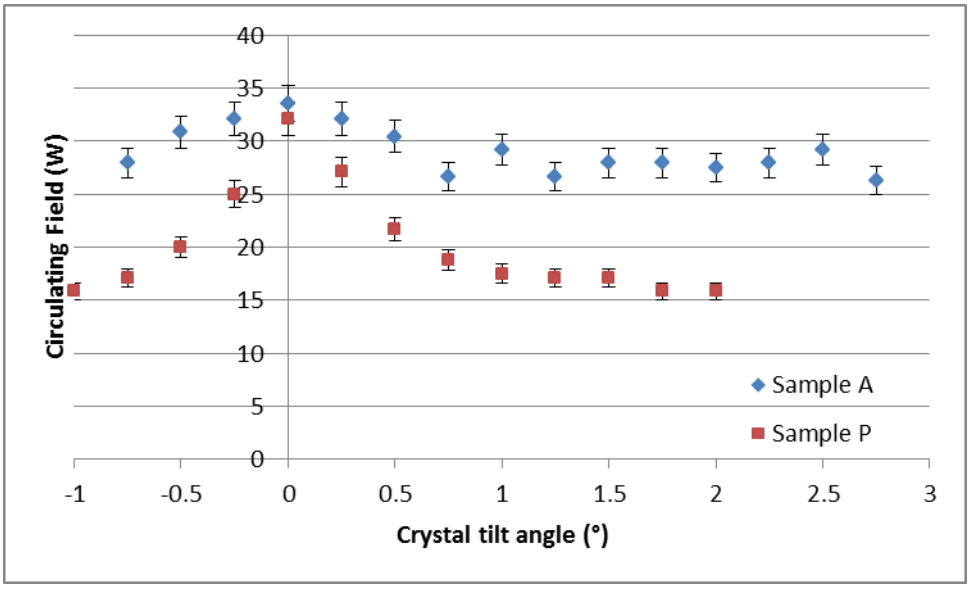

Figure 5.12 : Reduction in circulating field as a function of angle for Samples A and P for λ = 1055nm

An attempt was made to characterise the loss per surface of the PPLN by measuring the transmission. For Sample P, on axis, there was negligible reduction, but at 2° there was ~6.5% loss per surface. This is large compared to Sample A, which showed a loss of only 2.5% per surface. Sample W showed a toal transmission loss of ~5%.

This leaves some loss unaccounted for between the reduction in circulating field caused by the wedged crystal and the plane crystal tilted 2° off axis. This could be due to poor

surface quality on the wedged crystal prior to coating (Mr. Ulrich Wostenbrink in Germany).

5.3 Performance due to improved AR coating on plane and angled PPLN facets

Giving the problems resourcing this project, it was not possible to carry out the concluding experiments during the EngD funded period. A two-week period in November 2012 was agreed to return to St Andrews to test the crystals on their arrival. By this point, the diode pump laser had degraded by several Watts. This reduction in pump power meant that there was insufficient circulating field to bring the OPO above threshold to test the new crystals. The only conclusions that could be made were that the wedge did improve frequency stability compared to the planar PPLN at the same circulating field.

One of the main findings from this section of work is that in theory the VECSEL offers an excellent opportunity to have an additional OPO tuning mechanism. However, in reality, as shown in Figure 5.10 it is imperative to have a good understanding of the coatings that are being used to ensure optimal operation of the ICOPO. From an engineering point of view and for production, higher specification coatings are required or a single grating period in the PPLN would be required for this to be a marketable item using pump tuning. The VECSEL offers distinct advantages, in particular a smaller footprint and no relaxation oscillations. Consequently if it were possible to realise stable single frequency operation of the VECSEL ICOPO, it would have system benefits over the more complex single frequency Nd-based system, which requires an additional nonlinear element to control the relaxation oscillations.

If this work were to be continued, the next logical step would be to replace the pump diode to achieve OPO threshold and evaluate the frequency stability with the ICOPO running. The fact that the PPLN coating showed high losses when tilted off-axis, contrary to the supplier's expectations – when they had advised that the coating should not suffer any additional loss at such a small angle – suggests that it may be worth evaluating a Brewster-cut piece of PPLN. The main concern with Brewster-angled elements is the astigmatism introduced and whether this can be adequately compensated by cavity design and the effect this would have on the OPO efficiency from the perspective of mode matching in the crystal. This is examined in section 5.5.

5.4 Addition of Frequency selective components

The other route for investigation highlighted in Chapter 4 was the use of additional frequency selective elements (etalons) to increase the loss in the cavity to an extent where there is only one allowed mode above threshold.

Having been discussed theoretically in section 4.1.2, three following etalons were tested in the cavity (between January and June 2012 before the degradation of the pump diode as described in 5.3):

- 10GHz 10mm quartz etalon with 60% reflectivity coating
- 100µm uncoated quartz etalon
- 75µm uncoated YAG etalon

The 10GHz etalon did provide an improvement in the frequency stability with longer bursts of single frequency oscillation, but due to the thickness, could not be used for tuning of the cavity as the walk-off loss would be too large. Additionally, the high FSR meant that the OPO drifted in and out of resonance as the single frequency detuned the laser wavelength from its phase matching solution in the grating. Ideally a variable air-spaced etalon would have been a better choice, however, as this project had no formal funding associated with it and a home-made alternative would have insufficient mechanical stability to make a simple comparison, only the off-the-shelf components could be evaluated. The position of this etalon in the cavity was important as the coating reflectivity is so high that it forms a stable laser cavity if too far from the VECSEL chip, acting as an output coupler – for this reason it is positioned within one focal length of the first intracavity lens where the cavity it forms with the VECSEL chip is unstable.

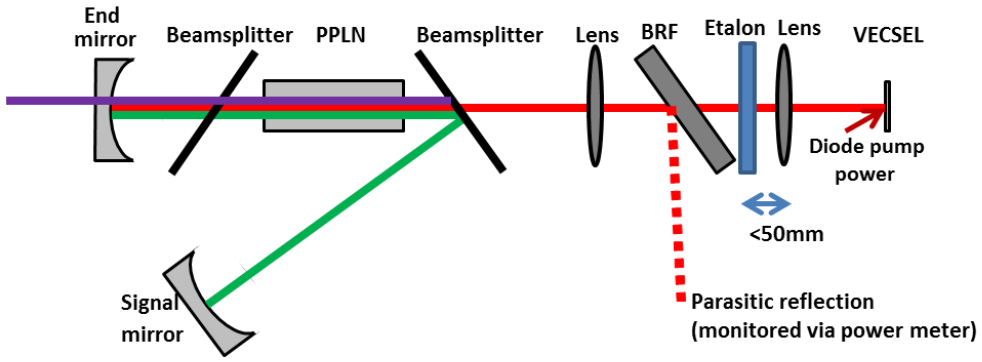

Figure 5.13: Cavity layout for trialling etalons (detailing the part of the cavity where etalons were placed)

The 100μm quartz etalon was used in place of the YAG etalon as it was simpler to mount. It is a reasonable substitution as it has a comparable FSR (YAG etalon ~ 1.1GHz vs 100 μm quartz ~ 0.98 GHz). The high FSR of the 100 μm quartz etalon made its alignment very sensitive to position, but did enable steadier single frequency behaviour (seconds at a time) from the OPO when paired with the 10mm quartz etalon. The idler power was very low, and due to thermal effects on the cavity length the OPO drifted on and off resonance. In order to progress this to be a useful mid-IR source, effort should be directed towards stabilizing cavity length as the etalon is rotated using a piezo mounted end mirror.

5.5 Brewster cut PPLN Cavity Design

Having determined that improvements in the crystal coating results in improvement the frequency stability it may be worth considering a design that removes the requirement for a coating. Cutting the crystal facets at Brewster's angle was a method of getting round the early, poor quality coatings which were available and enables much higher incident fields. This is because the damage threshold of the coating, rather than the crystal, is the limiting factor for power handling. Opting to use Brewster angled elements however adds system complexity due to the astigmatism and coma that are introduced via the significantly angled facets.

The cavity design is based on that in two key papers [5.2], [5.3] which dealt with Brewster cut crystals used for second harmonic generation in dye lasers. In addition to using Brewster cut PPLN to eliminate feedback which has de-stabilised the single frequency operation of the VECSEL IC-OPO, the extra Brewster surfaces will strengthen the polarisation dependant loss which keeps the laser vertically polarised to ensure efficiency of the OPO.

The following pages summarise the key expressions used to compensate for coma and astigmatism, and will then be applied to the VECSEL IC-OPO and a new cavity design formulated.

5.5.1 Key expressions used for Astigmatism and Coma compensation

Astigmatism occurs when the sagittal and tangential components of the beam have different foci. In this case, the vertical component sees a planar surface, and the horizontal component sees an angled surface, which causes magnification of the beam in the horizontal plane only, generating an elliptical beam. This ellipticity will affect the

interaction of the beam with other optical components in the cavity and could mean that a cavity could be stable in one plane, but not in the other. In order to correct for this, an additional angled mirror needs to be employed after the Brewster surface to correct for astigmatism at the focus.

Using geometrical optics, when the mirror angle is such that the following relationship is satisfied, the path length to the focus as seen by the tangential and saggital rays will be the same [5.2]:

$$\frac{[t(n_2^2-1)(n_2^2+1)]^{1/2}}{n_2^4} = f \sin I \tan I \tag{5.1}$$

Where t is the thickness of the PPLN, n_2 is the refractive index of the material, f is the focal length of the mirror and I is the angle of incidence on the mirror.

If a beam is not travelling at normal incidence through a series of optical elements, which will be the case for a Brewster element, there will be a variation of the effect (e.g focussing) of that element across the beam diameter, which deforms the beam, this is called coma. Coma occurs both at the Brewster surface, and at the spherical mirror which is being used to compensate for astigmatism.

To compensate for astigmatism and coma, the effects of coma at the various interfaces in the cavity should be combined with the effect of astigmatism. These combined effects can be eliminated by careful choice of the angle of incidence on the spherical mirror, given by [5.2]:

$$\tan I = \frac{n_2^3}{2(n_2^2+1)} \tag{5.2}$$

Where I is the angle of incidence on the mirror, and n_2 is the refractive index of the crystal. The purpose of this short section was to document the negative effects of coma and astigmatism and why they have to be considered when designing a cavity containing an optically active Brewster element. The key expressions have been

extracted from [5.2] and this should be consulted for the complete mathematical derivation.

5.5.2 Design

Equations 5.1 and 5.2 can be applied to the VECSEL ICOPO. For a pump wavelength of 1.05μm, the refractive index of PPLN is 2.161 which has a corresponding angle of incidence on the mirror of ~41°. To replicate the focussing conditions in the PPLN which have been used elsewhere in the thesis, a spot of radius 52 μm would be obtained by using a 38mm focal length lens. If a mirror of radius of curvature 76mm is substituted and the target focus is used to calculate the confocal parameter, b, of 16mm then the distance in the leg prior to the PPLN needs to be 90mm. The optical design for this is shown in Figure 5.14 with the 2nd 75mm lens being modelled in place of the curved mirror which would be used for the astigmatism/coma compensation.

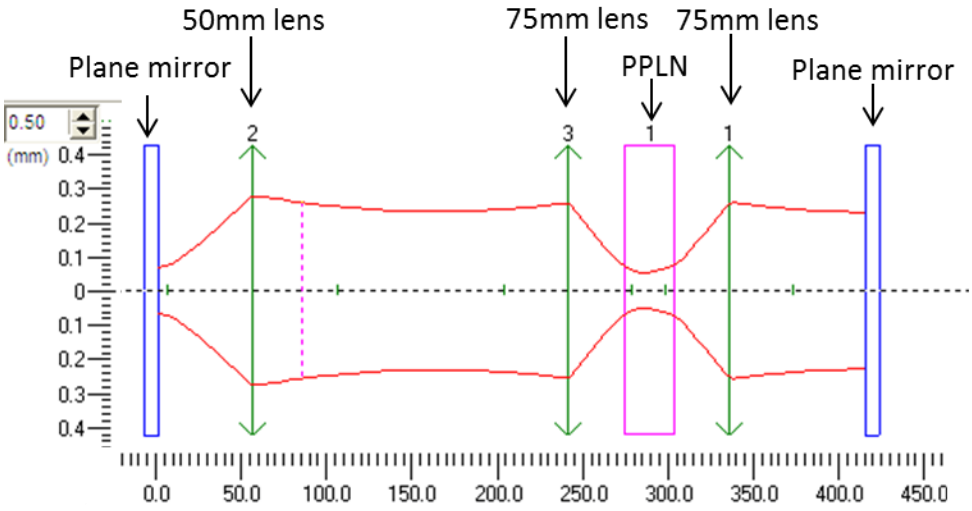

Figure 5.14 : Cavity configuration required to accommodate comatic aberations (using Psst! Simulation software)

The analysis shows that from Equation 5.2, an angle of 41° is needed to compensate for coma and astigmatism; which would require specially designed mirrors. This design was not pursued experimentally due to a lack of resources.

5.6 Conclusion

The work described in this chapter built, experimentally, on the discussions in Chapter 4, in seeking to understand and address the problem of frequency instabilities in the VECSEL based IC-OPO. This covered the impact of coating quality and cavity symmetry on parasitic feedback into the VECSEL cavity, the addition of etalons to

enhance spectral selectivity and a design study on the use of a Brewster angled PPLN crystal.

The favoured hypothesis to explain these instabilities was parasitic feedback from anti-reflection coatings in the cavity. Frequency analysis of existing PPLN was carried out and from this a new set of specifications was made, including angled facets on one of the crystals for comparison. The experimental results from the re-worked PPLN had disappointing results when characterised outwith the cavity, reporting higher losses than expected, possibly due to the flatness of the polish on the facets. When attempts were made to characterise these crystals inside the cavity, the circulating field was significantly lower and due to additional diode pump degradation this configuration could not be fully characterised.

Finally, an analysis was carried out on the practicalities of realising a cavity based on Brewster angled PPLN. In particular this focussed on the compensation requirements of coma and astigmatism in the cavity and the implications this has on the IC-OPO efficiency. This approach was deemed too high risk due to the investment required in new mirrors, and the practical risk of damaging the PPLN by adding the Brewster surfaces.

Ultimately the question of whether the VECSEL is well-suited to supporting an IC-OPO is still open. The lack of relaxation oscillations coupled with the lack of spatial hole burning due to the very thin gain region and the excellent thermal handling of the gain medium resulting in no thermal lenses make it a promising candidate; however there are a number of subtleties beyond this that are yet to be fully understood. As no solution was demonstrated with takes advantage of the single frequency VECSEL characteristics, a single frequency VECSEL IC-OPO would require etalons and cavity length stabilisation (both pump and signal) to prevent environmental fluctuations from having a significant effect on idler power.

5.7 References

[5.1] M. Schubert, “Personal communication via email,” 2013.

[5.2] M. Dunn, “Coma compensation in off-axis laser resonators,” *Optics Communications*, vol. 20, no. 2, pp. 214 - 219, 1977.

[5.3] A. Ferguson and M. Dunn, “A tunable, frequency-doubled, continuous-wave dye laser using ADA,” *Optics Communications*, vol. 23, no. 2, pp. 177–182, 1977.

[5.4] D. J. M. Stothard, C. F. Rae, and M. H. Dunn, “An Intracavity Optical Parametric Oscillator With Very High Repetition Rate and Broad Tunability Based Upon Room Temperature Periodically Poled MgO : $LiNbO_3$ With Fanned Grating Design,” *IEEE Journal of Quantum Electronics*, vol. 45, no. 3, pp. 256–263, 2009.

[5.5] T. J. Edwards, D. Walsh, M. B. Spurr, C. F. Rae, M. H. Dunn, P. G. Browne, "Compact source of continuously and widely-tunable terahertz radiation" Optics Express, vol. 14, no. 4, pp. 1582 - 1589, 2006

6 Optimisation of Output Coupling of a VECSEL Intracavity Optical Parametric Oscillator

6.1 Introduction

OPOs are attractive to the defence industry due to their ability to simultaneously provide 3 useful wavelengths (of which signal and idler can be tuned) with a single laser system for infrared countermeasure systems (as described in Chapter 1). If the balance of wavelengths is compared between extracavity and intracavity systems, the extracavity OPOs resonate only at the signal wavelength, thus the portion of the pump which is not downconverted can be used in addition to the idler and signal (if some output coupling is included in the OPO design). It has been shown in previous chapters that it is possible to out-couple a significant fraction of signal out of the OPO in the case where a higher threshold is required for optimal operation of the OPO.

In previous chapters the pros and cons of both the intracavity and extravavity approaches have been outlined; in this chapter experimental and modelled results are presented to quantify the differences. For countermeasure applications, the low power consumption of the intravity approach is attractive, but the lack of versatility in output wavelengths is less so.

In this chapter, a model is presented and developed to calculate a solution where there is out-coupling at both the pump and signal, as well as the idler. The experimental approach will be discussed initially before the equations which form the basis of the model are discussed. The model for output coupling of the IC OPO is intimately linked with the equations that describe the host laser, and an experimental evaluation of the model is presented in this chapter. The work in this chapter was performed at the University of St Andrews and details the first validation work on the initial expressions derived by Dunn in the Handbook of Optics (2001) [6.2].

6.2 Experimental Verification

The optimum output coupling loss for an OPO or laser can be determined experimentally by testing a range of mirrors with different reflectivities at the required wavelength, which can be straightforward if a laser of standard wavelength is being investigated, e.g. Nd:YAG. As mentioned in Chapter 5, the coatings required for an output coupler with an intracavity OPO are more sophisticated (and therefore more

expensive) than the standard single wavelength coating. To avoid the expense of procuring a range of suitable mirrors, Fresnel loss was exploited by using parallel plates mounted on rotation stages, allowing the angle of incidence to be adjusted around Brewster's angle. These were added to the intracavity OPO described in Chapter 6 in the pump-only, and signal-only arms to introduce 'useful' output coupling loss. This is shown below:

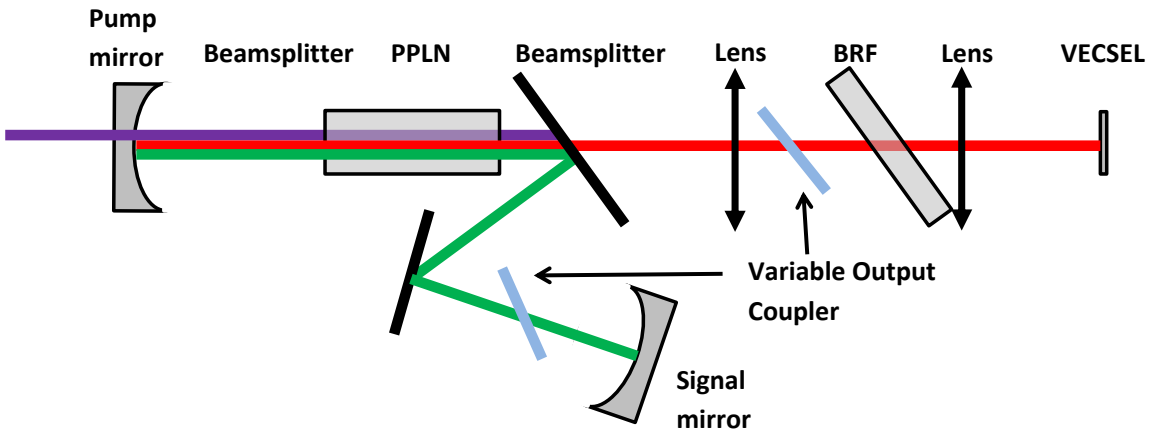

Figure 6.1: Cavity layout showing the rotatable plates used to add loss to the cavity. Red – pump; Green – signal; Purple - Idler

As mentioned in Chapter 4, the VECSEL is p-polarised through the addition of multiple Brewster surfaces in order to achieve maximum down conversion although the laser itself has no polarisation preference. This fact is exploited here by also using these surfaces (tuned slightly off Brewster angle) to alter the loss. For illustration, Figure 6.2 shows how Fresnel loss (expression shown below – 6.1) varies with angle (at the interface between air and a material with refractive index of 1.53) showing the range of losses (in the case for n_1 = air and n_2 = 1.53 (fused silica)) which could potentially be used.

$$R = \left(\frac{n_1 \cos\theta_1 - n_2 \cos\theta_1}{n_2 \cos\theta_2 + n_2 \cos\theta_2}\right) \qquad (6.1)$$

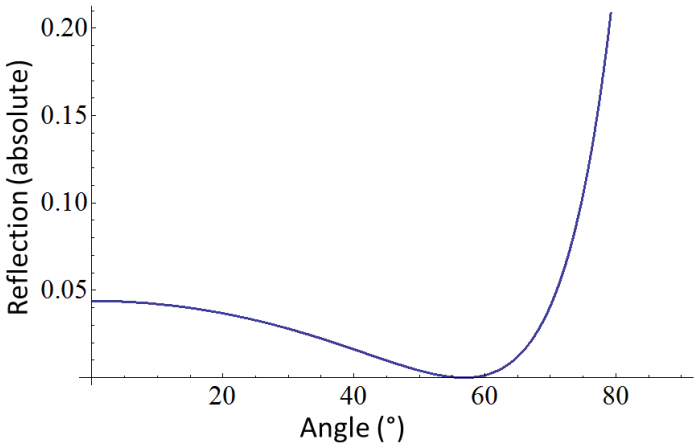

Figure 6.2: Calculated Fresnel reflection as a function of angle of incidence for p-polarised light on fused silica

The extent of the loss that can be introduced by this approach is somewhat limited by the space available in the signal arm of the OPO. However the loss introduced over the few degrees closest to Brewster's angle is very sensitive allowing a reasonable number of data points which can be used to verify the model. Microscope cover slips were used to minimise misalignment of the cavity which would have been more extreme had thicker plates been used.

6.3 Error Handling

The errors in the data presented in this chapter arise from one of two distinct avenues. What follows is a set of experimental results which have errors associated with the measurement (technique, power meter, accuracy of alignment), but also errors arising from the fit of the experimental data to the model where the accuracy of the input parameters is the largest source of error.

Practically, the use of cover slips to vary the output coupling through varying their rotational position to give Fresnel loss (discussed in Section 6.2) resulted in significant errors from two perspectives. Firstly, the angles through which the slide could be rotated were small, and the accuracy in positioning the slide was limited to ~1° rotational accuracy and secondly, the thickness of the slide (which was primarily selected to minimise misalignment during its rotation) resulted in etalon effects which significantly affected the power output from the OPO and consequently will uncertainty to the results (as the signal cavity modes are not always well aligned with the free spectral range of the etalon due to limitations in the mechanical tolerances of the

system). The uncertainty in the value of the loss (x-axis) has been left out in the error bars shown on the plots to increase clarity, as this is very small when one looks at how much the loss changes close to Brewster's angle in Figure 6.2. The value of error for the output powers (pump, signal or idler) has been set to 10% to reflect the variation in power which can be attributed to etalon effects.

Section 6.6 details a sensitivity analysis which looks at how small changes in key parameters effect not only the power which can be obtained from a set of characteristic inputs, but also the extent to which the shape of the curve changes. The reader is urged to, when looking at the results, presented in Section 6.3 and 6.4 to consider separately the trend shown in the data from the fit to the modelled result.

6.4 Modelling the System

This section begins by outlining the key equations used in the model, and showing where dependant variables are held throughout the model. These equations are numbered and referred to later in the chapter where the relevant experimental results are presented.

The model begins by modelling the laser cavity, which contains a term for the cavity lifetime, τ_{cav} which itself is dependent on cavity losses including crystal loss, parasitic loss and output coupling loss. By keeping this term dependant on these losses, the output coupling can be varied in the expressions used to calculate laser and down converted power.

6.4.1 The Approach

Laser dynamics are well understood and widely published, fundamentally equating gain and loss. The expression cited here is taken from Koechner's Solid State Laser Engineering text [6.1]. The theory of the output coupling of intracavity OPOs is well documented in the chapter 22 in the 2nd Edition of the 'Handbook of Optics'[6.2], and the equations for my model are taken from this.

Power as a function of varying output coupling of the parent laser is given by [6.1]:

$$P_{out} = A\frac{1-R}{1+R}I_S\left(\frac{2g_o l}{\delta - \ln R} - 1\right) \tag{6.2}$$

Where; A is the cross sectional area of the laser rod, I_s is the saturation intensity, g_o is

the small signal gain co-efficicent, δ is parasitic loss, l is gain length and R is output coupler reflectivity.

This equation is used to plot the laser output as a function of the output coupler reflectivity – see Figure 6.3. This plot indicates that ~8% is the optimal value of output coupling.

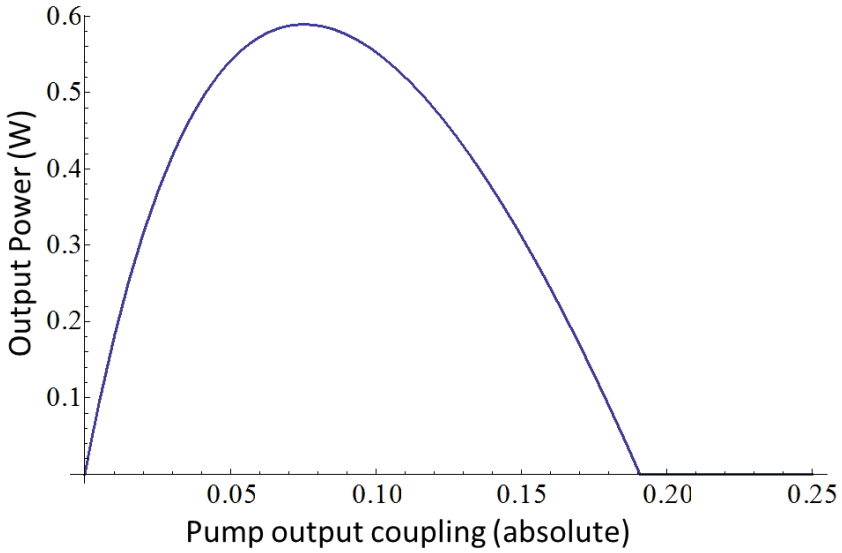

Figure 6.3: Calculated laser output power as a function of output coupling loss

In building up a set of useful equations for use in modelling of IC OPO outputs, the key parameter is not the laser output power, but rather the intensity (*I*) of the field inside the laser, which is critical to ensure that the OPO can operate above threshold. The key in being able to model output coupling is keeping a loss term as a variable when progressing through the equations, this has been done through the cavity lifetime parameter (τ_{cav}). Both τ_{cav}, and terms which are dependent on τ_{cav} have been emboldened in the expressions to highlight where the loss is kept active.

The intensity (*I*) within the cavity as a function of diode pumping power can be determined, starting from the rate equations:

$$\Lambda = \frac{\eta_{sp}\eta_{abs}P_{in}\lambda_p}{hcAl_l} \tag{6.3}$$

$$\boldsymbol{\Lambda_{th}} = \frac{L}{\sigma c l_l \boldsymbol{\tau_{cav}} \tau} \tag{6.4}$$

σ is the stimulated cross section, τ is the upper state lifetime of the laser media) and, Λ and Λ_{th} are the pumping rate and threshold pumping rate respectively. η_{abs} and η_{sp} are the absorption and spatial overlap coefficients, l_l is the length of the gain medium, P_{in} is the incident power and λ_p is the diode pump wavelength, τ_{cav} is the cavity lifetime, L is the laser cavity length).

The cavity lifetime, τ_{cav}, is comprised of losses, including output coupling loss, as follows:

$$\boldsymbol{\tau_{cav}} = \frac{2L}{\left(\log\frac{1}{1-l_{par}} + \log\frac{1}{1-l_{xtal}} + \log\frac{1}{1-\mathbf{l_{opc}}}\right)c} \tag{6.5}$$

where l_{par}, l_{xtal} and l_{opc} are parasitic, crystal and output coupling losses respectively.

Equating Λ and Λ_{th} and then solving for P_{in} gives the threshold for laser operation:

$$\mathbf{P_{th}}^{\mathbf{L}} = \frac{hAL}{\eta_{sp}\eta_{abs}\lambda_p\sigma\boldsymbol{\tau_{cav}}\tau} \tag{6.6}$$

The intensity inside the laser (intracavI) is given by:

$$\mathbf{intracavI} = \frac{I_{sat}}{2}\left(\frac{\Lambda}{\boldsymbol{\Lambda_{th}}} - 1\right) \tag{6.7}$$

where I_{sat} is the saturation intensity:

$$I_{sat} = \frac{h\upsilon_L}{\sigma\tau} \tag{6.8}$$

The intracavity intensity can be easily converted to circulating power by multiplying by the circulating beam radius.

Having dealt with the interactions of the host laser, the OPO can be described in terms of thresholds before combining the laser and OPO dynamics in order to understand the response of the OPO to varying laser losses.

The OPO threshold is described by the following equation:

$$P_{th}^{SRO} = \frac{n_p n_i n_s \varepsilon_o c^3 \pi (wP^2 + wS^2)}{4\omega_s \omega_i {d_{eff}}^2 l_{xtal}^2 h_m} \tag{6.9}$$

Where n_i, n_s and n_p are the refractive indices of the idler, signal and pump respectively, ω_s and ω_i are the signal and idler frequencies respectively, l_{xtal} is the crystal (PPLN) length, wP and wS are the signal and pump beam waists respectively, d_{eff} is the effective nonlinearity and h_m is the confocal parameter. From this, combined with the expressions relating to laser circulating field, the OPO threshold as a function of diode pump power can be obtained. This is a useful parameter as an intracavity OPO is nominally contained within a high finesse cavity and it may not always be possible to know the circulating field exactly.

The round trip saturated gain in the OPO is inversely proportional to the amount of field in the cavity via scaling parameters relating to small signal gain (K) and gain saturation (P_{sat}):

$$G_{sat} = \frac{KP}{(1 + {P_{IC}}/{P_{sat}})} \tag{6.10}$$

From there, the saturated gain can be substituted with the sum of the losses in the cavity (gain = loss in an oscillator) and alongside the knowledge that the amount of down-converted power is the total intracavity field multiplied by the nonlinear loss ($P_{DC} = P_{IC} loss_{NL}$) allows the expressions to be substituted into a form where experimental data can be used to calculate values:

$$P_{DC} = \sigma_{max}\left(P - P_{th}^{SRO}\right)\left[1 - \frac{P_{th}^{L}}{P_{th}^{SRO}}\right] \tag{6.11}$$

Another useful tool for working with OPOs is that unlike lasers, where it is always desirable to have a low threshold, it is possible to optimise the OPO threshold for maximum down conversion. The expression for this is as follows, and will be used to check whether the OPO which has been built is optimum:

$$P_{th}^{SRO} = \sqrt{P_{th}^{L} P} \tag{6.12}$$

In both of these expressions; P is power; SRO is single resonant oscillator; L is Laser; σ_{max} is the laser slope efficiency.

From the expressions for down conversion, the field can be partitioned into the signal and idler via energy conservation (as the idler is non-resonant) and the projected signal calculated:

$$P_{signal} = \frac{\omega_{sig}}{\omega_{idler}} \left[\frac{useful}{useful + parasitic} \right] P_{DC} \tag{6.13}$$

Now that the key expressions used in the model have been explained, in the next section the results from the model will be compared with experiment.

6.4.2 Model inputs

The values assigned to the model variables are shown in Table . The variables in bold are used as fitting parameters.

Table 6.1: Model Variables

Variable	**Symbol**	**Value assigned**	**Reference**
Cavity length	L	350mm	measured
Circulating mode field radius	ω	60μm	approximated along the whole cavity (modelled using Psst!)
Diode pump absorption	σ	10^7	(large number to suggest 100% pump absorption)
Gain length	l_{gain}	0.4718 μm	[3.3]
Laser wavelength	λ_l	1050nm	measured

Diode pump wavelength	λ_p	810nm	measured
Spatial overlap efficiency	$\boldsymbol{\eta_{sp}}$	**Estimated as 0.9 from fitting model to data**	
Pump absorption (cm^{-1})	η_{abs}	10^{10}	Assumes 100% absorption
Parasitic loss	$\boldsymbol{l_{par}}$	**Varies in the model**	
Output coupling loss	$\boldsymbol{l_{opc}}$	**Varied via Fresnel loss**	
Crystal length	l_{xtal}	30mm	measured
Crystal absorption	α_{xtal}	0.001	From PPLN datasheet
Cavity lifetime	τ_{cav}	Varies via cavity losses	
Upper state lifetime	T	2ns	[3]
Signal Wavelength	λ_s	These vary according to the experimental set-up	
Idler wavelength	λ_i		
Signal radius in crystal	ω_s	These vary to accommodate the experimental result	
Pump radius in crystal	ω_p		

The model makes a number of assumptions as to how the laser mode propagates within the cavity. For example, there was no information available for the gain length of the VECSEL used in this study, so data was taken from the literature [6.3] for a similar laser and the equations which are used to calculate thresholds assume that the beam diameter is constant throughout the cavity. The agreement obtained between the model and experiment is reasonable in most cases, but it is important to be aware of the limitations.

In this chapter 2, trade-offs are examined:

- The trade-off between output coupling of the pump only from the cavity and the effect this has on the amount of generated idler
- the trade-off between output coupling of the signal and the associated effect on the idler power attainable

6.4.3 Modelling the Laser

In order to gain good agreement with the IC OPO output coupling, it is important that the initial laser model is accurate. Figure 6.4 shows how circulating field increases with diode pump power. Good agreement between model and experiment at this stage gives confidence in the values used in the model for the parasitic losses in the laser cavity and thus confidence in τ_{cav}.

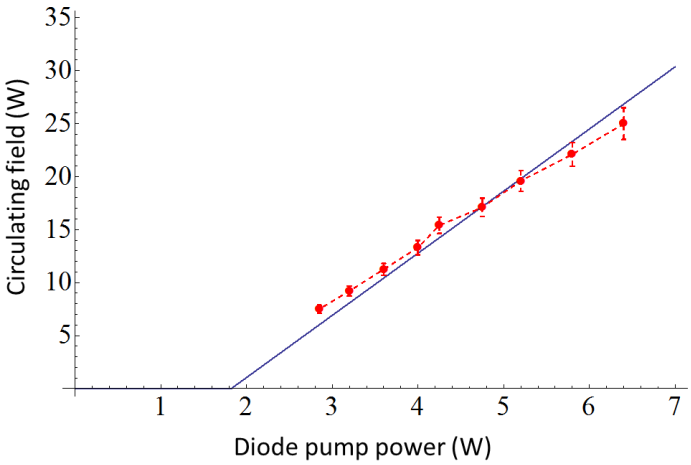

Figure 6.4: Plot showing the linear increase of circulating field with increasing diode pump power for a VECSEL laser only (experimental data – red, dashed; model – blue, solid)

The experimental data is shown for comparison in Figure 6.5 for the OPO both on and off to demonstrate the impact that down conversion has on the available pump field which can be extracted. The OPO was switched on/off by misaligning the signal only cavity mirror. The maximum output coupling from the angled plate is 567mW. The values used in the model are shown in Table 6.3.

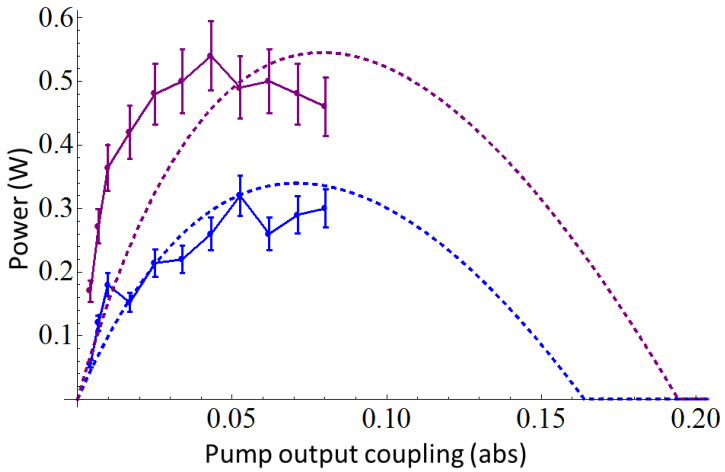

Figure 6.5: Pump output power with increasing output coupling from the pump cavity (model OPO on – blue, dashed; model OPO off – purple, dashed; experimental OPO on – blue, solid; experimental OPO off – purple, solid)

Table 6.2: Model values used in Figure 6.5

Model input	*Value*
Diode pump	6.5W
Parasitic loss (OPO off)	0.1
Parasitic loss (OPO on)	0.15

The maximum power attainable from each configuration is reasonably accurate, however the value of output coupling at which maximum power is achieved is different. This could be due to systematic error introduced from reading the rotation stage which has implications on the values of output coupling. The degree of sensitivity of the model to its input parameters is discussed more in section 6.7.

6.4.4 Modelling the OPO

In addition to the variation of the laser output with output coupling, it is important to also understand the impact of the associated reduction in circulating field on idler power. This is shown in Figure 6.6. From the set-up which gave the results shown in Figure 6.5, the idler output was also plotted as a function of pump output coupling loss. This shows a clear and obvious correlation that as the circulating field reduces, the idler

output also decreases. The OPO threshold was monitored though-out this measurement and was not seen to change.

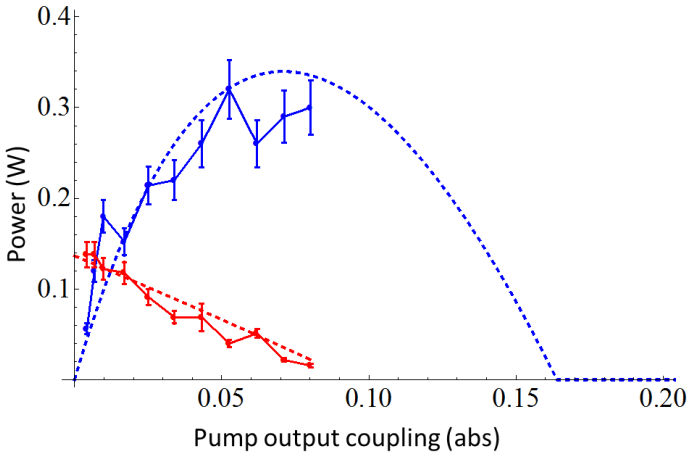

Figure 6.6: Plot showing the powers available at the pump and idler wavelengths with increasing output coupling of the pump field (experimental idler – red, solid; modelled idler –red, dashed; experimental pump - blue, solid; modelled pump- blue, dashed)

The modelled results for the laser output (no OPO) in Figure 6.6 are obtained by plotting the laser output as a function of output coupling loss, with the result for the OPO calculated by increasing the value of parasitic loss to accommodate the nonlinear loss of the OPO. The values of beam waists used in the model are not identical to those calculated using the ABCD matrices due to the aforementioned approximation of a constant beam waist throughout the cavity. The values used are shown in the table below:

	Laser (OPO on)	**Laser (OPO off)**	**Idler**
Diode pump	6.5W	6.5W	6.5W
Useful OPC (pump)	Varies	Varies	Varies
Parasitic loss (pump)	0.152	0.12	0.152
Useful OPC (signal)	-	-	0.002
Parasitic loss (OPO)	-	-	0.03
Signal/pump waists (OPO)	-	-	45/75µm

The OPO threshold would not be expected to change for different pump output coupling values as the OPO cavity is not being changed. This was confirmed by continuous monitoring of the parasitic reflection from the BRF (as indicated in Figure 5.1) in the pump only section of the cavity – this did not change as pump output coupling was varied confirming that the OPO threshold was constant at ~13W across the range.

None of the observations made so far address output coupling of the signal, but have served to verify the well-known relations relating laser output coupling, and the intuitive effect this has on idler field. The next section examines the balance between signal and idler output.

6.4.5 Modelling the ICOPO

The amount of idler generated is a function of the signal field, thus if too much signal is coupled out of the cavity the idler is compromised, both from the effects of increased threshold of the cavity and the net reduction in pump field available for down-conversion. In Figure 6.3, for all but the optimum power, there are 2 values of loss which give the same output power: with a high reflectivity mirror, most of the field is contained within the cavity and only a small amount is coupled out – resulting in a high intracavity field: in the other case, there is a high coupling loss and hence less field within the cavity. This becomes significant when examining the implications of what would be expected from an intracavity OPO. The intracavity OPO acts as an ideal output coupler; the intracavity field is clamped at the OPO threshold and a proportion of the pump field (the shaded area in Figure 6.7) is down-converted.

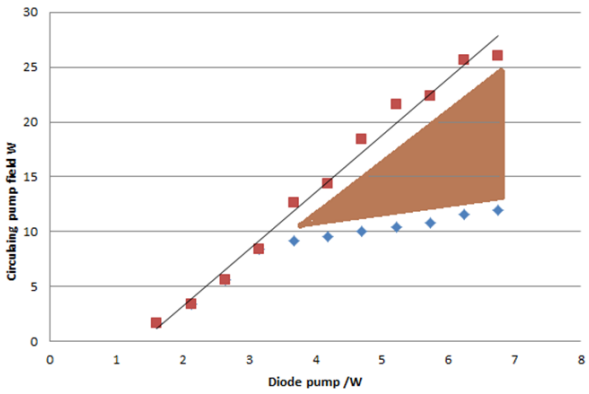

Figure 6.7: Circulating field as a function of diode pump power with the OPO on (blue) and off (red) – the shaded area shows the down converted power

By increasing the signal output coupling, the threshold is increased thus there will be less down conversion, and consequently less idler generated – this is confirmed experimentally in Figure 6.8.

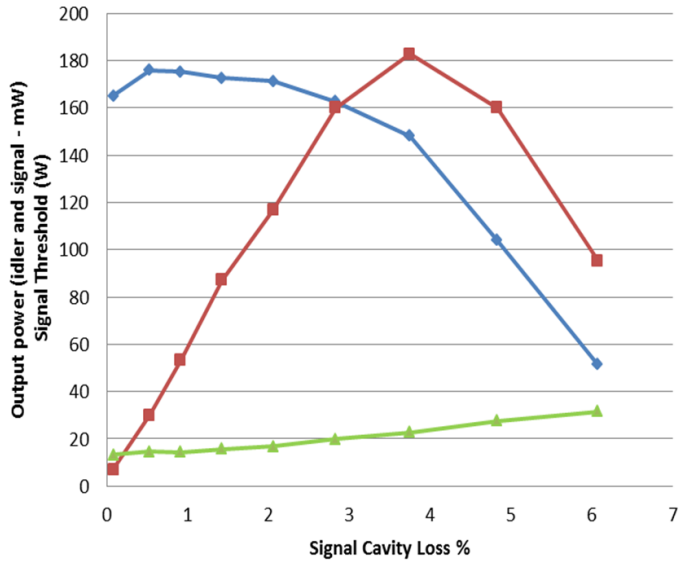

Figure 6.8: Experimental data showing the effect of signal output coupling on OPO threshold (green), idler (blue) and signal (red) output powers

As can be seen from this data (see Figure 6.8), both the signal and the OPO threshold increase with loss, the idler power decreases with loss and the signal output coupling is optimised at ~4% without a significant reduction in idler output.

6.5 Output coupling of pump and signal wavelengths – model vs. experiment

The OPO behaves like an ideal output coupler, which in this case is ~8% (see Figure 6.3). This is used as a value of loss in the model to calculate the curves shown in Figure 6.9, with the fitting parameters shown in Table 6.4. This is accompanied by an additional pump output of ~1W which does not vary when the signal output is varied.

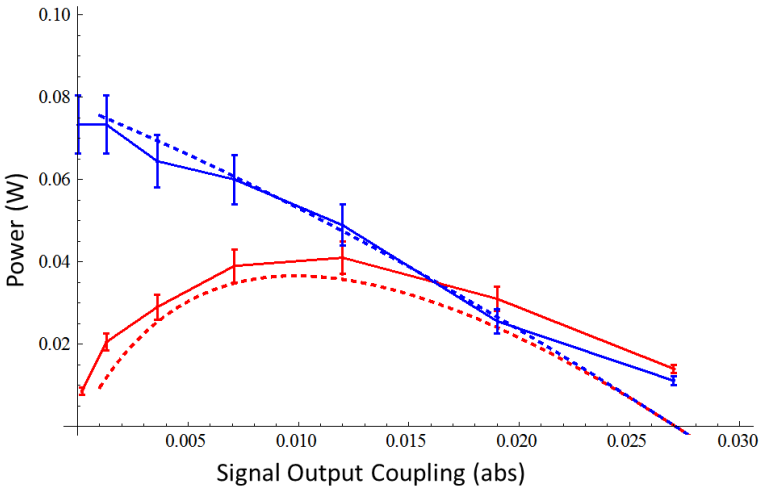

Figure 6.9: Plot showing the power attainable in the signal and idler wavelengths as a result of output coupling from the signal cavity (measured idler – blue, solid; measured signal – red, solid; modelled idler – blue, dashed; modelled signal – red, dashed)

Table 2.3: Values which provide the fit to experimental data shown in Figure 6.9

Parameter	**Value**
Laser output coupling (abs)	0.1
Laser parasitic loss (abs)	0.055
Useful OPO loss	(varied)
Parasitic OPO loss (abs)	0.07
Beam waist (pump)	45 µm
Beam waist (idler)	75 µm

6.6 Validation of data

By conservation of energy, it is possible to calculate the amount of generated signal from the amount of idler measured (and vice versa) via the following:

$$P_{signal} = P_{idler\ (measured)} \frac{\lambda_s}{\lambda_i} \left(\frac{useful}{useful + parasitic} \right) \tag{6.14}$$

In this expression, 'useful' and 'parasitic' refer to the loss of the OPO cavity. When plotted on the same graph, this gives a very good fit, confirming that the measurement error is small.

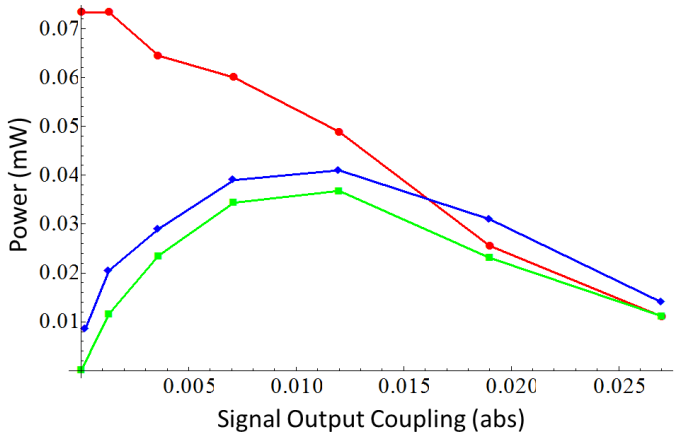

Figure 6.10: Experimental (green), and modelled (blue) signal output (as inferred by the idler power (red) via conservation of energy)

In the next section the predicted behaviours of the model are examined by varying a few key parameters, namely the parasitic loss of the laser, and the OPO.

6.7 Sensitivity analysis

Although modelling is a useful tool for calculating the behaviours that are expected from a given experimental set-up, attaining agreement between theory and experiment is often an iterative process as any model is always an approximation to reality. This nonlinear system is highly complex and given that many of the variables are interdependent the experimental results can be difficult to interpret and prone to error. The output power of both the laser and OPO cavity are highly sensitive to loss, and it is very difficult to measure this to the necessary accuracy.

Although reasonable agreement was obtained between the model and the experiment through an iterative technique, determining the loss values accurately by experiment is difficult. This suggests that practically, the IC-OPO is not best suited to tri-band output and another solution should be sought if a specific balance of powers is required.

The IC-OPO is a highly coupled system and small changes to the pump cavity have considerable impact on the OPO. In order to quantify the sensitivity of the system, a sensitivity analysis was carried out. This is described below, in which the impact of parasitic OPO loss and pump/signal spot overlap on the signal and idler output are examined.

Figure 6.11 shows the effect of increasing the parasitic OPO loss from 0 to 3%. This has a significant effect on the impact of signal output coupling, since the greater the loss in the signal cavity, the less down conversion there can be for a given amount of field.

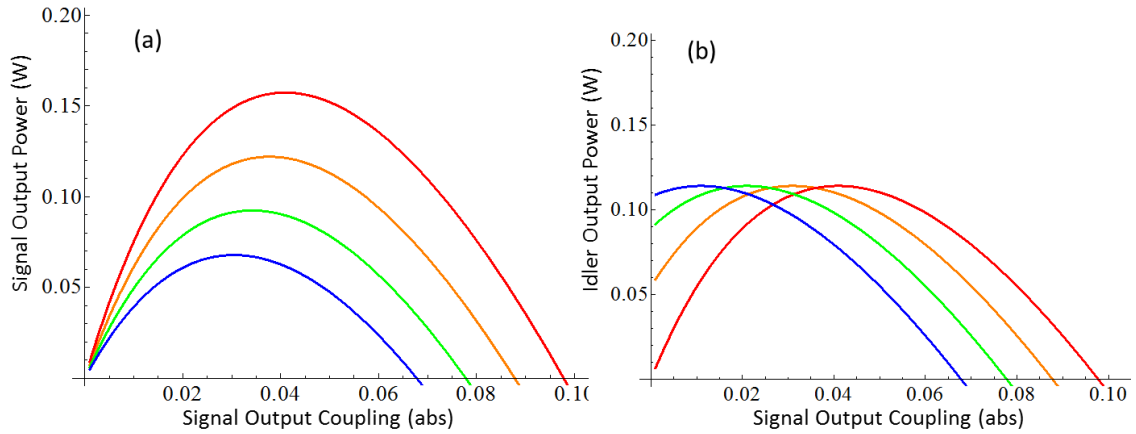

Figure 6.11: Effect of varying parasitic OPO loss on signal and idler output power from the ICOPO (0% - red, 1% - orange; 2% - green; 3% - blue)

The effect of increasing the pump loss is intuitive – as the pump field is reduced, the signal field is also reduced resulting in an overall reduction in idler power achievable.

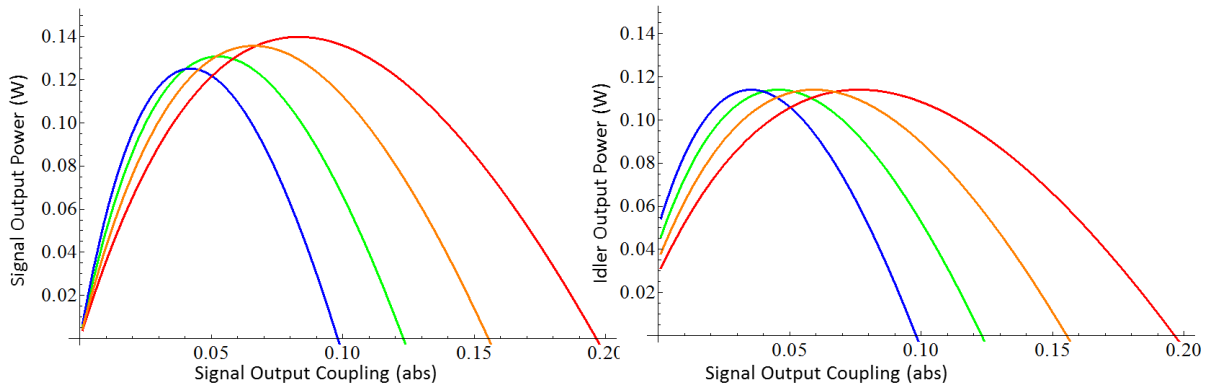

Figure 6.12: Effect of varying signal spot overlap with pump from 40 – 70 µm (Red to Blue) on signal and idler output power from the ICOPO (pump spot size is 45 µm) (40 µm - red, 50 µm - orange; 60 µm - green; 70 µm - blue)

In Figure 6.12, the impact of varying the signal spot overlap with the pump is examined. It is clear that, in terms of output powers, there is no difference between changing the size of pump spot relative to the signal spot or vice versa as in Equation 6.9 the spot sizes are simply summed. However, from a practical point of view, the signal spot size can be varied independently of the pump spot size with no effect on the operation of the

rest of the cavity as the signal spot is defined by its own cavity mirrors as shown in Figure 6.1, however changing the pump spot in the PPLN requires the adjustment of end mirrors and lenses which not only have a small effect on the cavity layout, but also change the focussing in the VECSEL thus affecting the pump cavity.

The most significant influence on the OPO output is the level of pump loss in the cavity (see Figure 6.13), where it can be seen that the magnitude of the pump field directly influences the magnitude of the idler output from the OPO.

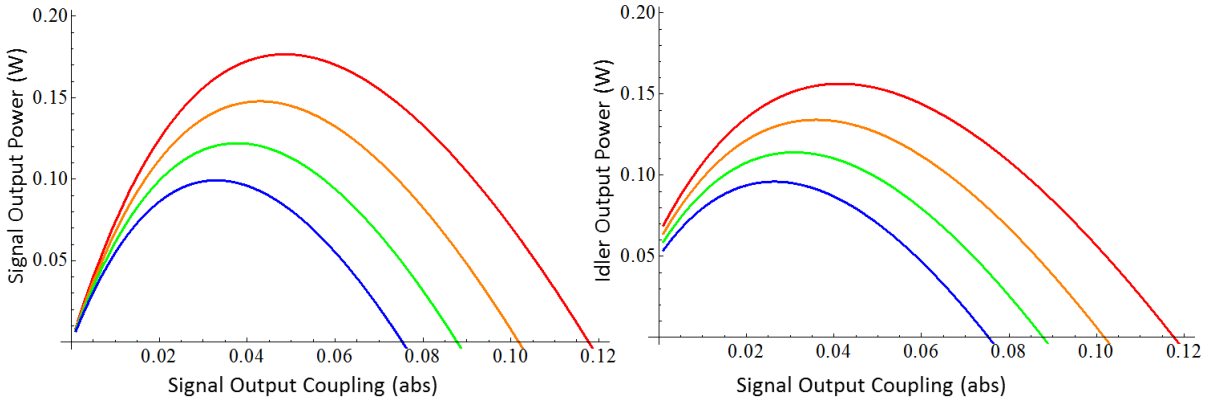

Figure 6.13: Effect of varying parasitic pump loss from 6 – 9 % (Red to Blue) on signal and idler output power from the IC OPO (6% - red; 7% - orange; 8% - green; 9% - blue)

Examining Figure 6.11 and Figure 6.12, it can be concluded that the signal and idler powers are most sensitive to parasitic losses from the OPO, with these being the most difficult parameters to characterise.

6.8 Conclusion

This chapter has demonstrated the simultaneous output coupling of 180mW of signal and 150mW of idler in the absence of pump output coupling. It can be concluded that the principle used to vary output coupling was effective, the implementation could be improved in a number of ways. This would include the mounting of the Brewster plate on a motorised rotation stage to achieve greater accuracy, the use of a wedged plate to mitigate against any parasitic etalon effects and the extension of the dog-leg arm of the signal cavity would be advantageous to allow a greater rotation of the Brewster plate. This would allow the loss to be increased to around 10%, at which point the circulating field would be diminished such that there would be no down conversion. If the experiment were to be developed further to gain additional understanding of the

parameters involved in the modelled equations, it would be useful to be able to monitor the signal intracavity field though a parasitic output in the same way that the intracavity pump field is monitored via the birefringent plate, or a beamsplitter. To do this, an accurately known output coupler for the signal would be required (which was not available), and the laser parameters must be more accurately defined.

The trends seen in the experimental data support the modelled results making this a positive first step in confirming the behaviour of an intracavity OPO with simultaneous output coupling.

6.9 References

[6.1] Koechner, "Chapter 5 - Optical Resonators" in *Solid State Laser Engineering*, 6th Ed., Springer Series in Optical Sciences , pp. 210 - 299, 2006

[6.2] M. Ebrahimzadeh and M. H. Dunn, "Ch. 22 Optical Parametric Oscillators," in *Handbook of Optics*, 2001, pp. 22.42 – 22.50.

[6.3] M. D. Calvez, S., Hastie, J. E., Kemp, A. J., Laurand, N., Dawson, "Chapter 5," in *Semiconductor Disk Lasers*, 1st ed., O. G. Okhotnikov, Ed. Wiley VCH, 2010, pp. 74–94.

7 Conclusion

7.1 Work completed

The aim of any engineering doctorate is to add value to a corporate portfolio in research areas that would not otherwise have been pursued and further strengthen a relationship between industrial and academic groups. This doctorate aimed to explore methods of generating mid-IR lasers for a number of applications relating to the defence sector. This included an investigation into the potential of exploiting fibre dynamics to create an ultrafast laser source with a simple architecture; using the extracavity OPO configuration with the aim of generating higher average power mid-IR output, the intracavity OPO configuration to generate lower power, spectrally pure output, and the investigation of output coupling from this intracavity OPO.

In Chapter 2, the aim was to ascertain whether it would be appropriate to simplify the ultrafast laser by using fibre-based techniques with a view to generating larger bandwidth spectral outputs for use as countermeasures. It was concluded that although there are a number of nonlinear effects which are present in the interaction of an intense field with a narrow core microstructured fibre, it is not possible to completely isolate and control them easily, if at all. During the time between the initial investigations into this area at the start of the doctorate and its conclusion, the field of ultrafast fibre lasers has advanced greatly. These advances would mean that a fibre laser based solution would be more appropriate for the application than generating the next best alternative in generating a broad bandwidth, high spectral power density source via supercontinuum generation to then filter a large percentage of the power as it is out with the region of interest.

Chapter 3 addressed the interest in longer wavelengths for use in countermeasures, expanding the experience of BAE Systems (ATC, Bristol) beyond PPLN to ZGP. This concluded in the demonstration of a pulsed, extracavity, line-narrowed degenerate PPLN OPO which was intended to be used for pumping ZGP (originally for OP-GaAs). On review of the experimental data and the specifications of the optics used, it became clear that the losses in the ZGP OPO were too high for the pump power (and bandwidth) which was available. A fuller discussion of the next steps for this work is detailed in the next section.

Chapters 4 and 5 brought the OPO into the cavity resulting in an OPO which could be operated in the continuous wave regime. The application for this OPO was spectroscopy, specifically for stand-off detection of volatile organic compounds. The narrower the spectrum of the laser, the higher the resolution and therefore more complex spectral signatures can be identified. The desire in substituting OP-GaAs in this example would be to extend the applicability of the technique to more substances. The frequency response of the VECSEL IC-OPO was not as stable as initially anticipated when following from the stable frequency behaviour of the VECSEL itself. This was attributed to the coating quality on the PPLN and to a certain extent, the other intracavity elements, resulting in parasitic cavities forming and feeding back into the parent laser causing dynamic fluctuations in the frequency behaviour. Attempts to control this were via the addition of etalons, and passive by wedging the PPLN facets and improving the coating quality. Ultimately, a firm test of the latter, more elegant, hypothesis was not possible due to resources (time as well as funding), however the preliminary tests showed promise.

Chapter 6 was slightly tangential to the preceding chapters in that the cavity architecture remained the same and the output coupling of the signal cavity was investigated with the initial aim of identifying an optimum point of operation. This was to address the needs of a user to be able to utilise the lower powers made efficiently attainable by the intracavity configuration, but more than a single wavelength is required. This experiment was validated with a model which had previously been untested experimentally, and the results were promising. Ultimately, there was a trade-off between the pump and signal circulating fields as it is not possible to achieve significant power across the 3 wavelengths available. The small, but significant and variable losses in the cavity made it difficult to reconcile exactly with the model leading to the idea that it may have been more straightforward to have used Nd-based IC-OPO to carry out the initial testing of the model.

7.2 Future work

A number of technologies have been demonstrated alongside potential application; however, not all demonstrations yielded the results that were intended. This section outlines the work that would be required to gain the information required to enable a true comparison between the technologies demonstrated and the current state of the art/fielded systems.

7.2.1 ZGP OPO

As described in Chapter 3, the advantage of using a PPLN OPO is that it allowed for the characterisation of whatever nonlinear material was suitably sourced by tuning the wavelength using wither the diffraction grating used to narrow its linewidth, or by tuning the temperature to affect the phase matching. The resultant system achieved ~3.4W for 12 W of input power which when used to pump the ZGP OPO proved insufficient, with the conclusion that the ZGP OPO losses (coatings, material loss) were too high to be overcome by the power that was available.

If the funding for this project never came under question, the first port of call would have been to buy a new laser which has a direct emission wavelength suitable for pumping ZGP, such as the TLPN-1-1-20-M laser from IPG [7.1] which has M^2<1.1, 20W average power with the same repetition rates as the 1064nm laser used for the work in Chapter 3. Alternatively, given that changing the pump source changes the phase matching wavelengths which would result in a requirement for new mirrors, another (more budget conscious option) would be to resurrect the Thulium fibre laser (to then pump Ho:YAG) held by the BAE Systems Advanced Technology Centre in Great Baddow (Essex). Direct emission sources have a naturally narrow linewidth source with enough power in band to get the system above threshold (or at least with such a well-defined source there would be less ambiguity about the reasons for it not reaching threshold, thus helping trouble-shoot the cavity design). This 2.09μm source would phase match (with the ZGP crystal described previously) to signal and idler wavelengths of 3.45μm and 5.31μm respectively (see Table 3.2) which would result in a non-degenerate OPO requiring new mirrors (unlike the design in Chapter 3), but with more pump power available this is not foreseen as being a problem.

If it is accepted that loss was the only reason that the system in Chapter 3 failed to operate successfully and that additional power would circumvent this problem, the three options can be compared more critically in terms of overall system performance (assuming that optically the same result can be achieved for all). Thermal management is one of the most significant problems in designing modest to high power lasers (>10W). Fibre lasers offer advantages in that they may not need active cooling as the fibre itself has sufficient surface area to allow the heat from the pump laser/quantum defect to escape, whereas a VECSEL, like most solid state lasers, needs active water cooling which is an inconvenience for the laser user. From a space perspective, the

VECSEL has advantages in that the cavity can be made very short (<5cm [7.2]), whereas the bend radius of a fibre laser has to be accommodated (the length of the fibre can be negated to a certain extent as it can be coiled). Realistically, with the availability of direct emission pump sources for materials like ZGP, the OPO was only ever a diagnostic tool so a final system for the countermeasure application would look more like that described by Elder [7.3] using the Thulium fibre laser approach.

7.2.2 IC-OPO for gas sensing

The design exists for a continuous wave, single frequency IC-OPO based on the addition of a frequency doubling crystal to the cavity to suppress relaxation oscillations cause by the use of Neodymium as a gain material [7.4] which would exhibit comparable powers to what has been achieved from the VECSEL system (if the VECSEL IC-OPO could achieve single frequency operation). If the baseline assumption that the VECSEL IC-OPO is capable of single frequency operation is correct, if not yet demonstrated, then it would be unfair to try to compare an unknown system configuration with the Nd-based system. This section will outline some work which would further inform the understanding of the behaviour which has been observed with the VECSEL IC-OPO system.

The nature of the research carried out in Chapters 4 and 5 were subject to significant amounts of uncertainty due to the inability to fully characterise the materials which were being trialled. There were no diagnostics in place to fully understand the crystal coatings nor the integrity of the material itself. If the initial assumption is true – that there should be no reason that the VECSEL should not be able to accommodate an intracavity OPO – then the crystals have to be brought into question as intracavity doubling systems based on VECSELs have been demonstrated [7.5]. Access to spectrophotometers to verify the coatings on the crystals before trialling them in the set-up would have allowed the coating quality claimed by the manufacturer to be verified and more useful comparisons to be made between samples. Moving away from PPLN, it would have been useful to evaluate the frequency stability of other birefringently phase matched nonlinear materials, such as BBO, in the same set-up to conclude if the material itself was the problem.

Finally, it would have been advantageous for the operator to have gained experience with both the Nd-based system and the VECSEL-system in order to evaluate the relative alignment sensitivities of the two systems. It could be that the VECSEL is naturally

more sensitive compared to the Nd-system and the fluctuations which were observed were due to air currents and mechanical instabilities rather than fundamental laser dynamics.

This section has highlighted the existence of an IC-OPO technology which is capable of generating single frequency idler output in the wavelength region of interest for high resolution spectroscope of hydrocarbons. It has also served to outline some of the configurations which should be trailed in order to further understand the limitations of using PPLN intracavity with a VECSEL.

7.3 Final conclusion

This thesis has focussed on the development of mid infrared laser based sources for use in defence applications. The sponsorship by BAE Systems provided an opportunity to collaborate on some important engineering problems which have the potential to affect the lives of men and women on the ground in areas of conflict. The down side of working with an industrial sponsor is that you are also subjected to the trials and tribulations of the market with regards to evolving economic circumstances affecting the availability of funding. The funding for the work described in this thesis fell into the void between commercial interest (deployment within 1 – 3 years) and fundamental research interest. Despite this, this thesis saw the first experimental verification of the equations developed for the optimisation of the output coupling from an ICOPO and extended the experience of BAE Systems ATC in the realm of mid-IR generation and application areas of supercontinuum generation for countermeasures.

7.4 References

[7.1] IPG Laser http://www.ipgphotonics.com/Collateral/Documents/English-US/TLPN-1-1-20-M.pdf accessed 8/4/14

[7.2] J.-M. Hopkins, A. J. Maclean, E. Riis, N. Schulz, M. Rattunde, C. Manz, K. Kohler, J. Wagner and D. Burns, "Tunable, single-frequency, diode-pumped 2.3 μm VECSEL" *Optics Express*, vol. 15, no. 13, pp 8212 – 8217, 2007

[7.3] I. Elder, "Thulium fibre laser pumped mid-IR laser," *Proceedings of SPIE*, vol. 7115, pp. 711505–711505–11, 2008.

[7.4] D. J. M. Stothard and M. H. Dunn, "Relaxation oscillation suppression in continuous-wave intracavity optical parametric oscillators.," *Optics express*, vol. 18, no. 2, pp. 1336–1348, Jan. 2010.

[7.5] D. Paboeuf, P. J. Schlosser and J. Hastie, "Frequency stabilization of an ultraviolet semiconductor disk laser", *Optics Letters*, vol. 38, no. 10, pp 1736 – 1738, 2013

8 Published Papers

M. A. Martin, D.J.M. Stothard and M. H. Dunn, "Intracavity Optical Parametric Oscillator based on Vertical External Cavity Surface Emitting Lasers (VECSELs) and Brewster Cut Periodically Poled Lithium Niobate (PPLN)", Photon 12, Durham (UK), 3 – 6th September 2012

Presentation at Photon 12 (Durham) – accepted, but not presented

Abstract: Relaxation oscillations in continuous wave, intracavity optical parametric oscillators are a well-recognised problem. One solution to this is to use a Vertical External Cavity Surface Emitting laser (VECSEL) as a pump source. This development is one step closer to realising a mode-hop free tunable, single frequency source for high resolution spectroscopy in the mid infrared. There are a number of strategically significant compounds with spectral fingerprints in this region of the spectrum for which the intracavity solution provides a highly compact source.

The use of a planar nonlinear crystal in a standing wave configuration has resulted in dynamic frequency fluctuations as a result of coupled-cavity effects arising from plane facet reflections with the additional requirement of complex tri-band dielectric coatings being difficult to realise. We have developed a cavity design based around a Brewster cut crystal of Periodically Poled Lithium Niobate (PPLN) to both eliminate the instabilities resulting from the plane surfaces of the crystal and the need for crystal coatings. By moving from a linear to a Z-shaped or bow-tie cavity design astigmatism introduced at the Brewster surfaces is compensated.

The power and frequency characteristics of the device will be discussed in the context of this novel cavity design alongside a comparison with previous work carried out using intracavity schemes.

M. A. Martin, M. A. Watson, “Infrared Laser Sources for BAE Systems: EngD programme – Mhairi Martin”, End of Year report 2012, BAE Systems TES report no. 109860-1, Oct 2012